# DEVELOPMENT OF $CO_2$ EOR TECHNIQUES FOR UNLOCKING RESOURCES IN TIGHT OIL FORMATIONS

A Thesis

Submitted to the Faculty of Graduate Studies and Research

In Partial Fulfillment of the Requirements

For the Degree of

Master of Applied Science

In

Petroleum Systems Engineering

University of Regina

By

Chengyao Song

Regina, Saskatchewan

October, 2013

Copyright 2013: Chengyao Song

**UNIVERSITY OF REGINA**

**FACULTY OF GRADUATE STUDIES AND RESEARCH**

**SUPERVISORY AND EXAMINING COMMITTEE**

Chengyao Song, candidate for the degree of Master of Applied Science in Petroleum Systems Engineering**,** has presented a thesis titled, ***Development of $CO_2$ EOR Techniques for Unlocking Resources in Tight Oil Formations,*** in an oral examination held on September 12, 2013. The following committee members have found the thesis acceptable in form and content, and that the candidate demonstrated satisfactory knowledge of the subject material.

| | |
|---|---|
| External Examiner: | Dr. Amornvadee Veawab, Environmental Systems Engineering |
| Supervisor: | Dr. Daoyong Yang, Petroleum Systems Engineering |
| Committee Member: | Dr. Yongan Gu, Petroleum Systems Engineering |
| Committee Member: | Dr. Peng Luo, Petroleum Systems Engineering |
| Chair of Defense: | Dr. Hilary Horan, Faculty of Business Administration |

# ABSTRACT

Tremendous resources of tight oil are located in North America and widely distributed in 24 oil reservoirs, which are characterized by both low permeability and low porosity. Although long horizontal wells together with massively fracturing techniques have been utilized to promote fluid injectivity and productivity, primary recovery factor of a tight oil reservoir still remains as low as only 5-10 % of original oil in place (OOIP). Due to low permeability, waterflooding results in low injectivity. Although $CO_2$ injection may be the most suitable enhanced oil recovery (EOR) option under immiscible or miscible conditions, its flooding mechanisms and performance have not been well understood. The traditional injection strategy including continuous $CO_2$ injection, water-alternating-$CO_2$ injection ($CO_2$-WAG), simultaneous water and $CO_2$ injection, and $CO_2$ huff-n-puff injection may perform rather differently in tight formations compared to the conventional reservoirs. Therefore, it is of practical and fundamental importance to evaluate the suitability of $CO_2$ EOR techniques for unlocking resources from tight oil formations.

In this study, techniques have been developed to experimentally and numerically evaluate performance of $CO_2$ injection in tight oil reservoirs for the purpose of enhancing oil recovery. Experimentally, coreflooding experiments have been performed to evaluate performance of waterflooding, continuous $CO_2$ flooding, $CO_2$-WAG flooding, and $CO_2$ huff-n-puff processes in tight oil formations,

respectively, while effects of various operational parameters on recovery performance are examined. Subsequently, numerical simulation is performed to match the experimental measurements and optimize the operational parameters. Finally, field-scale simulation is further conducted to evaluate the performance of various $CO_2$ EOR schemes in a tight oil formation.

As for experimental measurements and simulation, the $CO_2$-WAG flooding is found to result in higher sweep efficiency, leading to better recovery performance compared to waterflooding and continuous $CO_2$ flooding. As for $CO_2$ huff-n-puff process, oil recovery is experimentally found to be lower than that of $CO_2$ flooding. There exists a good agreement between the experimentally measured and numerically simulated oil recovery and pressure, indicating that the overall mechanisms of $CO_2$ injection in tight oil reservoirs have been captured by numerical simulation, while the operational parameters can be optimized to maximize oil recovery form tight oil formations.

As for field-scale simulation, miscible $CO_2$-WAG flooding is found to result in higher oil recovery efficiency compared to other $CO_2$ flooding schemes, while $CO_2$ huff-n-puff processes show favourable recovery performance, provided that enough wells in the field are put into production. Oil recovery is found to be improved by optimizing the operational parameters during $CO_2$ injection processes, while production and injection pressures play dominant roles on oil recovery in tight formations.

# ACKNOWLEDGEMENTS

I would like to acknowledge my academic supervisor, Dr. Daoyong (Tony) Yang, for his excellent guidance, valuable encouragement, and timely support throughout the course of my graduate studies.

I also wish to thank the following individuals or organizations for their support and encouragement during my graduate studies at the University of Regina:

- My past and present research group members: Dr. Huazhou Li, Mr. Chuck Egboka, Mr. Sixu Zheng, Mr. Yin Zhang, Miss Xiaoli Li, Mr. Deyue Zhou, Mr. Feng Zhang, Miss Min Yang, and Ms. Ping Yang;
- Natural Sciences and Engineering Research Council (NSERC) of Canada for a Discovery Grant to Dr. Yang;
- Petroleum Technology Research Centre (PTRC) for an innovation fund to Dr. Yang;
- Faculty of Graduate Studies and Research (FGSR) at the University of Regina for awarding the Teaching Assistantship (2013 Winter);
- Saskatchewan Research Council (SRC) for providing the analytical results of crude oil and reservoir brine;
- Many wonderful friends who extended their love and friendship to me during my stay in Regina.

# DEDICATION

To my beloved parents, Mrs. Guiying Meng and Mr. Guangming Song, for their continuous support and unconditional love.

# TABLE OF CONTENTS

ABSTRACT ..... i

ACKNOWLEDGEMENTS ..... iii

DEDICATION ..... iv

LIST OF TABLES ..... vii

LIST OF FIGURES ..... viii

NOMENCLATURE ..... xiv

CHAPTER 1 INTRODUCTION ..... 1

1.1 Tight Oil Resources ..... 1

1.2 Development of Tight Oil Resources ..... 2

1.3 Purpose of the Thesis Study ..... 3

1.4 Outline of the Thesis ..... 4

CHAPTER 2 LITERATURE REVIEW ..... 5

2.1 Introduction ..... 5

2.2 $CO_2$ EOR Mechanisms ..... 7

2.3 $CO_2$ EOR Techniques ..... 11

2.3.1 Continuous $CO_2$ flooding ..... 11

2.3.2 $CO_2$-WAG flooding ..... 15

2.3.3 $CO_2$ huff-n-puff ..... 17

2.4 Performance Optimization ..... 19

2.5 Summary ..... 20

CHAPTER 3 EXPERIMENTAL AND NUMERICAL EVALUATION OF $CO_2$ EOR PERFORMANCE ..... 22

3.1 Experimental ..... 22

3.1.1 Materials ..... 22

3.1.2 Experimental setup ..... 25

3.1.3 Experimental scenarios ..... 28

3.1.4 Experimental procedures ..... 30
3.2 Numerical Simulation ..... 33
3.2.1 Numerical model ..... 33
3.2.2 Simulation procedure ..... 34
3.3 Results and Discussion ..... 37
3.3.1 Experimental measurements ..... 37
3.3.2 History matching ..... 55
3.3.3 Sensitivity analysis ..... 77
3.4 Summary ..... 90
CHAPTER 4 PERFORMANCE EVALUATION OF FIELD-SCALE $CO_2$ INJECTION ..... 93
4.1 Field Background ..... 93
4.2 Reservoir Geological Model ..... 95
4.3 Simulation Procedure ..... 97
4.4 Result and Discussion ..... 100
4.4.1 Reservoir pressure estimation ..... 100
4.4.2 History matching ..... 102
4.4.3 Sensitivity analysis ..... 108
4.5 Summary ..... 129
CHAPTER 5 CONCLUSIONS AND RECOMMENDATIONS ..... 134
5.1 Conclusions ..... 134
5.2 Recommendations ..... 136
REFERENCES ..... 138
APPENDIX ..... 150

# LIST OF TABLES

**Table 3.1** Physical properties of crude oil ..... 23

**Table 3.2** Compositional analysis results of crude oil ..... 24

**Table 3.3** Properties of reservoir brine ..... 26

**Table 3.4** The measured porosity, permeability, and initial oil saturation of Scenarios #1-9 ..... 31

**Table 3.5** Summary of the properties of the eight pseudo-components ..... 35

# LIST OF FIGURES

**Figure 2.1** Producing and prospective tight oil plays in North America.....6

**Figure 3.1** Schematic diagram of the experimental setup.....27

**Figure 3.2** A digital image of the experimental setup.....29

**Figure 3.3** Schematic diagram of 3D view of the displacement model. .....36

**Figure 3.4** Measured oil recovery, cumulative water production, and pressure drop versus pore volume of water injected for Scenario #1 .....38

**Figure 3.5** Measured oil recovery, cumulative gas production, and pressure drop versus pore volume of $CO_2$ injected for Scenario #2.....40

**Figure 3.6** Measured oil recovery, cumulative gas production, and pressure drop versus pore volume of $CO_2$ injected for Scenario #3.....42

**Figure 3.7** Measured oil recovery, cumulative water production, cumulative gas production, and pressure drop versus pore volume of $CO_2$ or water injected for Scenario #4 .....44

**Figure 3.8** Measured oil recovery, cumulative water production, cumulative gas production, and pressure drop versus pore volume of $CO_2$ or water injected for Scenario #5 .....46

**Figure 3.9** Measured oil recovery, cumulative water production, cumulative gas production, and pressure drop versus pore volume of $CO_2$ or water injected for Scenario #6 .....48

**Figure 3.10** Measured oil recovery, cumulative gas production, and pressure drop versus time for Scenario #7.....51

**Figure 3.11** Measured oil recovery, cumulative gas production, and pressure drop versus time for Scenario #8.....53

**Figure 3.12** Measured oil recovery, cumulative gas production, and pressure drop versus time for Scenario #9.....54

**Figure 3.13** Water and oil relative permeability and capillary pressure for Scenario #1.....56

**Figure 3.14** Simulated oil production and injection pressure versus time for Scenario #1.....57

**Figure 3.15** Relative permeability for **(a)** Water-oil system and its capillary pressure and **(b)** Gas-liquid system and its capillary pressure for Scenario #2 ...59

**Figure 3.16** Simulated oil production and injection pressure versus time for Scenario #2.....60

**Figure 3.17** Relative permeability for **(a)** Water-oil system and its capillary pressure and **(b)** Gas-liquid system and its capillary pressure for Scenario #3 ....62

**Figure 3.18** Simulated oil production and injection pressure versus time for Scenario #3 .....63

**Figure 3.19** Relative permeability for **(a)** Water-oil system and its capillary pressure and **(b)** Gas-liquid system and its capillary pressure for Scenario #4 ....65

**Figure 3.20** Simulated oil production and injection pressure versus time for Scenario #4 .....66

**Figure 3.21** Relative permeability for **(a)** Water-oil system and its capillary pressure and **(b)** Gas-liquid system and its capillary pressure for Scenario #5 ....67

**Figure 3.22** Simulated oil production and injection pressure versus time for Scenario #5 .....69

**Figure 3.23** Relative permeability for **(a)** Water-oil system and its capillary pressure and **(b)** Gas-liquid system and its capillary pressure for Scenario #6 ....70

**Figure 3.24** Simulated oil production and injection pressure versus time for

Scenario #6 ..... 71

**Figure 3.25** Relative permeability for **(a)** Water-oil system and its capillary pressure and **(b)** Gas-liquid system and its capillary pressure for Scenario #7 .... 73

**Figure 3.26** Simulated oil production and injection pressure versus time for Scenario #7 ..... 74

**Figure 3.27** Relative permeability for **(a)** Water-oil system and its capillary pressure and **(b)** Gas-liquid system and its capillary pressure for Scenario #8 .... 75

**Figure 3.28** Simulated oil production and injection pressure versus time for Scenario #8 ..... 76

**Figure 3.29** Relative permeability for **(a)** Water-oil system and its capillary pressure and **(b)** Gas-liquid system and its capillary pressure for Scenario #9 .... 78

**Figure 3.30** Simulated oil production and injection pressure versus time for Scenario #9 ..... 79

**Figure 3.31** Production profiles with different production pressures for **(a)** Scenario #2 and **(b)** Scenario #9..... 80

**Figure 3.32** Sensitivity analysis for Scenario #4: **(a)** WAG ratio and **(b)** Injection pressures..... 82

**Figure 3.33** Sensitivity analysis for Scenario #4: **(a)** Cycle time and **(b)** Injection pressure ..... 85

**Figure 3.34** Sensitivity analysis for Scenario #4: **(a)** Water slug size and **(b)** Injection pressure..... 87

**Figure 3.35** Production profiles with different injection pressures for Scenario #9 .. 89

**Figure 3.36** Production profiles with different soaking times for Scenario #9..... 91

**Figure 4.1** Location map of an oilfield selected in the Bakken formation..... 94

**Figure 4.2** **(a)** Cumulative oil production, **(b)** Cumulative water production, and **(c)**

Cumulative gas production of each well in the selected region.....96

**Figure 4.3** Schematic diagram of 3D view of the reservoir geological model .....98

**Figure 4.4** Distribution of initial oil saturation for **(a)** Layer #1, **(b)** Layer #2, **(c)** Layer #3, **(d)** Layer #4, and **(e)** Layer #5 .....99

**Figure 4.5** Calculated reservoir pressure versus time .....101

**Figure 4.6** Relative permeability for **(a)** Water-oil system and its capillary pressure and **(b)** Gas-liquid system and its capillary pressure for the field-scale reservoir simulation .....103

**Figure 4.7** Simulated reservoir pressure and its calculated value from material balance versus time .....104

**Figure 4.8** Distribution of residual oil saturation after primary recovery process for **(a)** Layer #1, **(b)** Layer #2, **(c)** Layer #3, **(d)** Layer #4, and **(e)** Layer #5105

**Figure 4.9** Distribution of residual water saturation after primary recovery process for **(a)** Layer #1, **(b)** Layer #2, **(c**) Layer #3, **(d)** Layer #4, and **(e)** Layer #5.....106

**Figure 4.10** Distribution of residual gas saturation after primary recovery process for **(a)** Layer #1, **(b)** Layer #2, **(c)** Layer #3, **(d)** Layer #4, and **(e)** Layer #5 .....107

**Figure 4.11** Schematic diagram of **(a)** Pattern #1, **(b)** Pattern #2, and **(c)** Pattern #3 for waterflooding processes (Injector: Orange color; Producer: Black color) .....109

**Figure 4.12** Simulated oil recovery versus time for different well patterns of waterflooding processes.....110

**Figure 4.13** Distribution of residual oil saturation in waterflooding processes for **(a)** Layer #1, **(b)** Layer #2, **(c)** Layer #3, **(d)** Layer #4, and **(e)** Layer 5 ... 111

**Figure 4.14** Distribution of residual water saturation in waterflooding processes for **(a)** Layer #1, **(b)** Layer #2, **(c)** Layer #3, **(d)** Layer #4, and **(e)** Layer 5 ..... 112

**Figure 4.15** Distribution of residual gas saturation in waterflooding processes for **(a)** Layer #1, **(b)** Layer #2, **(c)** Layer #3, **(d)** Layer #4, and **(e)** Layer 5113

**Figure 4.16** Oil recovery of continuous $CO_2$ flooding with different production pressures..... 115

**Figure 4.17** Distribution of residual oil saturation in continuous $CO_2$ flooding processes for **(a)** Layer #1, **(b)** Layer #2, **(c)** Layer #3, **(d)** Layer #4, and **(e)** Layer #5 ..... 116

**Figure 4.18** Distribution of residual water saturation in continuous $CO_2$ flooding processes for **(a)** Layer #1, **(b)** Layer #2, **(c)** Layer #3, **(d)** Layer #4, and **(e)** Layer #5 ..... 117

**Figure 4.19** Distribution of residual gas saturation in continuous $CO_2$ flooding processes for **(a)** Layer #1, **(b)** Layer #2, **(c)** Layer #3, **(d)** Layer #4, and **(e)** Layer #5 ..... 118

**Figure 4.20** Oil recovery profiles with different WAG ratios for miscible $CO_2$-WAG flooding processes..... 120

**Figure 4.21** Oil recovery profiles with different cycle time for miscible $CO_2$-WAG flooding processes..... 122

**Figure 4.22** Distribution of residual oil saturation in $CO_2$-WAG flooding processes for **(a)** Layer #1, **(b)** Layer #2, **(c)** Layer #3, **(d)** Layer #4, and **(e)** Layer #5 ..... 123

**Figure 4.23** Distribution of residual water saturation in $CO_2$-WAG flooding processes for **(a)** Layer #1, **(b)** Layer #2, **(c)** Layer #3, **(d)** Layer #4, and **(e)** Layer #5 ..... 124

**Figure 4.24** Distribution of residual gas saturation in $CO_2$-WAG flooding processes for **(a)** Layer #1, **(b)** Layer #2, **(c)** Layer #3, **(d)** Layer #4, and **(e)** Layer #5 ..... 125

**Figure 4.25** Oil recovery profiles with different soaking times for miscible $CO_2$ huff-n-puff processes ..... 127

**Figure 4.26** Oil recovery profiles with different injection pressures for $CO_2$ huff-n-puff processes..... 128

**Figure 4.27** Distribution of residual oil saturation in $CO_2$ huff-n-puff processes for **(a)** Layer #1, **(b)** Layer #2, **(c)** Layer #3, **(d)** Layer #4, and **(e)** Layer #5..... 130

**Figure 4.28** Distribution of residual water saturation in $CO_2$ huff-n-puff processes for **(a)** Layer #1, **(b)** Layer #2, **(c)** Layer #3, **(d)** Layer #4, and **(e)** Layer #5 ..... 131

**Figure 4.29** Distribution of residual gas saturation in $CO_2$ huff-n-puff processes for **(a)** Layer #1, **(b)** Layer #2, **(c)** Layer #3, **(d)** Layer #4, and **(e)** Layer #5..... 132

# NOMENCLATURE

***Notations***

$B_g$ = Formation volume factor for gas, $ft^3/scf$

$B_o$ = Formation volume factor for oil, bbl/STB

$B_w$ = Formation volume factor for water, bbl/STB

$c_g$ = Gas compressibility, $psi^{-1}$

$c_o$ = Oil compressibility, $psi^{-1}$

$c_r$ = Pore compressibility, $psi^{-1}$

$c_w$ = Water compressibility, $psi^{-1}$

$E_{f,w}$ = Rock and water compression/expansion term defined in Eq. [4.1]

$E_g$ = gas cap expansion term defined in Eq. [4.1]

$E_o$ = Oil and solution gas expansion term defined in Eq. [4.1]

$G_l$ = Cumulative gas injected, $Sm^3$

$k_{rg}$ = Relative permeability to gas for the liquid-gas system

$k_{rog}$ = Relative permeability to liquid for the liquid-gas system

$k_{row}$ = Relative permeability to oil for the water-oil system

$k_{rw}$ = Relative permeability to water for the water-oil system

$m$ = Initial gas cap size defined in Eq. [4.1]

$N$= Original oil in place, $m^3$

$N_p$= Cumulative oil production, $m^3$

$R_p$= Gas-oil ratio, scf/STB

$R_{so}$= Solution gas-oil ratio, scf/STB

$S_g$= Gas saturation, %

$S_o$= Oil saturation, %

$S_w$= Water saturation, %

$W_e$= Cumulative aquifer influx, $m^3$

$W_l$ = Cumulative water injected, $Sm^3$

$W_p$= Cumulative water production, $Sm^3$

# CHAPTER 1 INTRODUCTION

## 1.1 Tight Oil Resources

As world oil consumption is escalating and conventional oil reserves are depleting, the vast tight oil resources discovered in North America have recently drawn much more attention. Such an unconventional resource has been emerged as one of the crucial alternatives to the depleting conventional oil resources. The tight oil reservoirs are characterized by extremely low permeability and low porosity compared to the conventional oil reservoirs (Miller *et al*., 2008). It is, therefore, a great challenge to produce oil from such a tight formation economically and effectively.

The global tight oil resources exceed 100 billion barrels which are extensively distributed around the world, while most of the reserves are difficult to be efficiently recovered under the currently available technology (Ashraf and Satapathy, 2013). In North America, the tight oil reserves are estimated to be over 30 billion barrels, stored in 24 oil reservoirs of Canada and the United States. Some important tight oil formations including the Bakken formation, Cardium formation, Niobrara formation, Antelope formation, and Tuscaloosa formation present great recovery potential (Forrest *et al*., 2011). Although the volumes of original-oil-in-place (OOIP) are huge, daily production of tight oil is only 400,000 barrels in North America with a large amount of tight oil untouched (Elsevier, 2012).

## 1.2 Development of Tight Oil Resources

As for a tight oil formation with permeability lower than 1 mD, the primary recovery factor remains as low as only 5-10% of OOIP, even if long horizontal wells have been drilled and massively fractured (Manrique *et al.*, 2010). Waterflooding is subsequently initiated to improve oil recovery after primary recovery stage. In this way, oil production is improved and reservoir pressure is maintained. Although the waterflooding presents high recovery efficiency at the beginning, oil production decreases sharply and water production increases quickly once water starts to break through. Due to low fluid injectivity resulting from low permeability of tight oil formations, it is difficult for waterflooding to be widely applied to improve oil recovery (Iwere *et al.*, 2012).

$CO_2$ has both lower viscosity and density compared to water, resulting in a superior fluid injectivity (Jarrell *et al.*, 2002), which is the key to displace oil in tight formations (Yu *et al.*, 2011). $CO_2$ injection is found to achieve good recovery performance in some reservoirs with low permeability of 1-2 mD by the underlying mechanisms of oil viscosity reduction, oil swelling, interfacial tension reduction, solution gas drive, gravity drainage, reservoir permeability improvement, and light-components extraction (Ghedan, 2009). The applied $CO_2$ injection strategies include continuous $CO_2$ flooding, water-alternating-$CO_2$ ($CO_2$-WAG) flooding, and $CO_2$ huff-n-puff, among which the latter two processes appear to be more efficient and more economical for recovering oil from such tight formations (Kane, 1979; Monger and Coma, 1988).

Although $CO_2$ injection is found to achieve good recovery performance, the mechanisms governing $CO_2$ injection of tight oil formations lower than 1 mD have not been well understood (Shoaib and Hoffman, 2009). The traditional $CO_2$ injection strategies may result in rather different EOR performance in such tight formations compared to the conventional reservoirs. Therefore, it is of practical and fundamental importance to explore the major mechanisms of $CO_2$ injection in tight oil formations, and subsequently optimize the $CO_2$ injection processes for more effectively and efficiently unlocking resources from tight oil formations.

## 1.3 Purpose of the Thesis Study

The purpose of this thesis is to comprehensively investigate the suitability of $CO_2$ EOR techniques for unlocking resources from tight oil formations. The primary objectives of this study include:

1) To perform coreflooding experiments to examine effects of various $CO_2$ injection-production strategies on oil recovery;

2) To conduct numerical simulation for history matching the experimental measurements in order to identify the underlying mechanisms associated with $CO_2$ injection processes in tight oil reservoirs;

3) To perform sensitivity analysis on the operational parameters during $CO_2$ injection processes in order to maximize oil recovery from tight oil formations; and

4) To conduct comprehensive field-scale simulations to evaluate the recovery performance and optimize the injection-production strategies.

## 1.4 Outline of the Thesis

This thesis is comprised of five chapters. Chapter 1 is an introduction to the research including research topic and objectives. Chapter 2 provides a literature review on the recovery techniques applied in tight oil formations together with the mechanisms associated with $CO_2$ EOR techniques. Chapter 3 presents the experimental and numerical evaluation of oil recovery under various $CO_2$ injection-production strategies with tight core samples. Chapter 4 evaluates reservoir performance of various $CO_2$ injection schemes for a tight oil formation by conducting comprehensive field-scale simulation. Finally, Chapter 5 summarizes the major scientific findings of the study and provides some recommendations for future research.

# CHAPTER 2 LITERATURE REVIEW

## 2.1 Introduction

In North America, unconventional oil resources, including oil shale, shale gas, heavy oil, oilsands, and tight oil, are estimated to be over 200 billion barrels (Forrest *et al*., 2011). Such resources are nearly two times larger than the currently recoverable conventional oil resources. The tight oil resources account for 30 billion barrels, widely distributed in 24 oil reservoirs of Canada and the United States, among which only 14 reservoirs are under development (See **Figure 2.1**) (Forrest *et al.*, 2011).

Although various development schemes have been attempted to exploit the tight oil resources in North America for the past decades, a primary recovery factor can only achieve 5-10% of the original oil in place (OOIP) (Manrique *et al.*, 2010). In order to promote both productivity and injectivity from tight oil formations, horizontal wells have been extensively applied with massively hydraulic fracturing techniques, leading to a significant increase of oil production from the Bakken formation (Lolon *et al.*, 2010).

During the secondary oil recovery stage, waterflooding is implemented to maintain the reservoir pressure and provide the driven force (Park, 1966). However, the oil recovery performance is not enhanced obviously. This is attributed to the following two facts: (1) the poor physical properties of tight oil formations (i.e., low permeability, strong water sensitivity and low porosity) lead to a low injectivity, poor

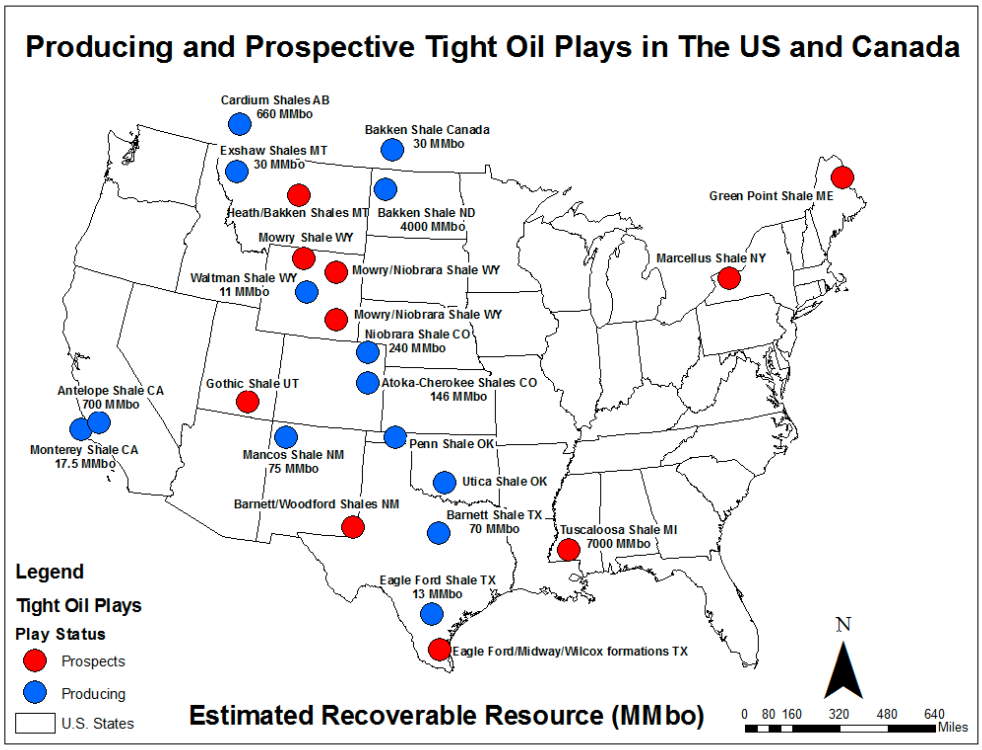


**Figure 2.1** Producing and prospective tight oil plays in North America (Forrest *et al.*, 2011)

pressure conductivity and unfavourable productivity (Iwere *et al.*, 2012), and (2) the early water breakthrough leads to a rapid depletion of reservoir energy (Joshi, 2003). By 2009, the daily production of tight oil approached only 400,000 barrels in North America (Elsevier, 2012), while a large amount of tight oil is still untouched.

Although $CO_2$ injection may be the most suitable option for enhanced oil recovery (EOR) or tertiary recovery under immiscible or miscible conditions, its flooding mechanisms and performance have not been well understood. The traditional injection strategy including continuous $CO_2$ injection, water-alternating-$CO_2$ injection ($CO_2$-WAG), simultaneous water and $CO_2$ injection, and $CO_2$ huff-n-puff injection may perform rather differently in tight formations compared to the conventional reservoirs. Therefore, it is of fundamental and practical importance to understand the flow behaviour and develop viable $CO_2$ techniques for significantly enhancing oil recovery in tight oil formations.

## 2.2 $CO_2$ EOR Mechanisms

$CO_2$ injection is a promising EOR method both on technical and economic grounds for tight oil formations together with positive environmental impacts (Arshad *et al.*, 2009; Faltinson and Gunter, 2011). Although the flooding schemes and the application conditions are varied, the main mechanisms of $CO_2$ EOR in tight oil formations are very similar, including oil viscosity reduction, oil swelling effect, interfacial tension reduction, permeability improvement, solution gas drive, gravity

drainage, and components extraction (Ghedan, 2009).

***Viscosity reduction***: When contacting with oil, $CO_2$ is able to easily dissolve into crude oil. Such dissolution leads to a significant reduction of oil density and viscosity. The decrease in oil viscosity will largely contribute to mobilizing the crude oil, and thus improving the ultimate oil recovery (Ghedan, 2009).

***Oil swelling***: Once $CO_2$ is dissolved into the crude oil, which is swollen and tends to expand. Such expansion results in an increase of oil saturation and decrease of residual oil in the reservoir (Rahman *et al*., 2010). Also, some reservoir water is displaced out by the swollen oil (Jha, 1986), which in turn contributes to improving the oil phase relative permeability. As such, a favourable condition has been developed for mobilizing the crude oil, and thus contributing to the enhancement of oil recovery.

***Reduction of interfacial tension (IFT)***: In miscible flooding, the IFT between crude oil and $CO_2$ theoretically tends to be zero. However, in most cases, the near-miscible or immiscible flooding is implemented instead of miscible flooding due to economic reasons and technique limitations (Zekri *et al*., 2006). Under these conditions, dissolution of $CO_2$ into crude oil is able to significantly decrease both oil/gas and oil/water IFT (Ghedan, 2009), which directly leads to a reduced capillary force. Since capillary force usually functions as a resistance to oil flowing especially in tight reservoir, IFT reduction increases the capillary number by reducing the capillary force, and thus enhances oil recovery.

***Improvement of formation permeability***: In addition to oil, $CO_2$ is able to dissolve into other formation fluids so that the $CO_2$-dissolved fluids will appear as somewhat slightly acidic. Such acidic fluids will react with the rock matrix with component of carbonate to dissolve some minerals (Rahman *et al.*, 2010). Formation permeability is then improved as some blockages for fluid flowing in porous media will be effectively removed.

***Solution gas drive***: Due to change of pressure and temperature in a reservoir, the solution gas in oil may be released from crude oil, and forms a free gas. Such released free gas will greatly drive the oil into wellbore or fractures, which is one of the most important mechanisms for $CO_2$ EOR (Bank *et al.*, 2007).

***Gravity drainage***: If a matrix block is surrounded by $CO_2$ or there exists some fractures in a reservoir wherever filled with $CO_2$, there must be a density difference between $CO_2$ in the fracture and fluid in the matrix. When the displacing forces resulting from density difference exceeds the capillary force that resists fluid flowing in the matrix, there will undergo a gravity drainage process, i.e., oil will flow into fractures and be produced out until the gravitational forces are equalized by the capillary forces (Kazemi and Jamialahmadi, 2009). Gravity drainage is generally dominated in naturally fractured reservoirs, especially for the medium or high permeability fractured reservoirs (Karimaie and Torsaeter, 2010).

In naturally fractured reservoirs, there usually exists a large amount of micro-fractures which are likely to boost the free-fall gravity drainage. Also, the natural fractures are usually longer and more complex, contributing to the efficiency of

gravity drainage. In addition, a larger permeability results in a lower capillary force. This will weaken the resistance of fluid flowing in porous media so that liquid transferring from matrix to fractures is facilitated. Thus, gravity drainage plays a dominant role in the fractured reservoirs with medium or high permeability. As for a tight oil reservoir, due to the dominant capillary force, effect of gravity drainage on oil recovery may not be so significant. Compared with the naturally fractured reservoirs, the hydraulic fractures formed in tight formations are not able to reach such a large scale either in length or complexity, thus the gravity drainage in tight formations is further weakened (Li *et al*., 2000).

***Light-components extraction***: In fractured tight reservoirs, the injected $CO_2$ is more likely to flow into the fractures with higher permeability, and molecular diffusion process takes place between $CO_2$ in the high permeability fractures and crude oil in the low permeability matrix. $CO_2$ tends to dissolve into the oil in the matrix, while light and intermediate fractions of the oil are extracted to the injected $CO_2$ and tend to be miscible via multiple contacts with $CO_2$. Though gravity drainage may still improve oil recovery, its impact is significantly decreased due to the presence of huge capillary force and absence of large-scale natural fractures, while light-components extraction plays a dominant role in the recovery of tight oil reservoir (Morel *et al*., 1993).

## 2.3 $CO_2$ EOR Techniques

On the basis of $CO_2$ EOR mechanisms, the recovery performance, however, would be various with the different development schemes for tight oil formations (Ghaderi *et al*., 2012). According to laboratory investigations and field applications, $CO_2$ injection is able to result in favourable oil production, though there exists some limitations for various flooding schemes (Arshad *et al*., 2009). Hence, an appropriate development scheme is crucial for recovering the tight oil reservoirs.

### 2.3.1 Continuous $CO_2$ flooding

***Immiscible $CO_2$ flooding***: During the immiscible $CO_2$ flooding process, $CO_2$ is continuously injected in to a reservoir with a pressure lower than the minimum miscibility pressure (MMP) between crude oil and $CO_2$ (Zhou *et al*., 2012). Partial of the injected $CO_2$ is dissolved into reservoir fluids, while the remaining $CO_2$ forms a free gas phase in the reservoir (Bagci, 2007). The main mechanisms for enhancing oil recovery by continuous $CO_2$ flooding are found to be viscosity reduction, oil expansion, interfacial tension reduction, light and medium components exaction and blowdown recovery (Kamal, 1985; Martin and Taber, 1992). The first three factors lead to an improvement of oil mobility and then an increase of recovery. The light and medium components extraction usually works in light or medium oil reservoirs. Some light components in crude oil are extracted out and become miscible with the injected $CO_2$ gas, and be produced out later (Uwabe *et al*., 2009). As for blowdown recovery,

it is associated with the residual $CO_2$ in the reservoir that is liberated as reservoir pressure decreases, leading to the residual oil movement in the reservoir so that more oil is produced (Bagci, 2007).

Compared to waterflooding, continuous $CO_2$ injection maintains higher injectivity together with better recovery performance in tight oil reservoirs (Zhou *et al.*, 2012). The pressure drop of immiscible $CO_2$ flooding is able to be significantly decreased compared to waterflooding, resulting in an obviously lower injection pressure, and thus a higher injectivity (Yang and Wang, 2010). It is also observed from various laboratory experiments that a nearly 20-30% of ultimate oil recovery is able to be enhanced by continuous immiscible $CO_2$ flooding compared to waterflooding, proving to achieve a superior recovery performance in tight oil reservoirs (Kuo *et al.*, 1990; Dennis *et al.*, 1993) .

In general, early gas breakthrough hinders a further improvement of oil recovery during immiscible $CO_2$ flooding process (Bagci, 2007). It is found from coreflooding experiments that $CO_2$ breakthrough of continuous $CO_2$ flooding usually comes earlier than waterflooding (Zhang *et al.*, 2010). The oil production tends to be significantly decreased when the gas production is higher than a certain value (Wang and Gu, 2011). In addition, the $CO_2$ flooding will also result in obvious asphaltene deposition in the reservoir, leading to a decrease of oil effective permeability, and thus a lower oil recovery (Cao and Gu, 2013).

During the development of tight oil formations, continuous $CO_2$ flooding is considered to be applicable for either the reservoirs suitable for gravity stable

displacement or the reservoirs where waterflooding could have significantly adverse impact on reservoir performance (Zhou *et al*., 2012). Immiscible $CO_2$ flooding has shown better recovery performance compared to waterflooding. In 1978, $CO_2$ is continuously injected into its pilot zones with low permeability of 3 mD in the Maljamar field under immiscible conditions and achieved a higher oil production compared to waterflooding, while its injection pressure was significantly lower (Moore and Clark, 1988).

Immiscible $CO_2$ flooding is also regarded as a favourable choice for some special low permeability reservoirs bearing medium or even heavy oil because of the inefficiency of waterflooding, i.e., Bati Raman field with medium oil and heavy oil produced in Turkey (Sahin *et al*., 2008). Such field-scale immiscible $CO_2$ flooding has been initiated for nearly 30 years and makes the Bari Raman field stands as the second largest oilfield in Turkey. However, the unstable displacement of immiscible $CO_2$ flooding always leads to considerable variation of oil production in the field, which not only deters an accurate production estimation, but also increases the operating difficulties on the field (Pittaway *et al*., 1985; Bagci, 2007).

***Miscible $CO_2$ flooding***: In order to further improve oil recovery from tight oil reservoirs, miscible $CO_2$ flooding technique was proposed and implemented (Brannan and Whitington, 1977). The $CO_2$ flooding under miscible conditions leads to a zero capillary entry pressure for $CO_2$ into the oil-filled pore space, making oil and $CO_2$ be one phase, resulting in a high local displacement efficiency (Kovscek and Cakici, 2005). Theoretically, an ultimate recovery factor of 100% is able to be obtained by

miscible $CO_2$ flooding (Craig and Owens, 1960). It is also found that the MMP between carbon dioxide and crude oil is significantly lower than that of other gases, e.g., nitrogen, flue gas or natural gas (Stalkup, 1983). Thus, $CO_2$ miscible injection is considered attainable under a broad spectrum of reservoir pressure. Compared to previous immiscible flooding, miscible $CO_2$ flooding usually yields better recovery results. According to the laboratory investigations with tight core samples, the continuous miscible $CO_2$ flooding is able to obtain an incremental recovery factor of at least 15% of OOIP compared to immiscible $CO_2$ flooding, presenting a superior recovery performance for development of tight oil reservoirs (Kovscek *et al*., 2008).

Field tests of the continuous miscible $CO_2$ flooding have been conducted in six oilfields in North America for unlocking tight oil resources, including Slaughter field, Levelland field, Goldsmith field, Crossett Devonian field, Midale field and Coulee field (Forrest *et al*., 2011). Oil recovery is significantly enhanced compared to previous waterflooding or immiscible $CO_2$ flooding, which is consistent with the experimental results (Folger and Guillot, 1996).

Despite of the favourable oil recovery performance obtained by applying continuous $CO_2$ injection, the limitations of this technique cannot be ignored. The continuous miscible $CO_2$ flooding is very sensitive to reservoir heterogeneity. The existence of fractures or high permeability regions provides a sudden permeability change in tight oil reservoirs, which usually leads to non-uniform oil displacement. As such, chance of early breakthrough will be increased, leading to a decrease of ultimate recovery factor (Arshad *et al*., 2009). On the other hand, a large amount of

$CO_2$ gas would be consumed during the continuous $CO_2$ flooding process. The shortage of $CO_2$ resources around the oilfields as well as the high cost of $CO_2$ flooding imposes negative effects on the extensive implementation of continuous $CO_2$ injection method (Ghedan, 2009).

### 2.3.2 $CO_2$-WAG flooding

In a $CO_2$-WAG process, $CO_2$ and water are injected alternatively with certain slug size into a reservoir, while production wells produce continuously (Manrique *et al.*, 2007). When $CO_2$ is injected into the reservoir, $CO_2$ dissolves into crude oil, leading to oil viscosity reduction, oil swelling, interfacial tension reduction, and mass transfer between oil and $CO_2$ phase. Water slugs injected contributes to controlling $CO_2$ displacement front (Fatemi and Sohrabi, 2013). In this way, $CO_2$-WAG flooding has been considered as an improvement for its continuous version.

In the presence of alternatively injecting water slugs, the chance of early breakthrough is decreased, sweeping efficiency is improved and fingering of $CO_2$ gas is minimized (Jiang *et al.*, 2012). According to laboratory investigations, even after $CO_2$ breakthrough, the gas production rate of $CO_2$-WAG flooding is still found to be lower than that of continuous $CO_2$ flooding (Arshad *et al.*, 2009). The $CO_2$-WAG injection is consequently found with obvious superiority on recovery performance. According to the coreflooding research, $CO_2$-WAG flooding is found with an increased recovery factor by 10-20% compared to both waterflooding and

continuous $CO_2$ flooding, while miscible $CO_2$-WAG flooding shows better recovery performance than immiscible $CO_2$-WAG flooding (Kudal *et al*., 2010).

Recovery performance of $CO_2$-WAG flooding is found to be significantly influenced by reservoir heterogeneity, rock wettability, WAG ratio, slug size, cycle time, production rate, and production pressure (Surguchev *et al*., 1992). Numerical efforts have been made to optimize $CO_2$-WAG flooding schemes in order to maximize oil recovery from tight oil formations. Guo *et al*. (2006) presents a comprehensive reservoir simulation of $CO_2$-WAG processes with a tight oil reservoir model. Sensitivity analysis is conducted on various operational parameters including WAG ratio, $CO_2$ slug size, cycle time, cycle number, injection rate, and production pressure. It is found that oil recovery tends to increase with the increase of injection pressure until it becomes higher than the MMP. Under the same cycle time, parameters including slug size, WAG ratio and injection rate are able to be optimized to maximize the final recovery factor. However, there are no common rules to estimate the optimal condition, which are usually associated with specific characteristics of formations and properties of crude oil (Rogers and Grigg, 2001; Zekri *et al*., 2011).

Compared to continuous $CO_2$ flooding, the $CO_2$-WAG process has seen extensive applications in the oilfields due to its less $CO_2$ consumption and better oil recovery performance (Christensen *et al*., 2001). At present, $CO_2$-WAG flooding is used to enhance oil recovery in five tight oilfields of North America, including the Kelly-Snyder field, Hanford San Andres field, South Wasson Clearfork field,

Levelland field, and Wasson Denver field (Forrest *et al*., 2011). According to field production results, the ultimate oil recovery of $CO_2$-WAG flooding can be improved by at least 10% of OOIP compared to that of either waterflooding or pure $CO_2$ flooding (Heeremans *et al*., 2006).

The following limitations hinder a further implementation of $CO_2$-WAG flooding for unlocking tight oil resources. Firstly, the nature of both low permeability and low porosity of tight oil formations makes the fluid injectivity of $CO_2$-WAG flooding still low, even though long horizontal wells have been drilled and massively fractured (Christensen *et al*., 2001). Secondly, the injected water leads to expansion of water-sensitive clay and minerals, plugging the flowing throat, resulting in a further decrease of reservoir permeability, and hence a low oil recovery (Merritt and Groce, 1992). Thirdly, the shortage of affordable and sufficient $CO_2$ sources around some oilfields makes $CO_2$-WAG flooding is difficult to be widely applied in those reservoirs (Ghedan, 2009).

### 2.3.3 $CO_2$ huff-n-puff

Both continuous $CO_2$ flooding and $CO_2$-WAG flooding are generally suitable for large-scale reservoir development. The production response is long, while investment is huge (MacAllister, 1989). As for small fault-block reservoirs with low flowability between wells, $CO_2$ huff-n-puff processes are more applicable (Halnes and Monger, 1990). During the $CO_2$ huff-n-puff process, $CO_2$ is usually injected into

reservoir at a certain pressure. Then the injection wells are shut in to make $CO_2$ and crude oil soak for a period of time. When contacting with $CO_2$, oil viscosity is decreased, oil starts to swell, light-components of crude oil are extracted to the $CO_2$ phase, and thus oil phase effective permeability is improved (Monger and Coma, 1988). After soaking for a certain period, the wells are switched on for production.

Although few theoretical investigations have been made about the $CO_2$ huff-n-puff process in tight oil formations, its general advantages and limitations can be summarized as follows (Haskin and Alston, 1989; Asghari and Torabi, 2007):

1) The recovery response of $CO_2$ huff-n- puff process is very fast;

2) Compared to $CO_2$-WAG flooding and continuous $CO_2$ flooding processes, $CO_2$ consumption of the huff-n-puff processes is significantly lower, while recovery efficiency is still higher;

3) The area affected by $CO_2$ huff-n-puff process, however, is so limited that only works around the injection wells even if long horizontal wells have been drilled with massive hydraulic fractures. Small development-scale leads to an unfavorable recovery results, and thus poor economic performance.

$CO_2$ huff-n-puff processes have been put into field practice for developing tight oil reservoirs in North America for decades. In 1976, a regional test of $CO_2$ huff-n-puff project was initially launched to enhance oil recovery in a tight oil field of Hill Upland in Texas, and the oil recovery was enhanced significantly in the pilot

region. However, the $CO_2$ huff-n-puff process only benefits the limited region around wells instead of a larger scale like $CO_2$-WAG flooding or continuous $CO_2$ flooding (Watts *et al*., 1982). Finally, the Hill Upland field failed to extensively apply this technique into the whole field, and the project came to an end in 1977.

## 2.4 Performance Optimization

According to simulation efforts made by Li *et al*. (2010), a modified $CO_2$ flooding scheme is proposed to minimize chance of early gas breakthrough in tight oil formations. At first, $CO_2$ is injected into the reservoir continuously, while production wells are shut in. After a certain period of time, injection wells are shut in and production wells are switched on for production. The production wells and injection wells work in a repeated way until such a recovery process is terminated. In this way, the gas breakthrough is better controlled compared to that of continuous $CO_2$ flooding, while formation damage from water injection is avoided compared to that of $CO_2$-WAG flooding and the controlling region of wells becomes larger compared to that of $CO_2$ huff-n-puff process (Li *et al*., 2010).

In order to better control the production process of continuous $CO_2$ flooding and improve sweep efficiency, a strategy of continuous $CO_2$ injection and cyclic production is also proposed (Li *et al*., 2010). In this strategy, $CO_2$ is injected continuously, while the production wells produce in a cyclic way. At first, both injection wells and production wells are switched on for a period of time until gas

production rate increases to a certain value. Then, production wells are shut in until the static pressure of production wells increases to an expected value. During this period, gas, oil and water will be re-distributed in the reservoir. After production wells are switched on again, oil will flow out from the production wells with a much lower gas-oil ratio, and then oil recovery is significantly enhanced.

## 2.5 Summary

Due to low injectivity and productivity, oil recovery cannot be favourably enhanced by waterflooding in tight oil formations. $CO_2$ flooding has attracted an increasing interest for unlocking the resources in oil reservoirs with low permeability. In addition to pressure maintenance, $CO_2$ flooding contributes to oil recovery in tight formations through viscosity reduction, oil swelling, interfacial tension reduction, permeability improvement, solution gas drive, gravity drainage and components extraction.

Obviously, Recovery performance of continuous $CO_2$ flooding is found to be enhanced compared to waterflooding. By improving sweep efficiency, reducing chance of early gas breakthrough and minimizing $CO_2$ fingering, the oil recovery is further improved with $CO_2$-WAG flooding. As for small fault-block reservoirs with low flowability between wells, $CO_2$ huff-n-puff process achieves better recovery performance compared to either waterflooding or $CO_2$ flooding. Though $CO_2$ injection is found with good EOR performance, most of the $CO_2$ injection projects

are implemented in the reservoirs of good permeability. The performance of improving oil recovery with traditional $CO_2$ injection schemes in tight oil reservoirs has not been well investigated. Optimization of $CO_2$ injection schemes in tight oil formations must result in a different recovery performance compared to high permeability oil reservoirs. Therefore, it is of practical and fundamental importance to evaluate the performance of $CO_2$ injection schemes in tight oil formations, and to propose appropriate methods to enhance oil recovery by $CO_2$ injection.

# CHAPTER 3 EXPERIMENTAL AND NUMERICAL EVALUATION OF $CO_2$ EOR PERFORMANCE

In this chapter, a coreflooding system is designed and applied to evaluate performance of $CO_2$ injection in tight oil formations (Song and Yang, 2012a; b; 2013). Experimentally, a set of nine coreflooding tests have been conducted to evaluate performance of different $CO_2$ injection schemes. Numerically, simulation techniques have been developed to history match the experimental measurements, while sensitivity analysis is conducted with the tuned numerical model in order to maximize the oil recovery from tight formations.

## 3.1 Experimental

### 3.1.1 Materials

The oil sample and reservoir brine used in this study are collected from a tight oil formation in Saskatchewan, Canada. As shown in **Table 3.1**, the density and viscosity of dead oil are measured to be 801.2 kg/m$^3$ and 2.17 cP at 20ºC and atmospheric pressure, respectively.

Compositional analysis results of the crude oil sample are tabulated in **Table 3.2.** Most components of the oil sample are lighter than $C_{20}$, while heavy components of $C_{30+}$ account for only 11.08 wt%. The minimum miscibility pressure (MMP) of the dead oil sample is experimentally determined to be 9.7 MPa at 63ºC by the

**Table 3.1** Physical properties of crude oil

| | | |
|---|---|---|
| Density ($kg/m^3$) | at 15ºC | 805.0 |
| | at 20ºC | 801.2 |
| | at 30ºC | 793.1 |
| Viscosity(mPa·s) | at 15ºC | 2.54 |
| | at 20ºC | 2.17 |
| | at 30ºC | 2.22 |
| Acid number (mg-KOH/g) | | 0.40 |
| Molecular weight (g/mol) | | 162 |

(Saskatchewan Research Council, 2012).

**Table 3.2** Compositional analysis results of crude oil

| Component | wt% | mol% | Component | wt% | mol% |
|---|---|---|---|---|---|
| $C_1$ | 0.00 | 0.00 | $C_{14}$ | 4.07 | 3.55 |
| $C_2$ | 0.00 | 0.00 | $C_{15}$ | 4.14 | 3.37 |
| $C_3$ | 0.13 | 0.53 | $C_{16}$ | 3.48 | 2.66 |
| i-$C_4$ | 0.14 | 0.41 | $C_{17}$ | 3.23 | 2.33 |
| n-$C_4$ | 0.56 | 1.67 | $C_{18}$ | 3.15 | 2.14 |
| i-$C_5$ | 0.34 | 0.80 | $C_{19}$ | 2.68 | 1.72 |
| n-$C_5$ | 0.56 | 1.35 | $C_{20}$ | 2.36 | 1.45 |
| Other $C_5$ | 0.05 | 0.13 | $C_{21}$ | 0.05 | 0.03 |
| i-$C_6$ | 0.43 | 0.87 | $C_{22}$ | 4.03 | 2.25 |
| n-$C_6$ | 0.42 | 0.84 | $C_{23}$ | 1.97 | 1.05 |
| Other $C_6$ | 0.47 | 0.94 | $C_{24}$ | 1.62 | 0.83 |
| $C_7$ | 10.74 | 18.55 | $C_{25}$ | 1.57 | 0.77 |
| $C_8$ | 10.16 | 15.39 | $C_{26}$ | 1.43 | 0.67 |
| $C_9$ | 5.79 | 7.82 | $C_{27}$ | 1.30 | 0.59 |
| $C_{10}$ | 6.06 | 7.37 | $C_{28}$ | 1.23 | 0.54 |
| $C_{11}$ | 5.34 | 5.92 | $C_{29}$ | 0.94 | 0.40 |
| $C_{12}$ | 4.75 | 4.82 | $C_{30}$ | 0.94 | 0.38 |
| $C_{13}$ | 4.78 | 4.49 | $C_{31+}$ | 11.08 | 3.37 |

(Saskatchewan Research Council, 2012).

Saskatchewan Research Council.

The density and viscosity of reservoir brine at 20ºC and atmospheric pressure are measured to be 1108.7 kg/$m^3$ and 1.24 cP, respectively. The measured compositions of reservoir brine are shown in **Table 3.3**. The synthetic water is prepared with 5.3 g/l of $CaCl_2$, 1.8 g/l of $MgCl_2$, 140.2 g/l of NaCl, 3.3 g/l of $K_2SO_4$, and 3.3 g/l of $Na_2SO_4$, respectively

The tight core samples with a diameter of 1.5 inches are collected from the same region where oil and brine samples are collected, while their permeabilities range from 0.08 mD to 0.83 mD. The research grade $CO_2$ used in the experiments is purchased from Praxair, Canada, with a purity of 99.998 mol%.

### 3.1.2 Experimental setup

The experimental setup used in this study consists of four subsystems, i.e., injection subsystem, displacement subsystem, production subsystem, and temperature control subsystem (see **Figure 3.1**). In the fluid injection subsystem, synthetic water, oil and $CO_2$ are stored in transfer cylinders, which are injected into the core samples at a constant rate with a high pressure syringe pump (500 HP, ISCO Inc., USA), respectively.

The major component of this setup is the displacement subsystem, which is comprised of a coreholder (Core Lab, USA) with maximum operating pressure of 5500 psi, and a high pressure nitrogen cylinder (Praxair, Canada) used to provide overburden pressure to the coreholder. The core samples are placed in the coreholder

**Table 3.3** Properties of reservoir brine

| Property | | Value | Major components (mg/l) | Value |
|---|---|---|---|---|
| Density (kg/m$^3$) | at 15ºC | 1110.2 | Chloride | 94340 |
| | at 20ºC | 1108.7 | Sulphate | 4100 |
| | at 40ºC | 1099.6 | Sodium | 56200 |
| Viscosity (mPa·s) | at 15ºC | 1.41 | Potassium | 1500 |
| | at 20ºC | 1.24 | Magnesium | 460 |
| | at 40ºC | 0.85 | Calcium | 1900 |
| Refractive index | at 25ºC | 1.3590 | Iron | 1.0 |
| Conductivity (mS) | at 25ºC | 125.4 | Barium | 0.25 |
| pH | at 25ºC | 6.87 | Manganese | 0.61 |

(Saskatchewan Research Council, 2012).

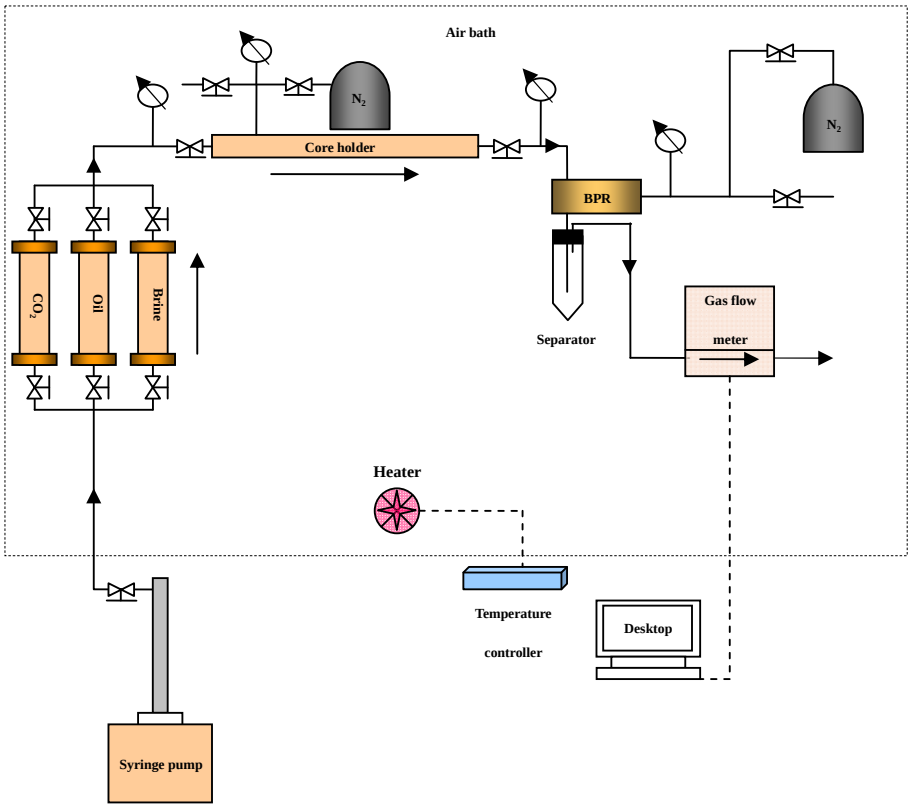


**Figure 3.1** Schematic diagram of the experimental setup

with a horizontal direction. The overburden pressure applied to the coreholder is usually maintained 3.0 MPa higher than the injection pressure under experimental condition.

In the production subsystem, a backpressure regulator (BPR) (EBIHP1, Equilibar, USA) is used to maintain the pre-specified production pressure throughout the experiments. The produced water and oil are collected by using an oil sample collector, which is actually a graduated tube with an accuracy of 0.05 ml. The gas production is measured by using a gas flow meter (DFM26S, Aalborg, USA) with an accuracy of 1 cc/min. The production data is recorded by a desktop computer.

The temperature control system is comprised of an airbath, a heater (HG1100, Makita, Canada), a temperature sensor, and a temperature controller (Diqi-Sense, USA). It is used to maintain a constant temperature environment of 63ºC throughout the experiments. A digital image of the whole experimental setup in this study is shown in **Figure 3.2**.

### 3.1.3 Experimental scenarios

The nine experimental scenarios include waterflooding (Scenario #1), continuous near-miscible $CO_2$ flooding (Scenario #2), continuous miscible $CO_2$ flooding (Scenario #3), miscible $CO_2$-WAG flooding with WAG ratio of 1.0 and slug sizes of 0.250 PV for both water and $CO_2$ (Scenario #4), miscible $CO_2$-WAG flooding with WAG ratio of 0.5 and slug sizes of 0.125 PV and 0.250 PV for water

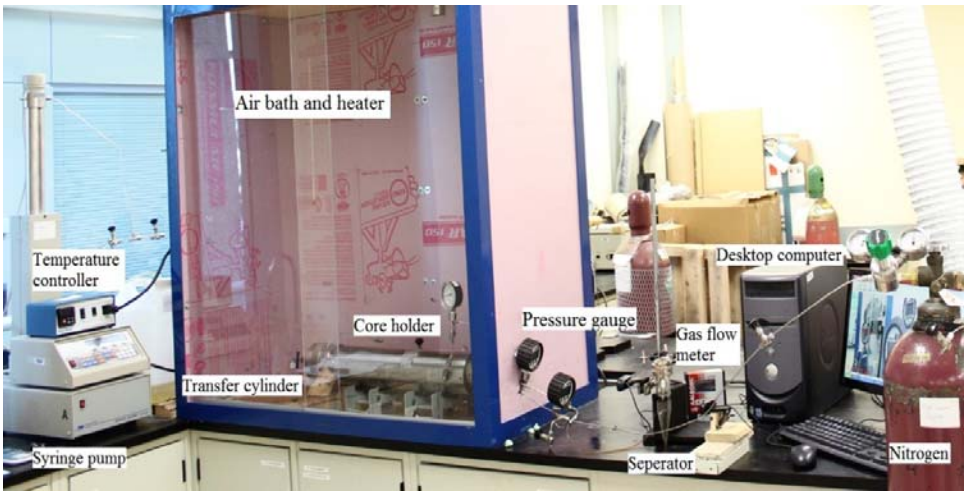


**Figure 3.2** A digital image of the experimental setup

and $CO_2$ (Scenario #5), miscible $CO_2$-WAG flooding with WAG ratio of 0.5 and slug sizes of 0.250 PV and 0.500 PV for water and $CO_2$ (Scenario #6), immiscible $CO_2$ huff-n-puff (Scenario #7), near-miscible $CO_2$ huff-n-puff (Scenario #8), and miscible $CO_2$ huff-n-puff (Scenario #9).

### 3.1.4 Experimental procedures

#### 1) Porosity measurement

Prior to each coreflooding experiment, dead volume is firstly determined (i.e., Scenario #1: 4.6 cc, Scenario #2: 4.6 cc, Scenario #3: 4.7 cc, Scenario #4: 4.5 cc, Scenario #5: 4.4 cc, Scenario #6: 4.7 cc, Scenario #7: 4.4 cc, Scenario #8: 4.3 cc, and Scenario #9: 4.3 cc). The porosity of core samples is subsequently measured. The procedure for porosity measurements is briefly described as follows. Core samples are first completely evacuated for 24 h by using a vacuum pump. Then the synthetic brine is injected into the rock samples. Consequently, porosity can be determined as the ratio of the brine volume inside core samples to the bulk volume of the core samples with consideration of the measured dead volume. The measured porosity in the nine sets of coreflooding experiments are shown in **Table 3.4**, where the porosity ranges from 17.7% to 23.6%.

#### 2) Permeability measurement

Absolute permeability of the core samples can be determined after the porosity tests. The procedure for permeability measurement is detailed as follows. Synthetic brine is injected into the core samples at different flow rates ranging from 0.100 to

**Table 3.4** The measured porosity, permeability, and initial oil saturation of Scenarios #1-9

| Scenario | Porosity (%) | Permeability (mD) | Initial oil saturation (%) |
|---|---|---|---|
| #1 | 23.1 | 0.27 | 55.2 |
| #2 | 20.6 | 0.79 | 44.1 |
| #3 | 17.7 | 0.08 | 43.8 |
| #4 | 18.9 | 0.29 | 57.9 |
| #5 | 22.3 | 0.23 | 59.1 |
| #6 | 23.6 | 0.44 | 51.4 |
| #7 | 18.6 | 0.56 | 42.9 |
| #8 | 23.1 | 0.81 | 64.2 |
| #9 | 20.7 | 0.83 | 59.6 |

0.500 cc/min by using a syringe pump. The resulted pressure drop under each flow rate is correspondingly measured when stabilized, then the absolute permeability of the core samples can be calculated by applying the Darcy's law. The absolute permeability of the nine scenarios is listed in **Table 3.4**.

**3) Initial oil saturation measurement**

Once the absolute permeability is determined, the core sample is subsequently flooded with light oil at a constant rate of 0.050 cc/min until irreducible water saturation has been reached. Initial oil saturation is calculated by knowing both volume of the oil injected and pore volume of the core sample. As shown in **Table 3.4**, the initial oil saturation of nine scenarios in this study ranges from 43.8% to 64.2%.

**4) Displacement experiments**

In Scenarios #1-6, either water or $CO_2$ is injected at a constant rate of 0.100 cc/min. During each displacement process, the cumulative oil production and pressure drop are measured. The production pressure in Scenario #1 is set to be 10.5 MPa. The production pressure in Scenario #2 is set to be 8.7 MPa, which is 1.0 MPa lower than the measured MMP in order to satisfy the so-called near-miscible condition (Fatemi and Sohrabi, 2013). As for Scenarios #3-6, the production pressure is set to be 14.0 MPa to ensure that the experiments are conducted under miscible conditions. It should be noted that, in Scenarios #2-6, once the $CO_2$ displacement is terminated, the BPR pressure is decreased in a stepwise manner to

initiate the blowdown recovery. As for each pressure level, oil production is recorded until the system pressure is reduced to the atmospheric pressure.

In Scenarios #7-9, $CO_2$ is injected into the coreholder for 3 h under constant pressure of 7.0, 9.3 and 14.0 MPa, respectively, in order to achieve immiscible, near-miscible, and miscible conditions. Subsequently, oil and $CO_2$ are soaked for another 6 h. Finally, oil is produced at the pre-specified pressure for 1 h. The $CO_2$ injection, soaking and production processes are repeated throughout the experiments. When oil production of certain cycle is less than 1% of OOIP, the experiment will be terminated (Asghari and Torabi, 2007).

## 3.2 Numerical Simulation

In order to obtain a better understanding on the mechanisms governing waterflooding and $CO_2$ EOR in tight oil formations, simulation techniques have been developed to history match the experimental measurements made in Scenarios #1-9, while sensitivity analysis is subsequently conducted to examine effects of the operational parameters on oil recovery.

### 3.2.1 Numerical model

#### 1) Fluid properties

According to the measured oil physical properties, compositional analysis, and MMP, the CMG WinProp module is used to build a PVT model to prepare fluid

properties, where the crude oil is treated as eight pseudo-components (See **Table 3.5**). Finally, a PVT model compatible with GEM compositional simulator is generated and incorporated into the displacement model.

**2) Gridblock**

By using the GEM simulator (Version 2009, Computer Modelling Group Ltd.), a grid system of 10×1×1 gridblock is applied throughout the simulations, though the size of each grid varies for Scenarios #1-9 (i.e., Scenario #1: 0.66×3.37×3.37 cm, Scenario #2: 0.64×3.38×3.38 cm, Scenario #3: 0.63×3.38×3.38 cm, Scenario #4: 0.62×3.38×3.38 cm, Scenario #5: 0.62×3.37×3.37 cm, Scenario #6: 0.64×3.38×3.38 cm, Scenario #7: 0.61×3.37×3.37 cm, Scenario #8: 0.64×3.37×3.37 cm, and Scenario #9: 0.63×3.38×3.38 cm). Meanwhile, homogeneous distribution of oil saturation, water saturation, porosity and absolute permeability are assigned to each model. A displacement model for Scenario #1 is shown in **Figure 3.3**.

### 3.2.2 Simulation procedure

Simulation techniques have been conducted to history match the experimental measurements made in Scenarios #1-9. The initial water saturation, initial oil saturation, absolute permeability, porosity and initial system pressure are set to be same as the values measured for each experimental scenario. The relative permeability and capillary pressure in the numerical model are respectively tuned to match the cumulative oil production and injection pressure profiles.

Once the experimental measurements are well matched, the tuned numerical

**Table 3.5** Summary of the properties of the eight pseudo-components

| | $C_3$-$C_6$ | $C_7$-$C_8$ | $C_9$-$C_{11}$ | $C_{12}$-$C_{15}$ | $C_{16}$-$C_{20}$ | $C_{21}$-$C_{24}$ | $C_{25}$-$C_{29}$ | $C_{30+}$ |
|---|---|---|---|---|---|---|---|---|
| Molar concentration | 0.08 | 0.42 | 0.18 | 0.08 | 0.08 | 0.05 | 0.07 | 0.04 |
| Critical pressure (atm) | 34.64 | 29.49 | 23.45 | 19.93 | 17.35 | 15.09 | 12.32 | 10.35 |
| Critical temperature (K) | 463.92 | 564.25 | 640.77 | 690.61 | 732.47 | 770.31 | 823.81 | 990.84 |
| Acentric factor | 0.23 | 0.34 | 0.48 | 0.58 | 0.68 | 0.78 | 0.94 | 1.16 |
| Molecular weight | 71.18 | 104.74 | 145.43 | 181.62 | 219.73 | 261.61 | 325.09 | 449.00 |
| Volume shift parameter | -0.01 | -0.01 | 0.05 | 0.08 | 0.10 | 0.12 | 0.18 | 0.12 |

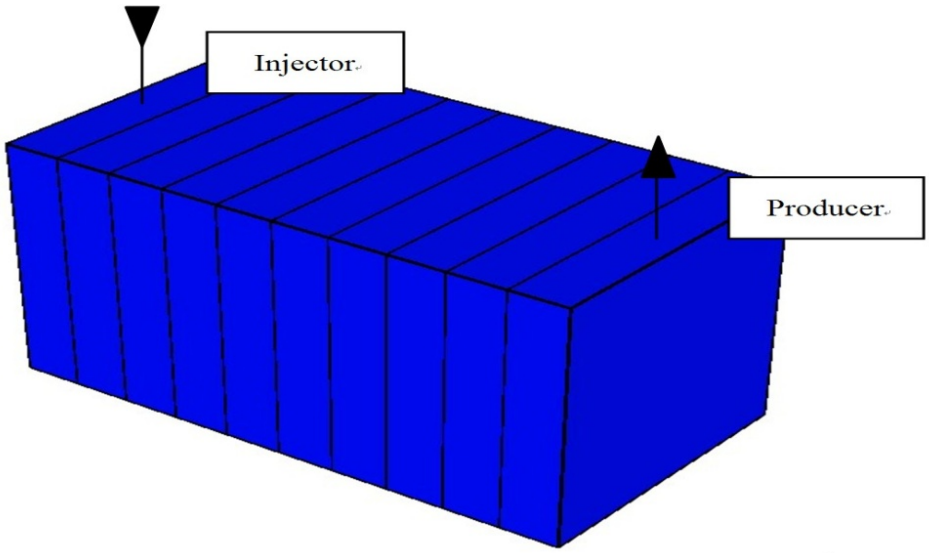


**Figure 3.3** Schematic diagram of 3D view of the displacement model.

models are further implemented to conduct sensitivity analysis on the production pressure for Scenarios #2 and #3; WAG ratio, cycle time, and slug size for Scenarios #4-6 as well as injection pressure, soaking time, and production pressure for Scenarios #7-9. Hence, effects of operational parameters on various $CO_2$ injection schemes are quantified, while oil recovery is further improved.

## 3.3 Results and Discussion

### 3.3.1 Experimental measurements

#### 1) Waterflooding

Scenario #1 evaluates performance of waterflooding in tight oil formation. As for Scenario #1, **Figure 3.4** shows the measured oil recovery, cumulative water production, and pressure drop, respectively. As can be seen from **Figure 3.4**, at the beginning, oil is recovered continuously, while no water is produced for the first 0.36 pore volume (PV) of water injected. After water breakthrough occurs, oil production rate starts to decline, while the cumulative water production starts to rise rapidly. Little incremental oil is produced after water breaks through, resulting in a low ultimate recovery of 51.5% of OOIP in this study. The low ultimate oil recovery is mainly attributed to the low permeability of the core samples used. The response of pressure drop is found to agree well with the oil recovery and cumulative water production profiles. The measured pressure drop increases with the PV of water injected until water breakthrough occurs around 0.360 PV of water injected.

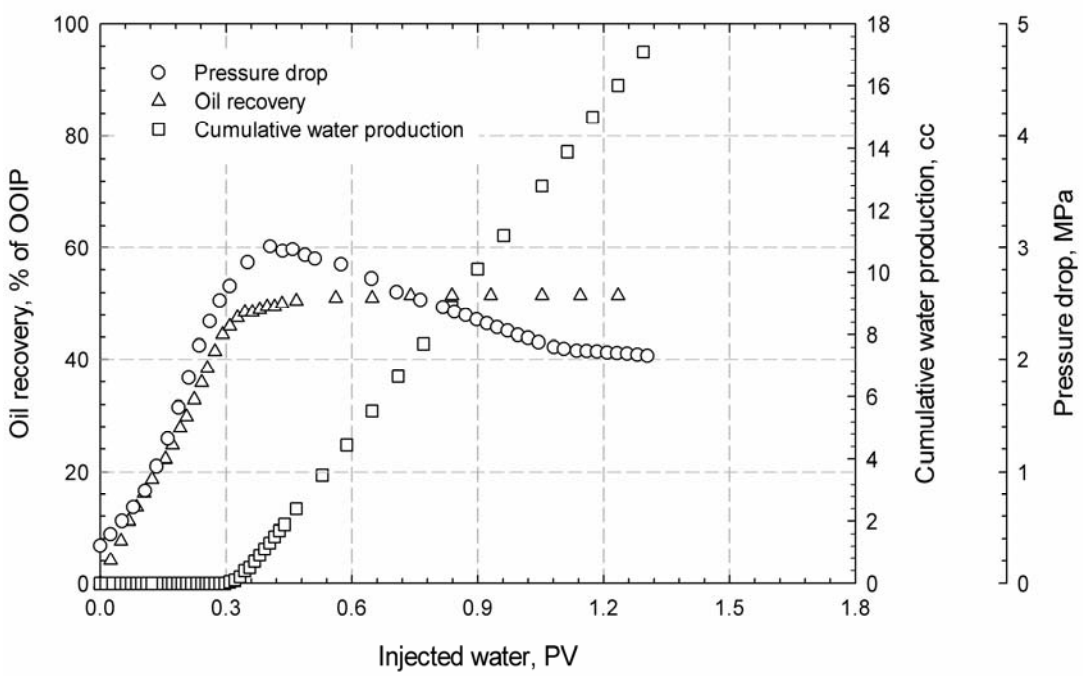


**Figure 3.4** Measured oil recovery, cumulative water production, and pressure drop versus pore volume of water injected for Scenario #1

**2) Continuous $CO_2$ flooding**

***Near-miscible $CO_2$ flooding***: Continuous near-miscible $CO_2$ flooding is implemented in Scenario #2, where the production pressure is maintained at 8.7 MPa. As for this scenario, **Figure 3.5** shows the measured oil recovery, cumulative gas production, and pressure drop, respectively. Oil production rate remains high at the beginning and then starts to decrease when $CO_2$ breakthrough occurs. A large amount of oil is already produced before $CO_2$ breakthrough, after which an additional 15.0% of OOIP is still recovered. As depicted in **Figure 3.5**, the pressure drop peaks at 0.380 PV of $CO_2$ injected. This agrees with the oil recovery profile. Excluding the blowdown recovery, 80.3% of OOIP is produced. Compared to the waterflooding process, a much higher oil recovery is achieved with the continuous near-miscible $CO_2$ flooding.

After near-miscible $CO_2$ flooding is completed, the blowdown recovery contributes to an incremental 7.5% of OOIP. It is found that a large amount of oil is produced when the production pressure is reduced from 1.5 MPa to atmospheric pressure, while little oil is produced when the production pressure is reduced from 8.7 MPa to 1.5 MPa. This is consistent with the findings in the literature (Zheng and Yang, 2013). The ultimate recovery factor by implementing continuous near-miscible $CO_2$ flooding is measured to be 87.8% of OOIP, demonstrating an obvious superiority of $CO_2$ flooding over waterflooding.

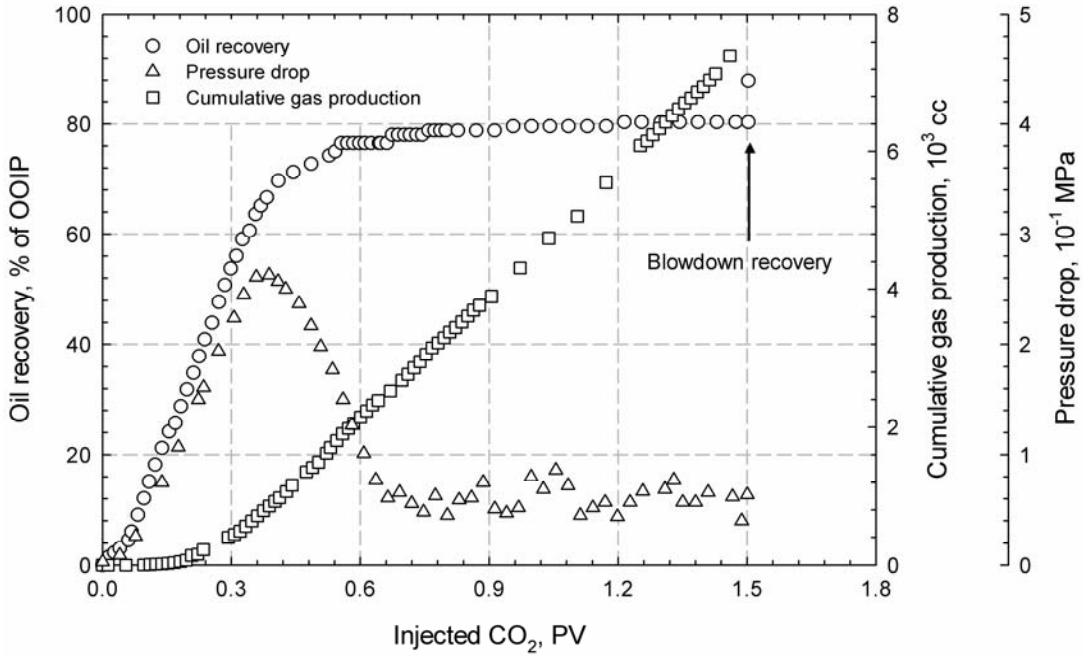


**Figure 3.5** Measured oil recovery, cumulative gas production, and pressure drop versus pore volume of $CO_2$ injected for Scenario #2

***Miscible $CO_2$ flooding***: As mentioned previously, MMP of this dead oil sample is experimentally determined to be 9.7 MPa by the Saskatchewan Research Council (SRC). A constant production pressure of 14.0 MPa is applied in order to ensure that the entire $CO_2$ flooding process is conducted under miscible conditions in Scenario #3. As for this scenario, **Figure 3.6** shows the measured oil recovery, cumulative gas production, and pressure drop, respectively. Excluding the blowdown recovery, 79.3% of OOIP has been recovered with the miscible $CO_2$ flooding process. This recovery factor is lower than that obtained in the near-miscible $CO_2$ flooding process (i.e., Scenario #2). Such a lower recovery factor is mainly caused by the following combinational effects: a) The absolute permeability of core sample used in Scenario #3 is 0.08 mD, which is one order lower than that in Scenario #2, i.e., 0.79 mD; and b) The recovery efficiency of light-to-medium oils with miscible $CO_2$ flooding is fairly close to that with near-miscible $CO_2$ flooding.

Blowdown recovery is conducted right after the continuous $CO_2$ flooding process. The production pressure is decreased to atmospheric pressure with 12 steps. Additional 15.2% of OOIP is recovered in the blowdown process, which is higher than that obtained under near-miscible conditions (i.e., Scenario #2). This might be due to the fact that the injection pressure for Scenario #3 is 4.0-6.0 MPa higher than that for Scenario #2, resulting in more $CO_2$ dissolved into crude oil, and hence a higher blowdown recovery. The ultimate recovery obtained in the miscible $CO_2$ flooding process (i.e., Scenario #3) is determined to be 94.6% of OOIP.

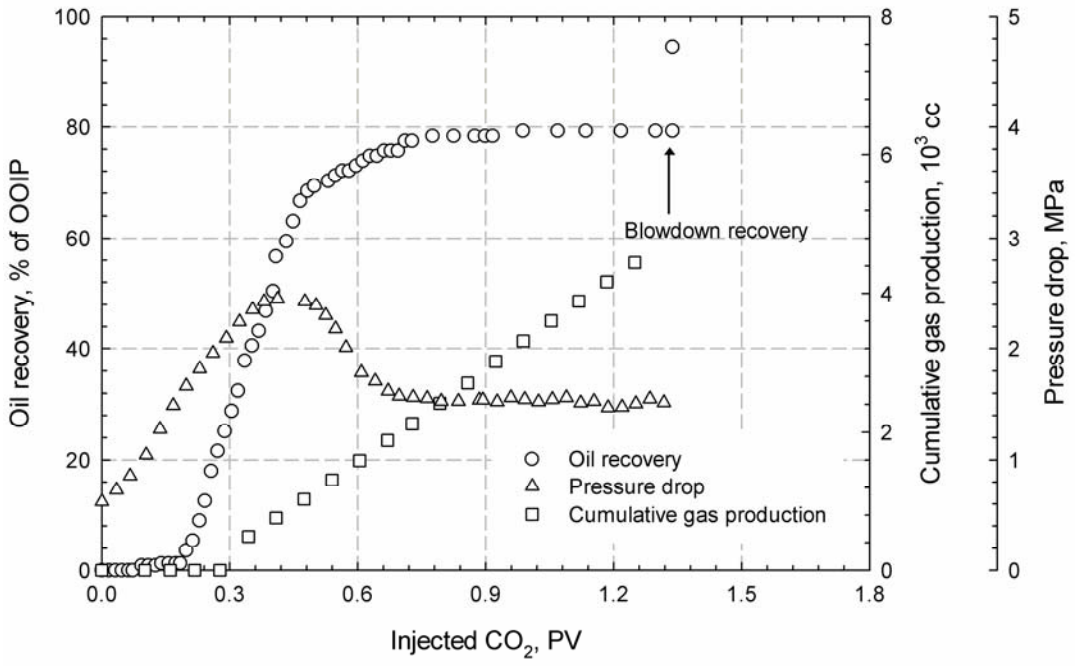


**Figure 3.6** Measured oil recovery, cumulative gas production, and pressure drop versus pore volume of $CO_2$ injected for Scenario #3

**3) $CO_2$-WAG flooding**

***WAG ratio=1.0, water slug size= 0.250 PV, $CO_2$ slug size=0.250 PV***: In order to improve both the macroscopic and microscopic sweeping efficiency of $CO_2$ displacement, the $CO_2$-WAG flooding process is investigated in Scenario #4. The slug sizes of water and $CO_2$ in each cycle are set to be 0.250 PV, while the production pressure is set as the same value used in the miscible continuous $CO_2$ flooding of Scenario #3.

As for Scenario #4, **Figure 3.7** shows the measured oil recovery, cumulative water production, cumulative gas production, and pressure drop, respectively. The oil recovery profile indicates that majority of oil is recovered from the first two cycles. The incremental oil recovery in the third cycle is significantly lower compared to the preceding cycles. The peak of pressure drops in later cycles tends to be higher than that of earlier cycles. Similar phenomenon is also documented in the literature (Prieditis *et al.*, 1991). It can be also observed in **Figure 3.7** that the pressure drop in each cycle usually increases rapidly as water injected, while it decreases significantly as $CO_2$ is injected. This implies that the fluid injectivity of the tight cores can be significantly improved in the $CO_2$ injection period (Ramsay and Small, 1964). The improvement of injectivity due to $CO_2$ injection underlines an important motivation to take advantage of $CO_2$ flooding for unlocking resources in tight oil formations. Prior to blowdown recovery, the recovery factor of miscible $CO_2$-WAG flooding is able to reach 88.8% of OOIP, indicating a superior efficiency compared to either continuous miscible or continuous near-miscible $CO_2$ flooding.

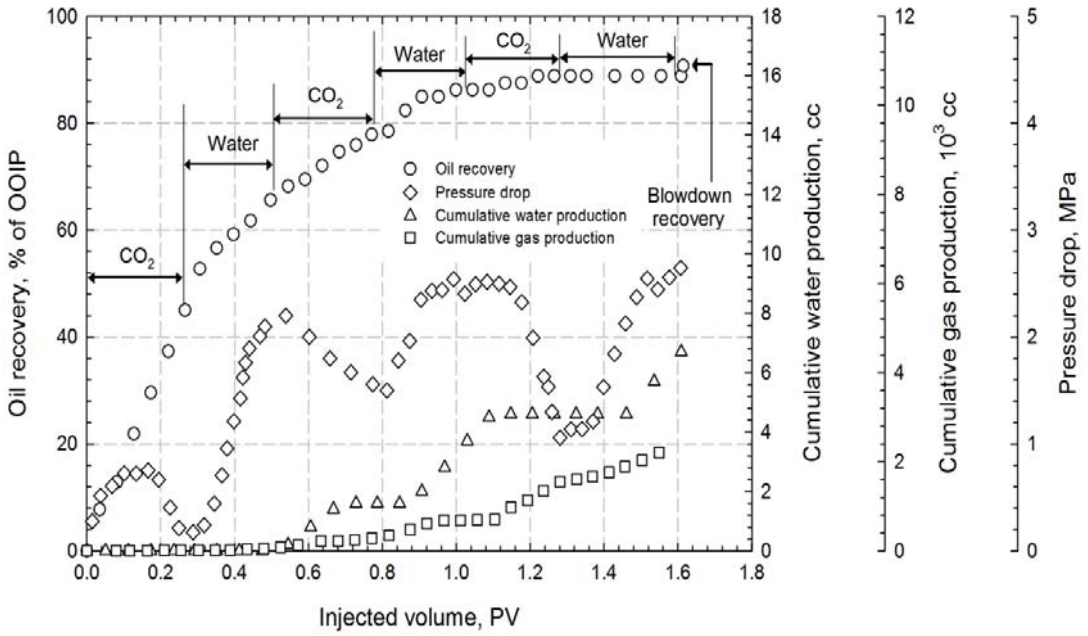


**Figure 3.7** Measured oil recovery, cumulative water production, cumulative gas production, and pressure drop versus pore volume of $CO_2$ or water injected for Scenario #4

Once miscible $CO_2$-WAG flooding is completed, a 12-step blowdown recovery is initiated. The blowdown process leads to an incremental oil recovery of 2.0%, which is much lower than that of both near-miscible $CO_2$ flooding and miscible $CO_2$ flooding. This is attributed to the fact that much less $CO_2$ (i.e., only 0.750 PV) is injected in the $CO_2$-WAG process, compared to 1.500 PV and 1.350 PV of $CO_2$ that are injected in near-miscible $CO_2$ flooding process and miscible $CO_2$ flooding process, respectively. An ultimate recovery factor of 90.7% of OOIP is achieved with this miscible $CO_2$-WAG flooding process.

***WAG ratio=0.5, water slug size=0.125 PV, $CO_2$ slug size=0.250 PV***: In order to examine the effect of different slug size on recovery performance, another set of miscible $CO_2$-WAG flooding (i.e., Scenario #5) is conducted. The $CO_2$ slug size is 0.250 PV, which is the same as that in Scenario #4, while the water slug size is set to be 0.125 PV, leading to a WAG ratio of 0.5. Four cycles are carried out during the displacement process. Both production pressure and fluid injection rate is the same as that in Scenario #4.

**Figure 3.8** shows the measured pressure drop, cumulative oil production, cumulative water production, and cumulative gas production in the experiment. It can be seen from the recovery profile that most oil is produced in the first two cycles, and the oil productivity is low in the last two cycles. It is also observed from the pressure drop profile that pressure drop tends to increase as water injected, while the subsequent $CO_2$ injection leads to a decrease of pressure drop. This further confirms the findings from Scenario #4 that $CO_2$ injection tends to improve the fluid

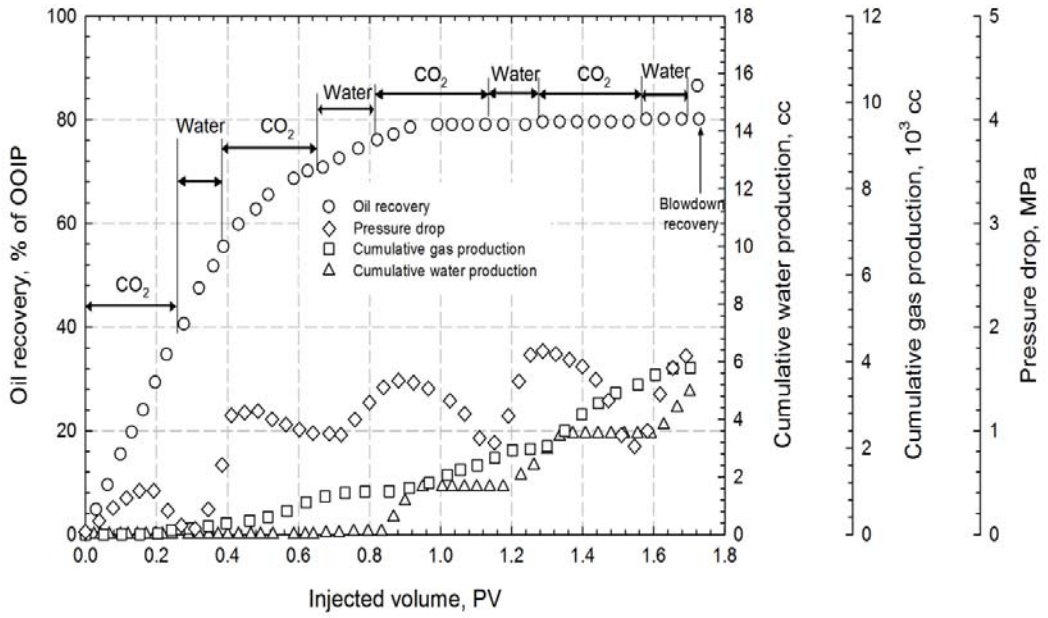


**Figure 3.8** Measured oil recovery, cumulative water production, cumulative gas production, and pressure drop versus pore volume of $CO_2$ or water injected for Scenario #5

injectivity in the $CO_2$-WAG process. Prior to the blowdown process, the recovery factor in Scenario #5 is able to reach 80.2%, which is lower than that in Scenario #4. This may be attributed to the fact that a shorter water slug size in Scenario #5 results in a decrease of sweep efficiency, thus a lower oil recovery.

After the displacement process, a stepwise blowdown recovery is conducted. 6.5% of OOIP is recovered in the blowdown process, which is higher than that in Scenario #4. This is because more $CO_2$ is injected into core sample in Scenario #5, resulting in more $CO_2$ dissolved into crude oil. Thus, the blowdown recovery is higher. An ultimate recovery factor of 86.5% of OOIP is achieved in Scenario #5.

***WAG ratio=0.5, water slug size=0.250 PV, $CO_2$ slug size=0.500 PV***: In order to examine the effect of cycle time on oil recovery and fluid injectivity performance, another set of miscible $CO_2$-WAG flooding is conducted in Scenario #6. The $CO_2$ slug size is increased to 0.500 PV, and water slug size is long to 0.250 PV, leading to a WAG ratio of 0.5, which is the same as that in Scenario #5.

Similar to Scenario #5, introduction of water into displacement process leads to an increase of pressure drop, while $CO_2$ tends to increase the fluid injectivity with a decrease in pressure drop. Compared with Scenario #5, pressure drop is further decreased by applying a longer $CO_2$ slug size (see **Figure 3.9**). However, different from previous scenarios, the introduction of $CO_2$ does not result in a decrease of pressure drop all the way, which presents to be constant at later period of $CO_2$ injection process in each cycle. It is found that fluid injectivity usually improves

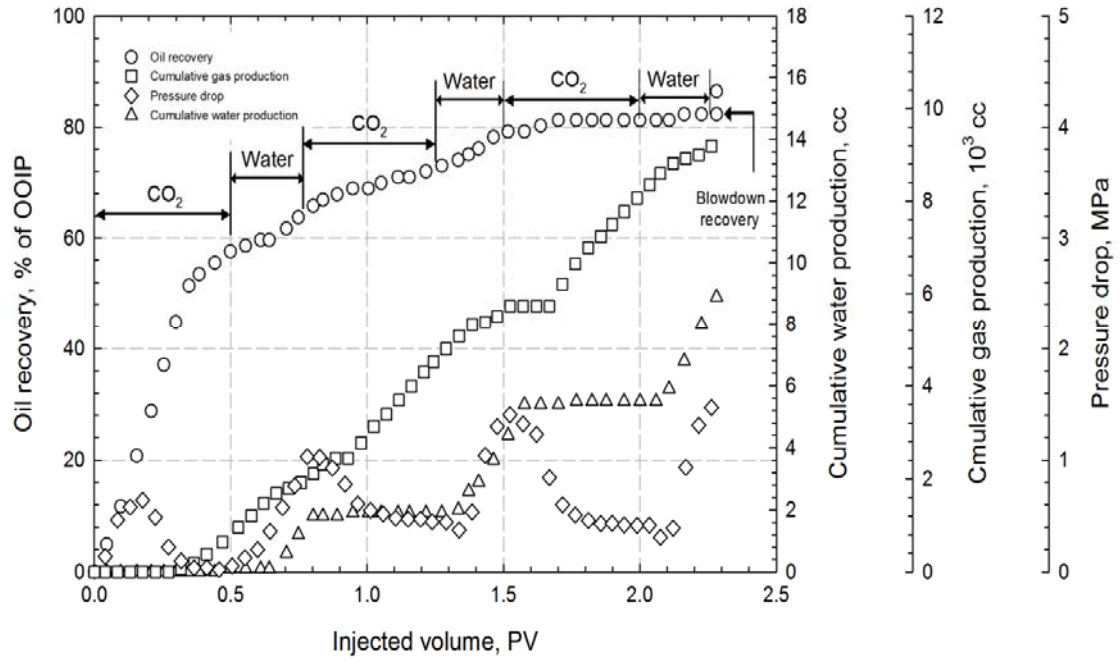


**Figure 3.9** Measured oil recovery, cumulative water production, cumulative gas production, and pressure drop versus pore volume of $CO_2$ or water injected for Scenario #6

with the increase of $CO_2$ slug size at first. Meanwhile, it tends to become constant by further increasing the $CO_2$ slug size. During the displacement process, oil recovery is estimated to be 82.3% of OOIP. It is higher than that of Scenario #5 due to the longer flooding period and higher permeability, but lower than Scenario #4, which may be attributed to the smaller WAG ratio and longer cycle time (Song and Yang, 2012b). Though the flooding time in Scenario #6 lasts up to 380 min of 2.200 PV, there is no significant improvement of oil recovery compared to that of Scenario #5. Thus, the longer cycle time in $CO_2$-WAG process is found to decrease the recovery efficiency.

Similarly, the blowdown process leads to an additional 4.1% of OOIP, which is lower than that in Scenario #5. This may be due to the lower injection pressure in Scenario #6, resulting in less $CO_2$ dissolved into crude oil, and thus a lower blowdown recovery compared to Scenario #5. However, the blowdown recovery in Scenario #6 is higher than that of Scenario #4. This may be attributed to fact that 1.500 PV of $CO_2$ is injected during the displacement process in Scenario #6 compared to only 0.750 PV of $CO_2$ injected in Scenario #4, leading to more $CO_2$ dissolved into crude oil, and thus a higher blowdown recovery.

**4) $CO_2$ huff-n-puff**

***Immiscible $CO_2$ huff-n-puff***: Performance of immiscible $CO_2$ huff-n-puff process is evaluated in Scenario #7, where $CO_2$ is injected into the coreholder for 3 h with a constant pressure of 7.0 MPa. Once the $CO_2$ injection is terminated, crude oil and $CO_2$ are soaked for another 6 h under a constant temperature. Subsequently, oil starts to produce for 1 h. A total of six cycles are repeated in this scenario.

**Figure 3.10** shows the measured oil recovery, cumulative gas production, and pressure drop as a function of time, respectively. The recovery profile indicates that most oil is produced during the first two cycles, followed by a much lower recovery after the third cycle. During the soaking process, the system pressure tends to decrease, though its decrease in the first cycle is minor compared to others. This may be ascribed to the fact that the pores in the cores are filled with oil and water initially, resulting in little $CO_2$ injected into core sample during first cycle.

As for the second cycle, pressure decrease during the soaking period is significantly improved due to more $CO_2$ injected into the core sample and dissolved into crude oil. From the third cycle to the sixth cycle, the pressure decrease during the soaking process becomes less significant again. This is because residual oil saturation in the core sample is much lower than that of the previous cycles. The ultimate recovery factor of immiscible $CO_2$ huff-n-puff process is only 42.8% of OOIP, indicating a significantly worse recovery performance compared to the previous $CO_2$ flooding schemes. This is attributed to the combinational effects: a) $CO_2$ and oil are immiscible; and b) $CO_2$ huff-n-puff is only able to affect a limited region around the wells.

***Near-miscible $CO_2$ huff-n-puff***: In order to examine effect of injection pressures on recovery performance, near-miscible $CO_2$ huff-n-puff injection is conducted in Scenario #8, where the injection strategy is same as that of Scenario #7. A total of four cycles are conducted in Scenario #8, while the injection pressure

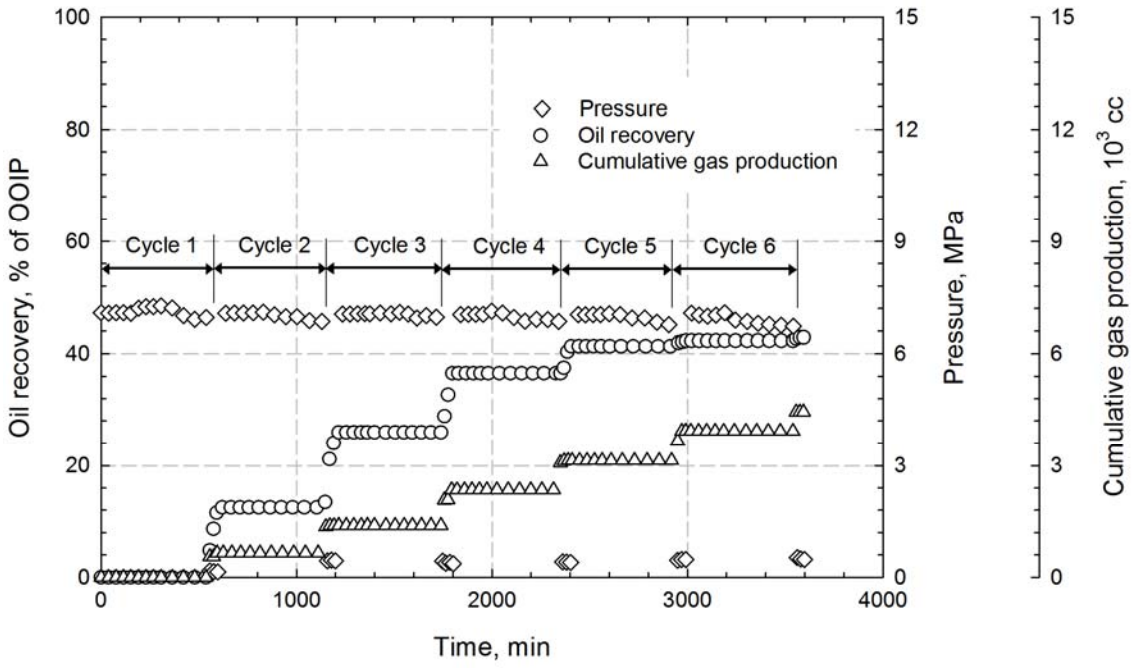


**Figure 3.10** Measured oil recovery, cumulative gas production, and pressure drop versus time for Scenario #7

increases to 9.3 MPa in order to maintain the near-miscible condition throughout the experiment.

The oil recovery, cumulative gas production, and pressure drop as a function of time are shown in **Figure 3.11**, where most oil is produced in the first two cycles. The oil production starts to decrease from the third cycle, while the pressure decrease in the second cycle is more obvious compared to the other cycles. This finding is same as that in Scenario #7. The ultimate oil recovery is 63.0% of OOIP in Scenario #8. This may be due to the higher injecting pressure, leading to more $CO_2$ dissolved into crude oil, and thus a higher ultimate oil recovery.

***Miscible $CO_2$ huff-n-puff***: Recovery performance of miscible $CO_2$ huff-n-puff injection is evaluated in Scenario #9 with a constant injection pressure of 14.0 MPa. The injection strategy is same as that of Scenario #8.

As observed in **Figure 3.12**, the pressure drop maintains a similar trend as Scenarios #7 and #8, while the ultimate recovery factor is measured to be 61.0% of OOIP. Compared to Scenario #8, the slightly lower recovery factor indicates that the miscible $CO_2$ huff-n-puff does not lead to a higher recovery, though the injection pressure is higher than the MMP of 9.7 MPa. This implies that recovery performance of $CO_2$ huff-n-puff process under near-miscible condition is fairly close to that of miscible condition and that it is unnecessary to overemphasize the pressure effect.

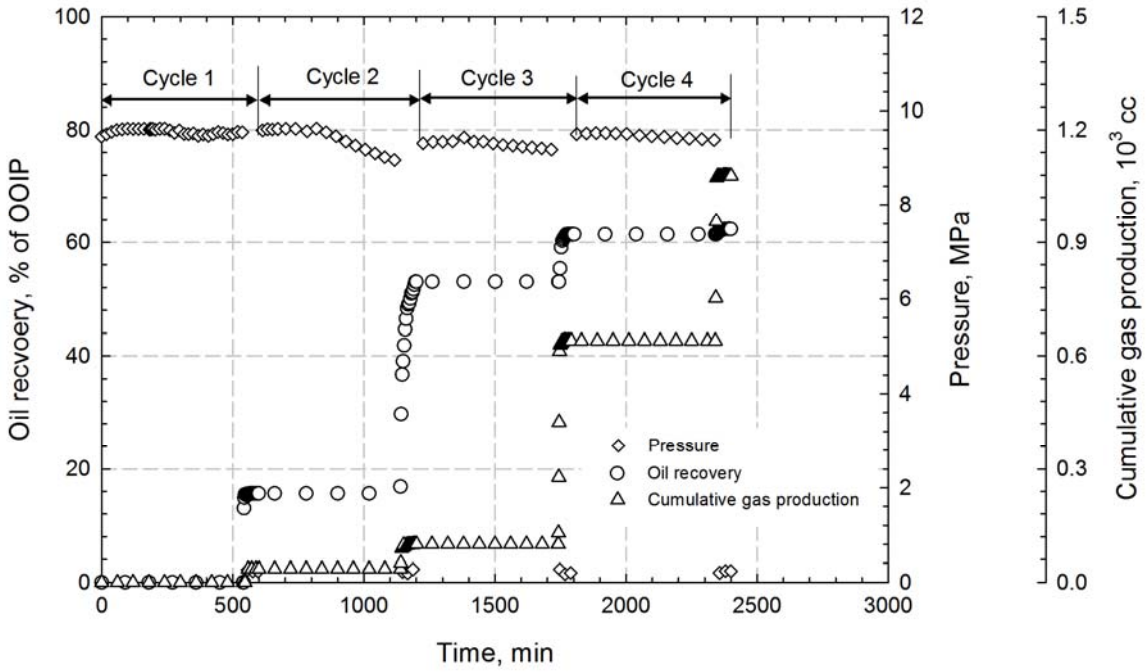


**Figure 3.11** Measured oil recovery, cumulative gas production, and pressure drop versus time for Scenario #8

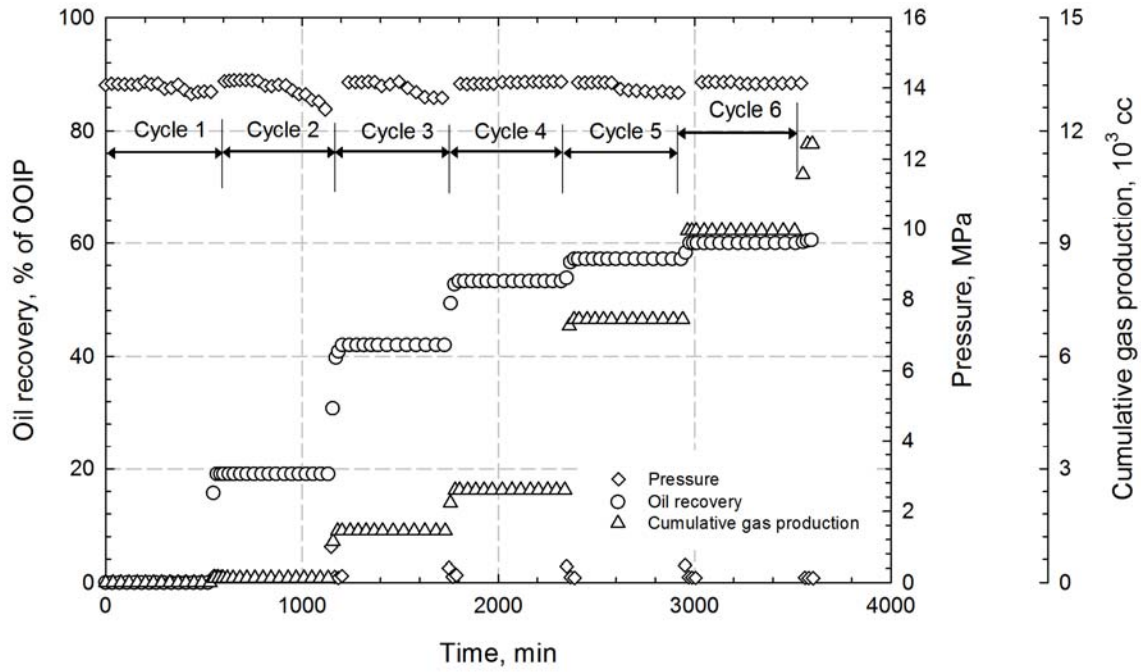


**Figure 3.12** Measured oil recovery, cumulative gas production, and pressure drop versus time for Scenario #9.

### 3.3.2 History matching

#### 1) Scenario #1 (Waterflooding)

The relative permeability curves and capillary pressure curves are tuned to history match the experimental measurements in Scenarios #1-9. **Figure 3.13** shows the tuned water and oil relative permeability curves and capillary pressure curve, respectively, for Scenario #1. As presented in **Figure 3.13**, the water relative permeability is rather low in the water saturation range from 0.32 to 0.50, while the oil relative permeability shows very low values in the water saturation range of 0.60-0.77. This is due to the low water or oil effective permeability in the corresponding water saturation ranges. According to the tuned water and oil relative permeability curves, irreducible water saturation is determined to be 0.32, resulting in a corresponding oil saturation of 0.68 at the endpoint, which is higher than the experimental measurement of initial oil saturation listed in **Table 3.4**. This is due to the fact that it is difficult to experimentally reach the irreducible water saturation for such tight core samples during the oil saturating process. Similar phenomenon is also found in the following Scenarios #2-9.

**Figure 3.14** shows the history matching results for Scenario #1, where the cumulative oil production history and injection pressure history are well matched. At the beginning (i.e., about 5 min), the measured injection pressure is higher than the simulated value. This is attributed to the fact that, during laboratory experiments, water starts being compressed and injected into the coreholder, while, during

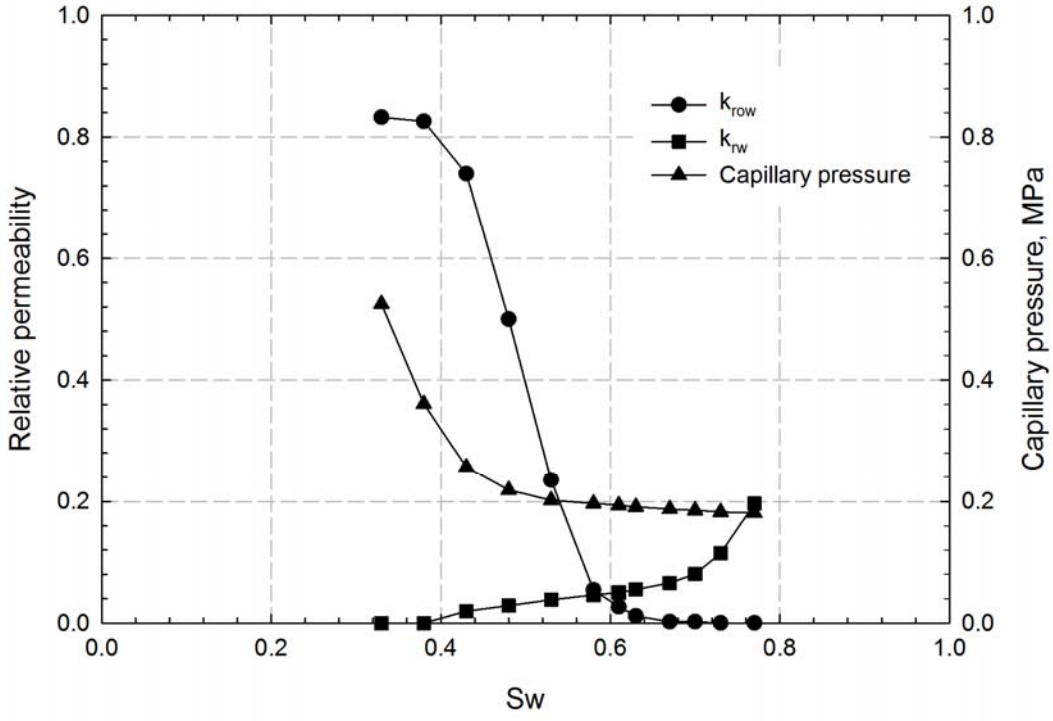


**Figure 3.13** Water and oil relative permeability and capillary pressure for Scenario #1

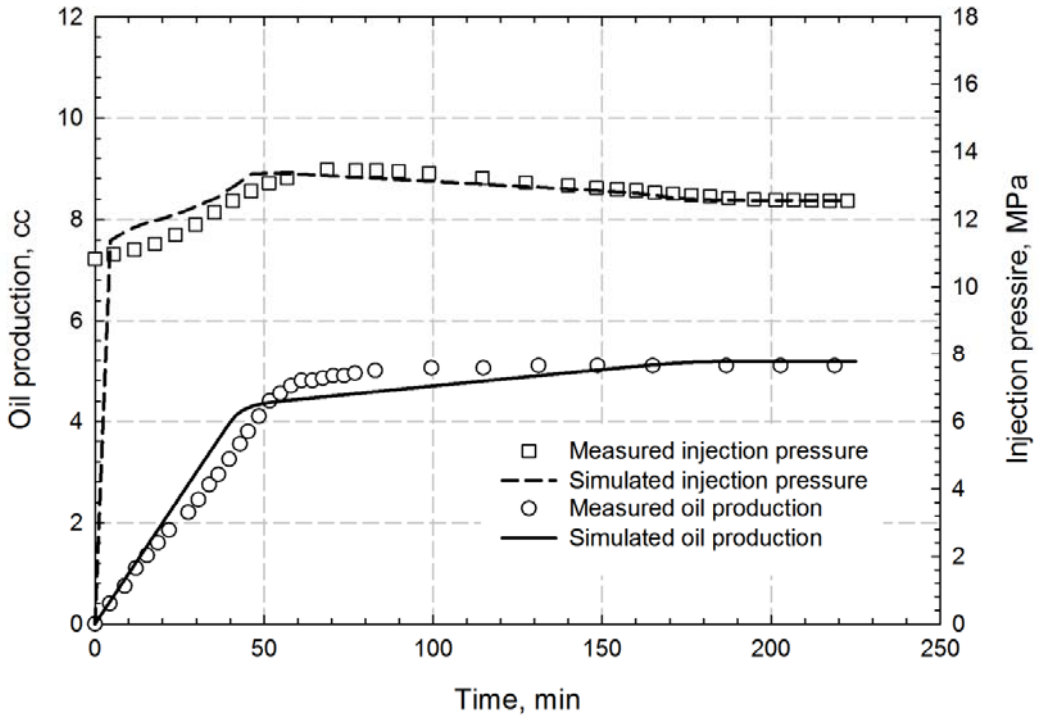


**Figure 3.14** Simulated oil production and injection pressure versus time for Scenario #1

simulation, water is usually injected instantly all the time. Similar operation is also implemented in $CO_2$ flooding processes for Scenarios #2-9 so as to ensure a constant injection rate of $CO_2$ under experimental conditions, resulting in a minor mismatch between the measured and simulated injection pressure at the beginning.

**2) Scenario #2 (Near-miscible $CO_2$ flooding)**

**Figures 3.15a** and **b** depict the tuned water and oil relative permeability curves, gas and liquid relative permeability curves, and capillary pressure curves, respectively, for the near-miscible $CO_2$ flooding process (i.e., Scenario #2). As shown in **Figure 3.15b**, gas phase relative permeability increases slightly when gas saturation is smaller than 0.40. Also, compared to the waterflooding process, the injection pressure and cumulative oil production is less sensitive to water and oil relative permeability curves.

**Figure 3.16** plots the history matching results of the measured cumulative oil production and injection pressure, respectively, for Scenario #2. In general, there exists a good agreement between the experimental measurements and simulation results for injection pressure, while a slight mismatch is found prior to gas breakthrough for cumulative oil production. This may be caused by the non-uniform distribution of oil saturation, resulting in different amount of dissolved $CO_2$ into oil. After $CO_2$ breakthrough, displacement process tends to be steady so that good history matching result is obtained. Compared to waterflooding, the simulated continuous near-miscible $CO_2$ flooding achieves a higher ultimate recovery factor, indicating the main mechanisms contributing to such a recovery enhancement (i.e., injectivity

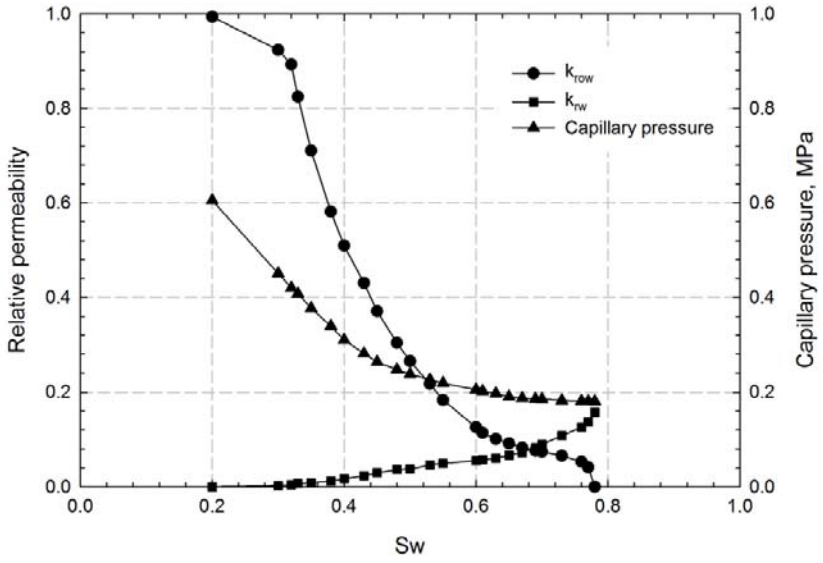


**(a)**

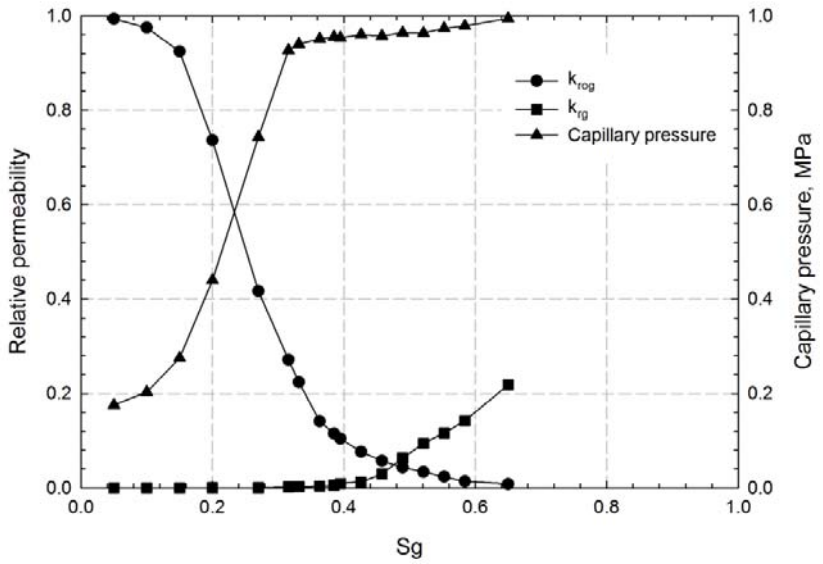


**(b)**

**Figure 3.15** Relative permeability for **(a)** Water-oil system and its capillary pressure and **(b)** Gas-liquid system and its capillary pressure for Scenario #2

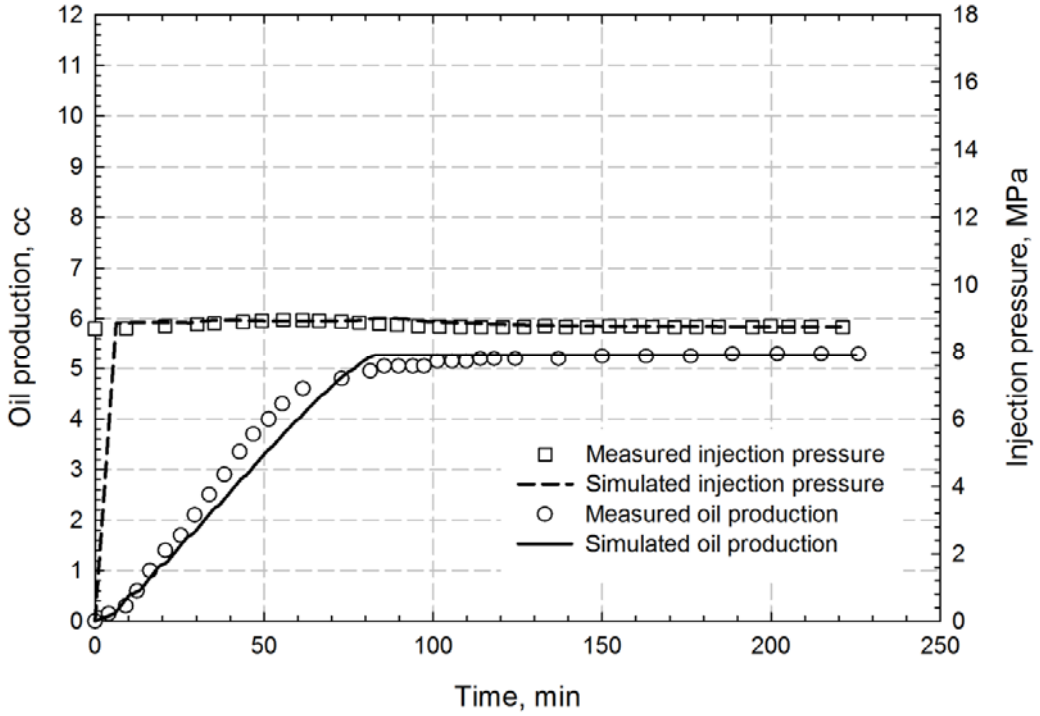


**Figure 3.16** Simulated oil production and injection pressure versus time for Scenario #2

improvement, oil swelling, viscosity reduction, IFT reduction, solution gas drive, and light-components extraction) are well simulated.

**3) Scenario #3 (Miscible $CO_2$ flooding)**

**Figures 3.17a** and **b** show the tuned water and oil relative permeability curves, gas and liquid relative permeability curves, and capillary pressure curves, respectively, for the miscible $CO_2$ flooding process (i.e., Scenario #3). It can be seen from **Figure 3.17b** that the gas phase relative permeability increases slightly when gas saturation is smaller than 0.50, while the liquid phase relative permeability is very low at a high gas-saturation region.

The history matching results for Scenario #3 are presented in **Figure 3.18**. Again, there exists a generally good agreement between the experimental measurements and simulated data, indicating the most important mechanism during miscible $CO_2$ flooding process is well simulated. However, compared to the simulated results, the experimental oil production is delayed for 5 min at the beginning. Such a slight mismatch is mainly caused by the compressibility of $CO_2$ under supercritical conditions, resulting in a delay of injection pressure increasing from 9.5 MPa to the entry pressure (i.e., around 15.0 MPa). The history matching results for Scenarios #2 and #3 reveal that the mechanisms of continuous $CO_2$ flooding in tight cores (i.e., injectivity improvement, swelling effect, viscosity reduction, IFT reduction, solution gas drive, gas displacement, miscibility effect between crude oil and $CO_2$, and light-components extraction) are identified and simulated with the numerical models.

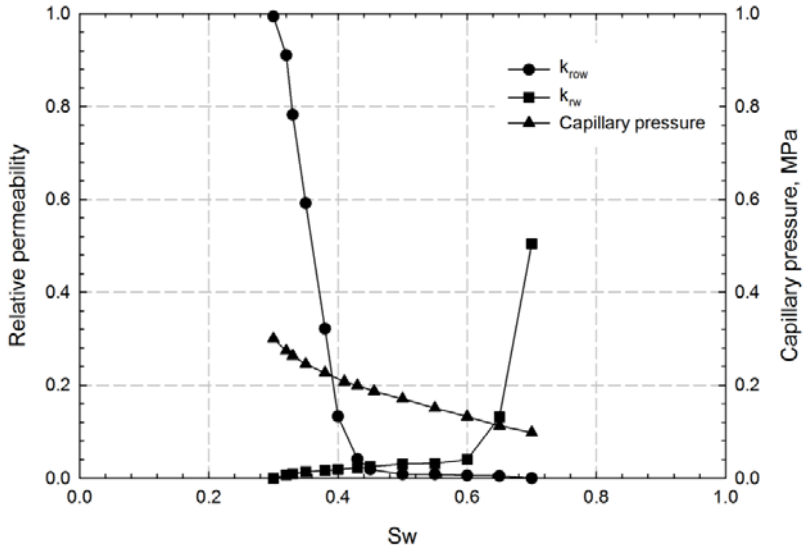


**(a)**

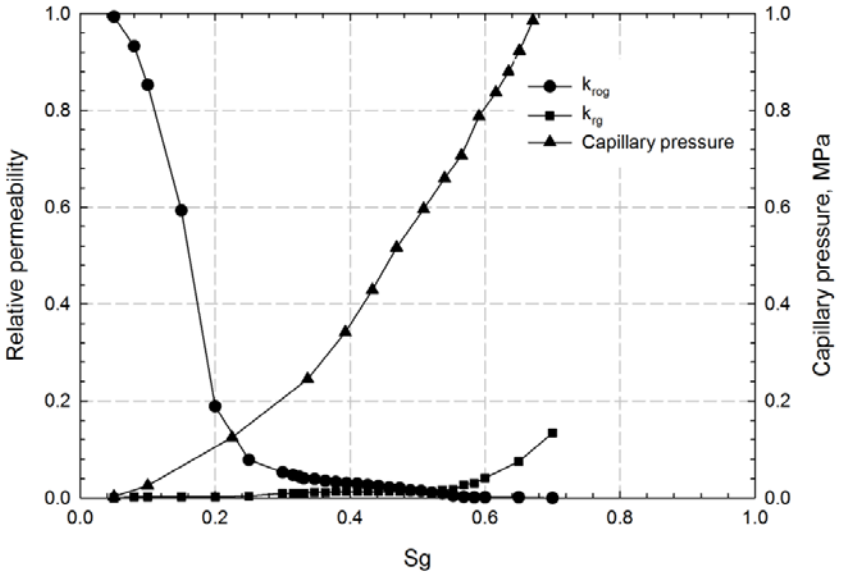


**(b)**

**Figure 3.17** Relative permeability for **(a)** Water-oil system and its capillary pressure and **(b)** Gas-liquid system and its capillary pressure for Scenario #3

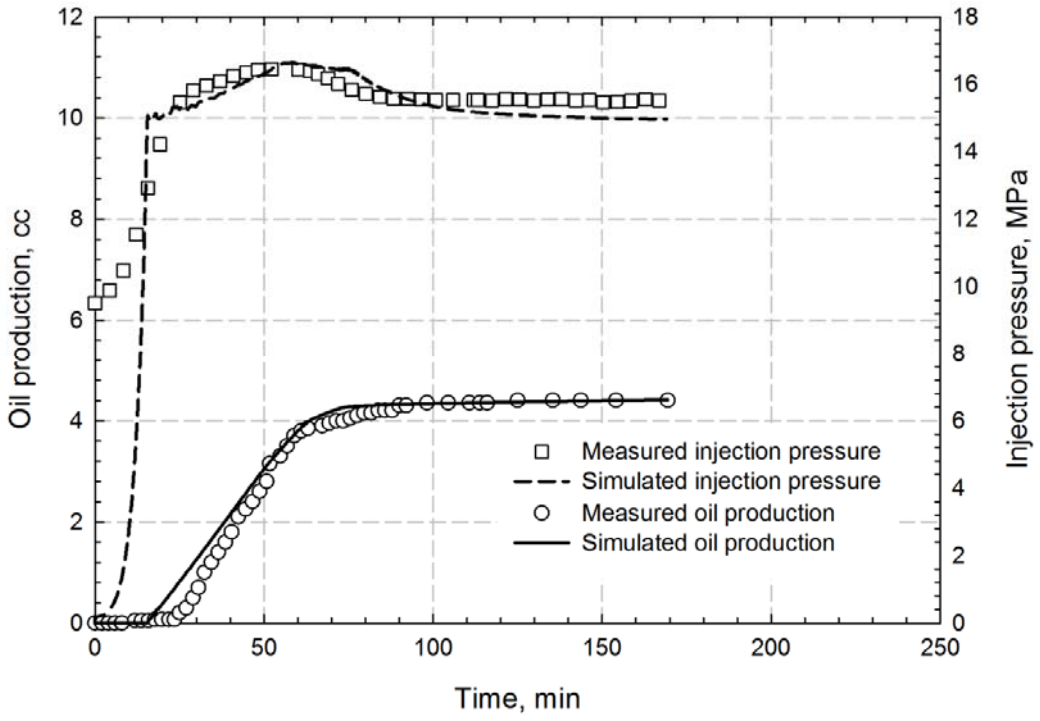


**Figure 3.18** Simulated oil production and injection pressure versus time for Scenario #3

**4) Scenario #4 ($CO_2$-WAG flooding, WAG ratio=1.0, water slug size=$CO_2$ slug size=0.250 PV)**

**Figures 3.19a** and **b** show the tuned water and oil relative permeability curves, gas and liquid relative permeability curves, and capillary pressure curves, respectively, for the miscible $CO_2$-WAG flooding process of Scenario #4.

History matching results for Scenario #4 are shown in **Figure 3.20**. It can be seen that there exists a generally good agreement between the measured and simulated injection pressure except for the minor mismatch at the beginning. As for cumulative oil production profiles, however, difference between the experimentally measured and numerically simulated data is observed during 60-110 min. This may be resulted from the dissolution of $CO_2$ into the synthetic water, leading to low displacement efficiency during water injection period, and thus a lower recovery compared to the $CO_2$ injection period. Compared to continuous $CO_2$ flooding, the higher simulated recovery is obtained from $CO_2$-WAG flooding process. This means that, besides the EOR mechanisms maintained in continuous $CO_2$ flooding process, the special mechanism of sweep efficiency improvement is successfully simulated in the $CO_2$-WAG flooding process.

**5) Scenario #5 ($CO_2$-WAG flooding, WAG ratio=1.0, water slug size=0.125 PV, $CO_2$ slug size=0.250 PV)**

**Figures 3.21a** and **b** show the tuned water and oil relative permeability curves, gas and liquid relative permeability curves and capillary pressure curves for Scenario #5, respectively. As can be seen from **Figure 3.21b**, the simulation results are very

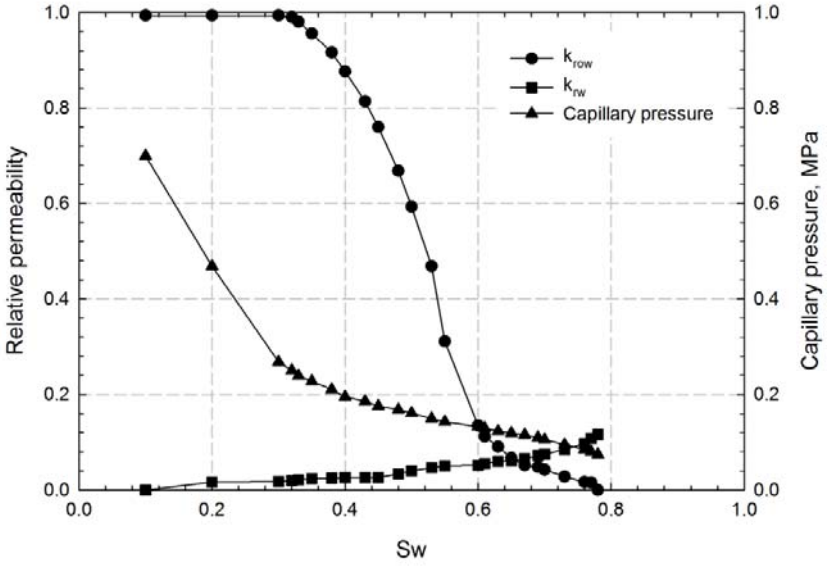


**(a)**

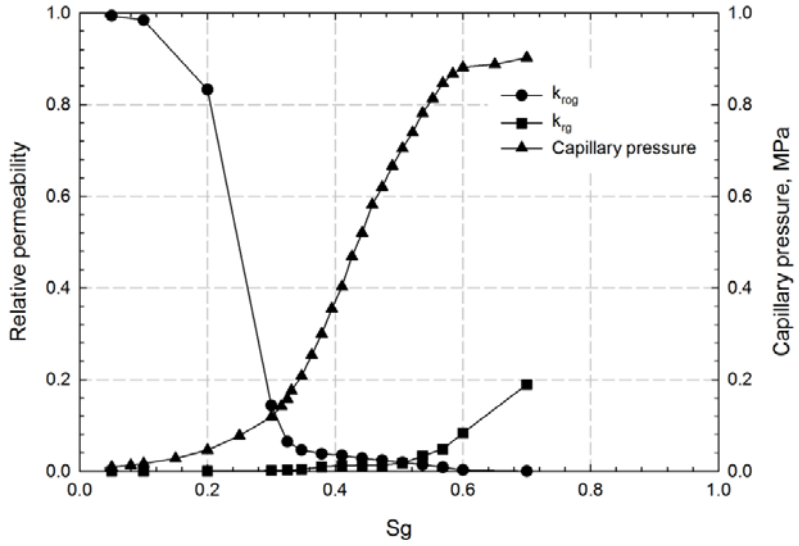


**(b)**

**Figure 3.19** Relative permeability for **(a)** Water-oil system and its capillary pressure and **(b)** Gas-liquid system and its capillary pressure for Scenario #4

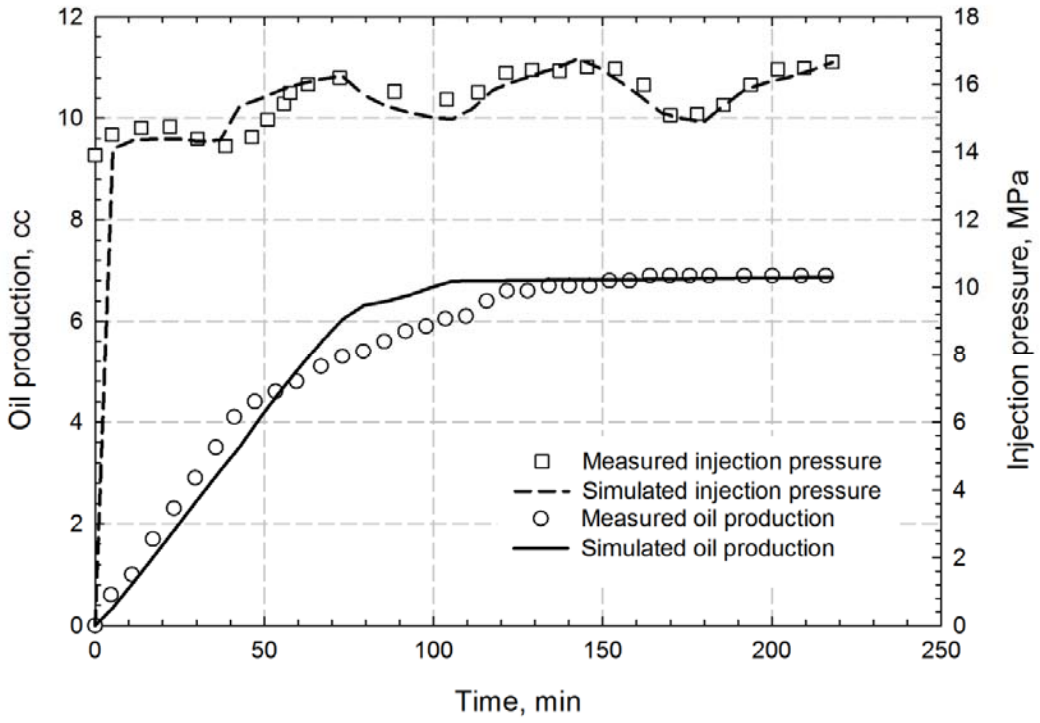


**Figure 3.20** Simulated oil production and injection pressure versus time for Scenario #4

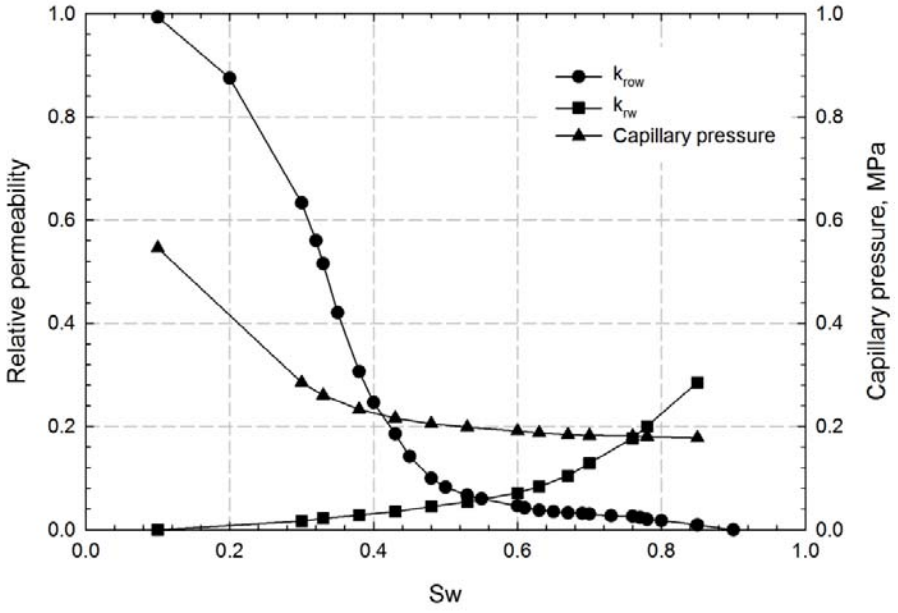


**(a)**

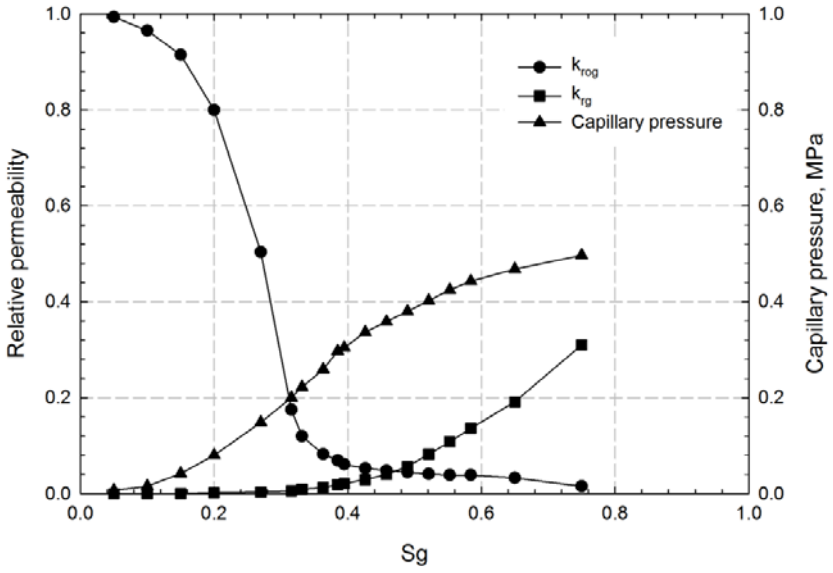


**(b)**

**Figure 3.21** Relative permeability for **(a)** Water-oil system and its capillary pressure and **(b)** Gas-liquid system and its capillary pressure for Scenario #5

sensitive to the gas phase relative permeability curve when gas saturation is smaller than 0.4, while the liquid phase relative permeability curve plays a key role on the simulated oil production and injection pressure as gas saturation is higher than 0.5.

The history matching results are presented in **Figure 3.22**, where the experimental measurements are well matched by performing numerical simulation except for the difference observed in cumulative oil production profiles between 80-130 min. Besides the reason outlined in Scenario #4, such a mismatch might also be caused by the non-uniform distribution of oil in the core sample, leading to an inconsistent $CO_2$ solubility into oil, and thus low recovery efficiency during this period.

**6) Scenario #6 ($CO_2$-WAG flooding, WAG ratio=0.5, water slug size=0.250 PV, $CO_2$ slug size=0.500 PV)**

**Figures 3.23a** and **b** show the tuned water and oil relative permeability curves, gas and liquid relative permeability curves and capillary pressure curves for miscible $CO_2$-WAG process in Scenario #6.

The history matching results for Scenario #6 are illustrated in **Figure 3.24**. The injection pressure history and cumulative oil production history are well matched by simulation for Scenario #6, while a minor mismatch of oil production profiles is observed during the range of 100-300 min. The similar phenomenon is also observed in previous $CO_2$-WAG flooding processes of Scenarios #4 and #5.

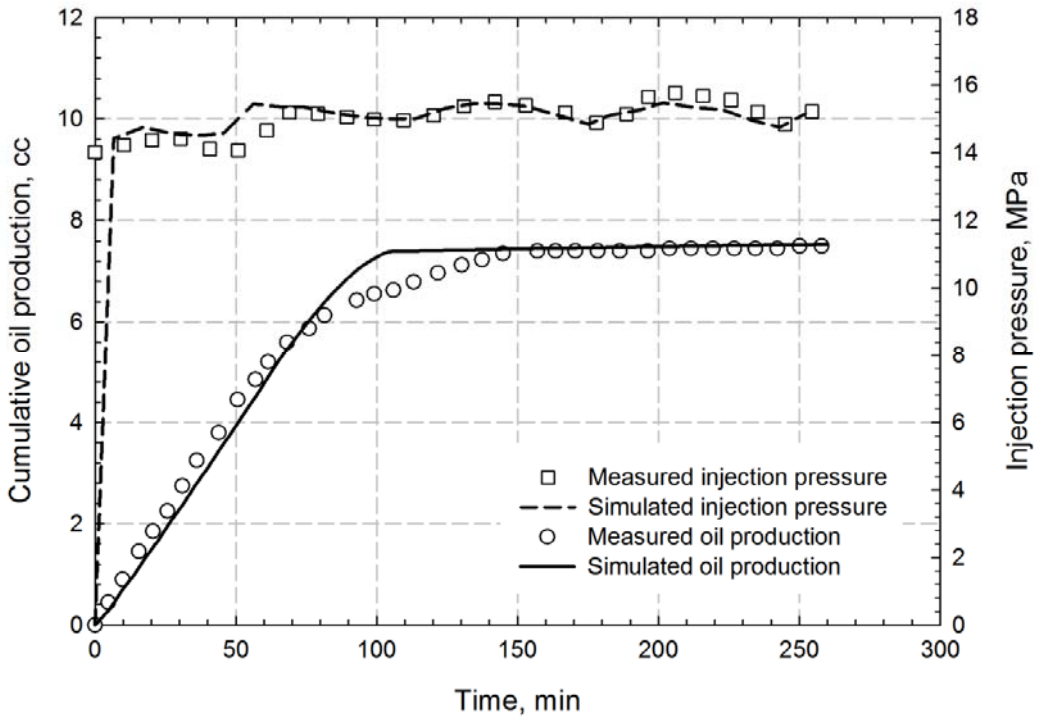


**Figure 3.22** Simulated oil production and injection pressure versus time for Scenario #5

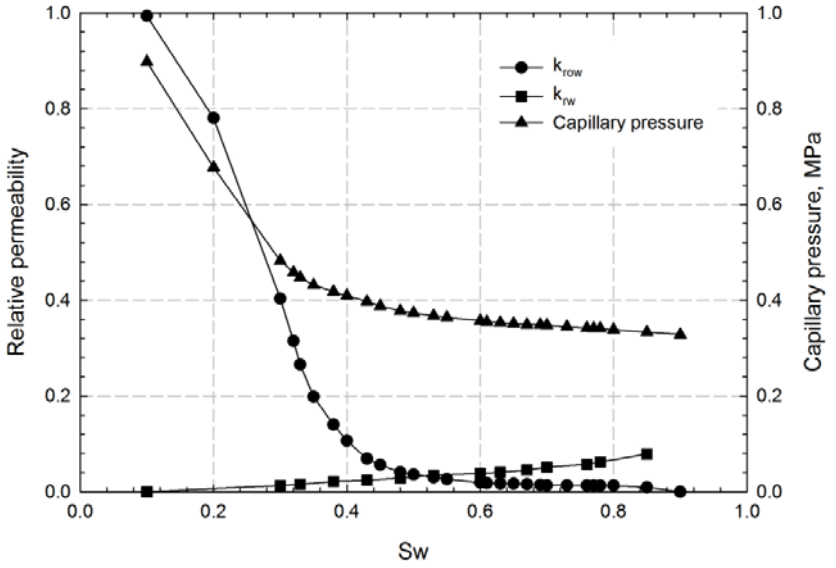


**(a)**

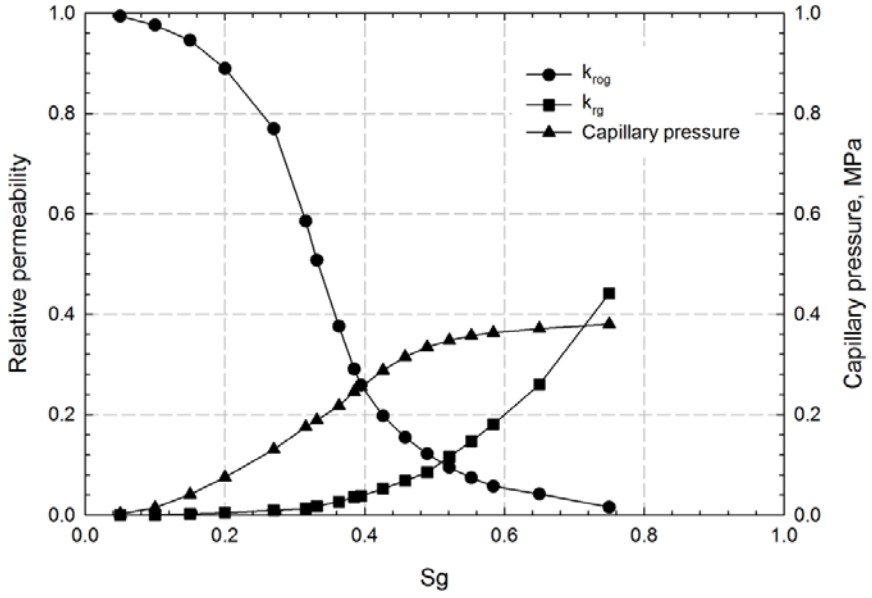


**(b)**

**Figure 3.23** Relative permeability for **(a)** Water-oil system and its capillary pressure and **(b)** Gas-liquid system and its capillary pressure for Scenario #6

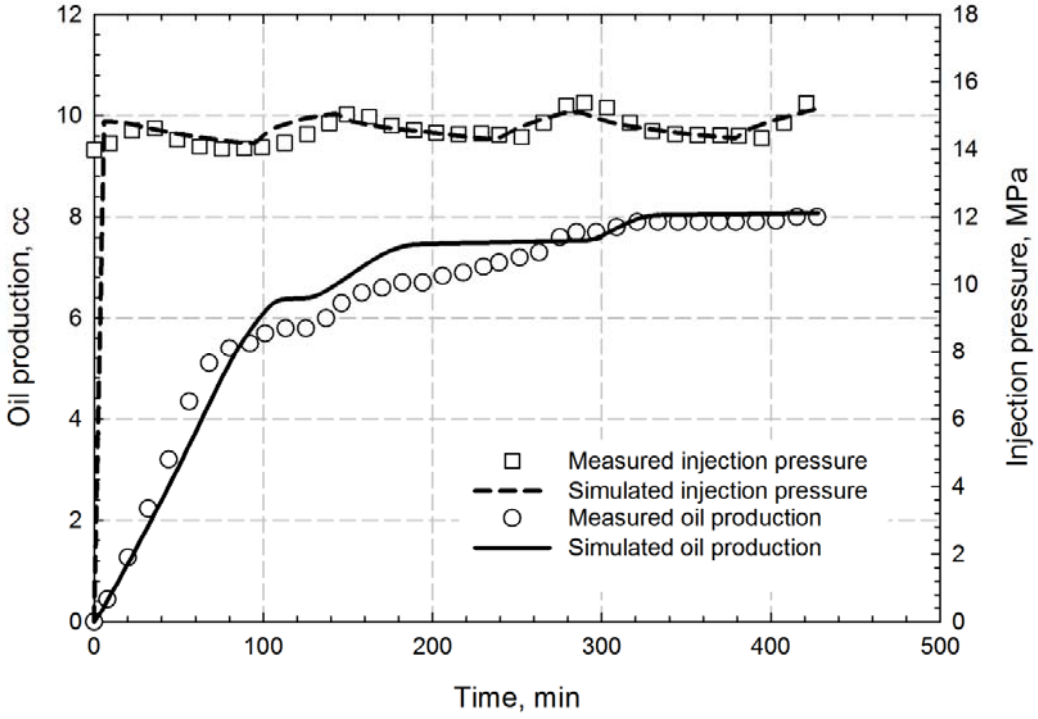


**Figure 3.24** Simulated oil production and injection pressure versus time for Scenario #6

**7) Scenario #7 (Immiscible $CO_2$ huff-n-puff)**

**Figures 3.25a** and **b** show the tuned water and oil relative permeability curves, gas and liquid relative permeability curves, and capillary pressure curves, respectively, for the immiscible $CO_2$ huff-n-puff process of Scenario #7. It is found that the oil phase relative permeability tends to increase with an increase of oil saturation. The capillary pressure of water and oil system tends to decrease with an increase in water saturation, while the capillary pressure of liquid and gas system tends to increase as gas saturation increases.

The history matching results are shown in **Figure 3.26**. It is found that there exists an excellent agreement between the experimental and simulated profiles with respect to oil production and pressure.

**8) Scenario #8 (Near-miscible $CO_2$ huff-n-puff)**

**Figures 3.27a** and **b** depict the tuned relative permeability curves, and capillary pressure curves for the near-miscible $CO_2$ huff-n-puff process (i.e., Scenario #8). It is found that either water phase relative permeability or gas phase relative permeability tends to increase with a decrease of oil saturation. Also, the simulated results are more sensitive to gas and liquid relative permeability curves, compared to water and oil relative permeability curves.

**Figure 3.28** presents the history matching results of the measured pressure and cumulative oil production throughout the experiment. An excellent agreement between the measured and simulated results is obtained.

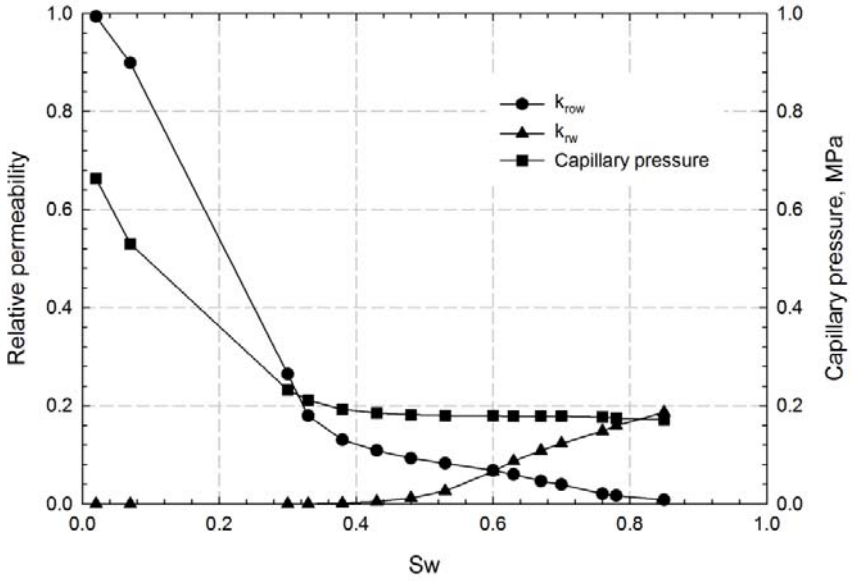


**(a)**

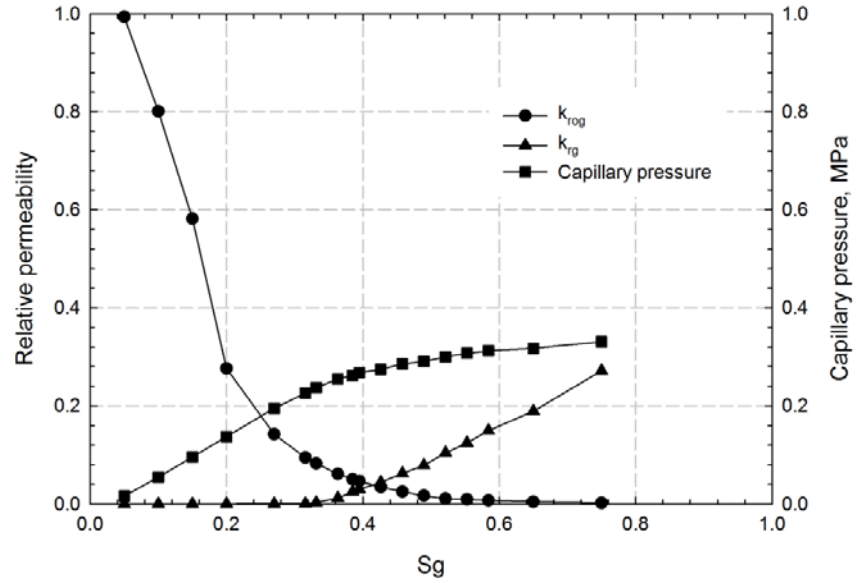


**(b)**

**Figure 3.25** Relative permeability for **(a)** Water-oil system and its capillary pressure and **(b)** Gas-liquid system and its capillary pressure for Scenario #7

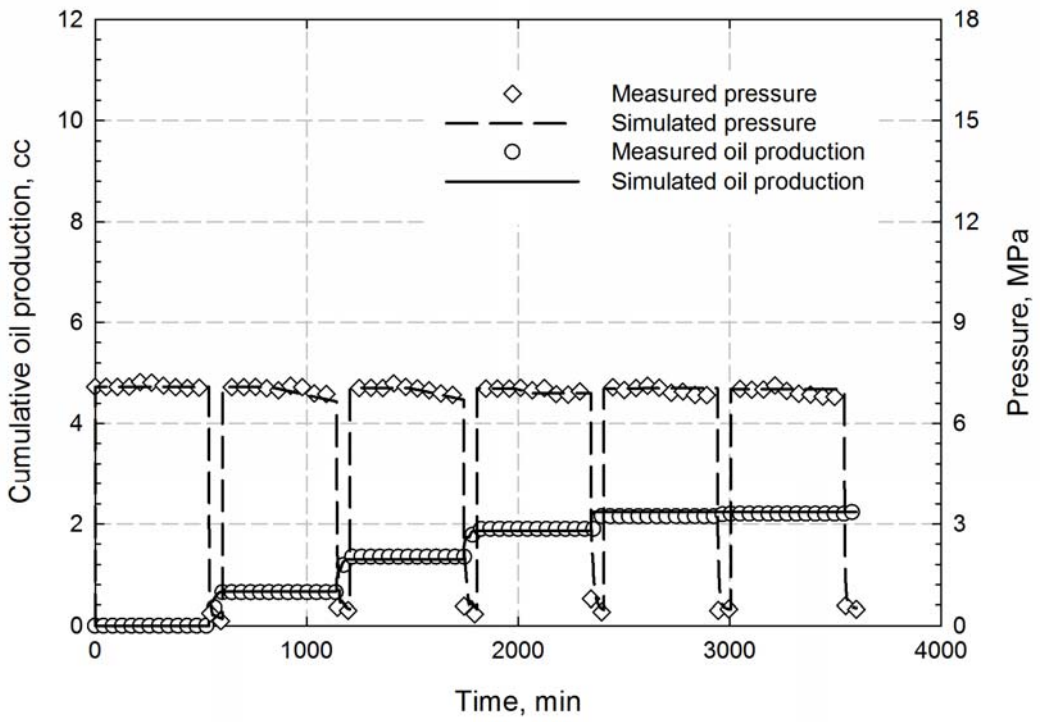


**Figure 3.26** Simulated oil production and injection pressure versus time for Scenario #7

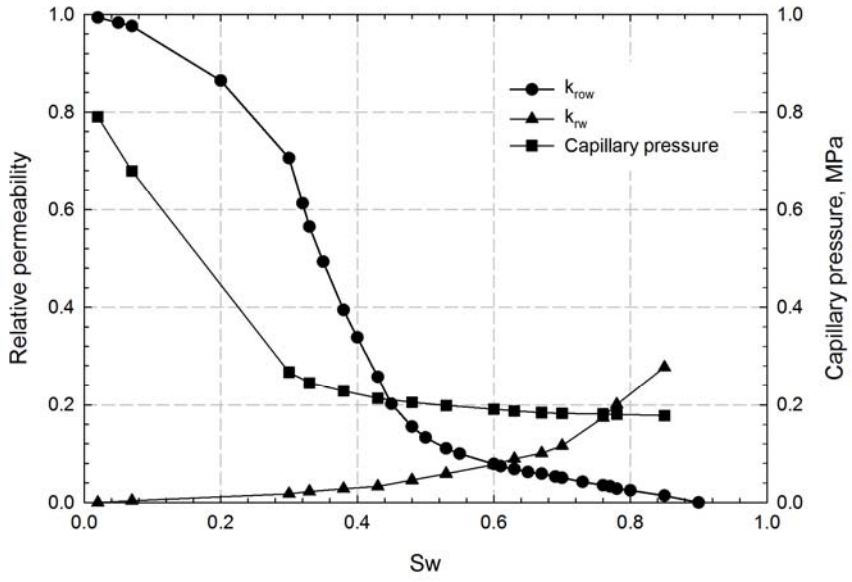


**(a)**

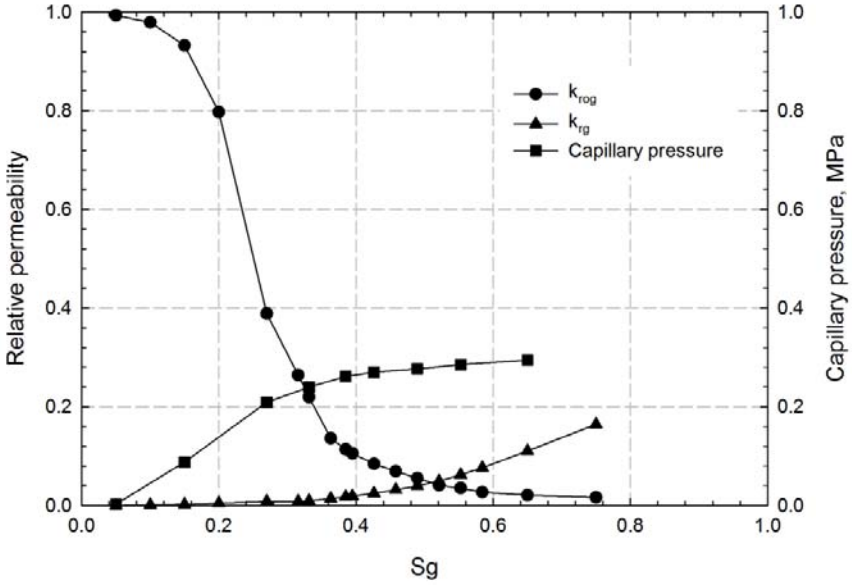


**(b)**

**Figure 3.27** Relative permeability for **(a)** Water-oil system and its capillary pressure and **(b)** Gas-liquid system and its capillary pressure for Scenario #8

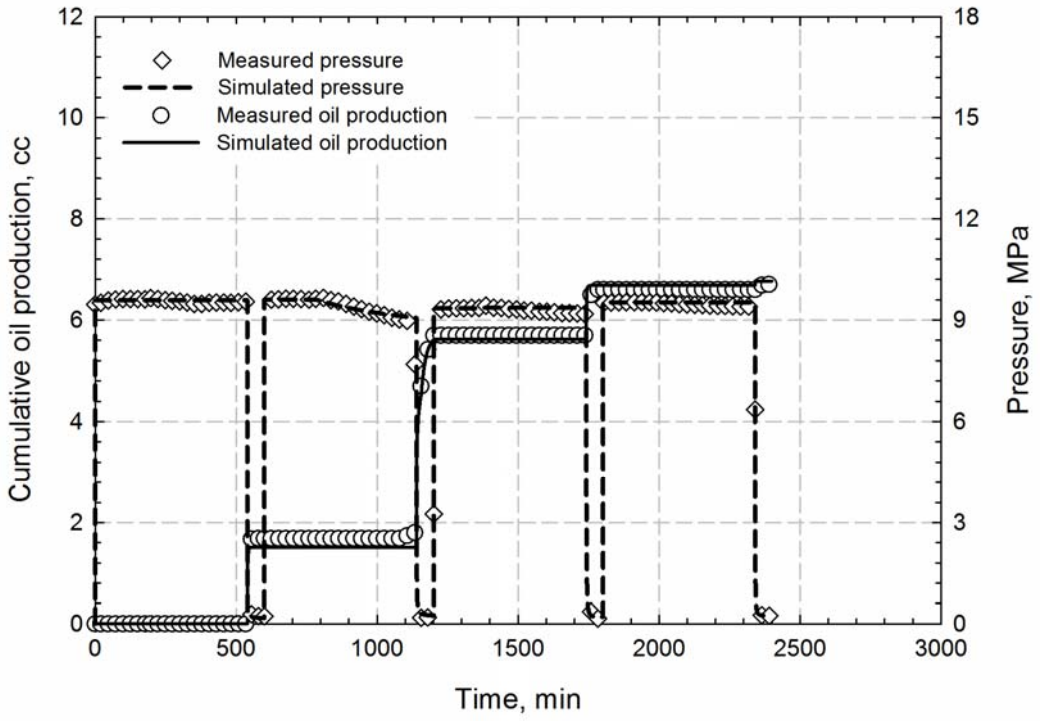


**Figure 3.28** Simulated oil production and injection pressure versus time for Scenario #8

**9) Scenario #9 (Miscible $CO_2$ huff-n-puff)**

The tuned water and oil relative permeability curves, gas and liquid relative permeability curves, and capillary pressure curves for miscible $CO_2$ huff-n-puff process (i.e., Scenario #9) are shown in **Figures 3.29a** and **b**. The history matching results for miscible $CO_2$ huff-n-puff process are depicted in **Figure 3.30**. The experimental pressure profile and cumulative oil production profile are well matched by simulation. According to the simulated results, pressure tends to decrease during the soaking time, while oil production appears to be high when the wells start to produce right after the soaking processes. This indicates the important mechanisms of solution and gas oil swelling drive underlying $CO_2$ huff-n-puff process may have been appropriately simulated by the numerical model.

### 3.3.3 Sensitivity analysis

In this section, sensitivity analysis is further conducted to examine effects of relevant operational parameters on performance of continuous $CO_2$ flooding, $CO_2$-WAG flooding and $CO_2$ huff-n-puff process.

**1) Production pressure**

***Continuous $CO_2$ flooding***: The tuned numerical model used in Scenario #2 is utilized to numerically examine effect of different production pressures ranging from 5.7 to 11.7 MPa on the production performance. As can be seen from **Figure 3.31a**, the ultimate oil recovery increases with an increase in production pressure.

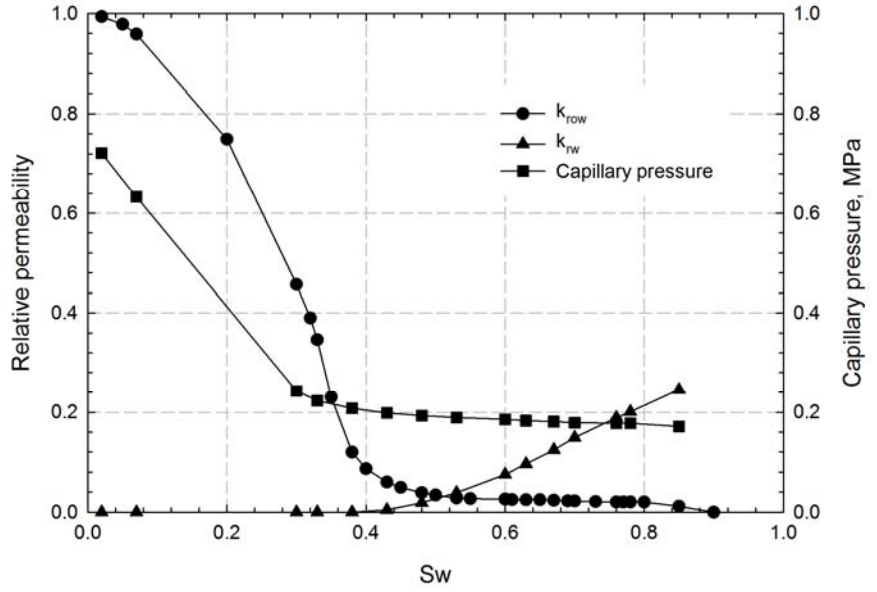


**(a)**

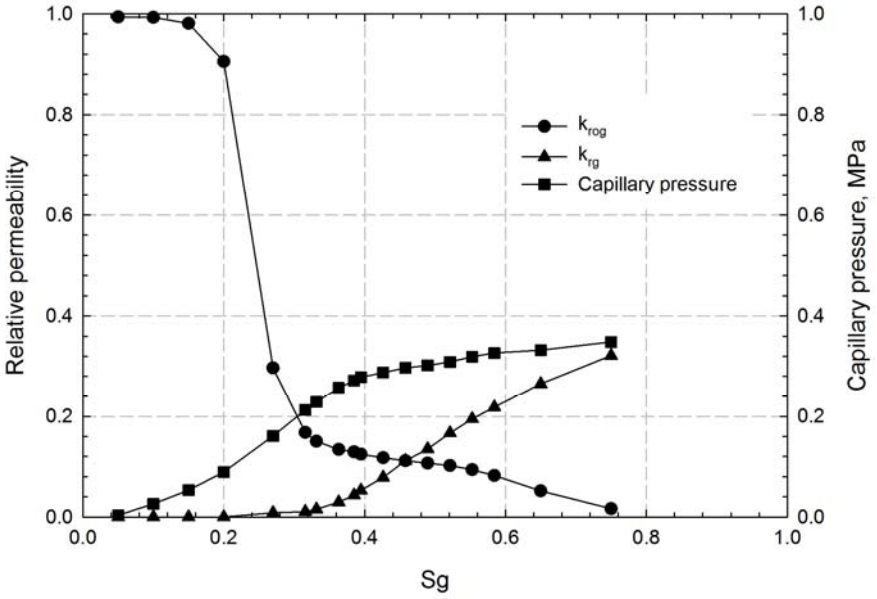


**(b)**

**Figure 3.29** Relative permeability for **(a)** Water-oil system and its capillary pressure and **(b)** Gas-liquid system and its capillary pressure for Scenario #9

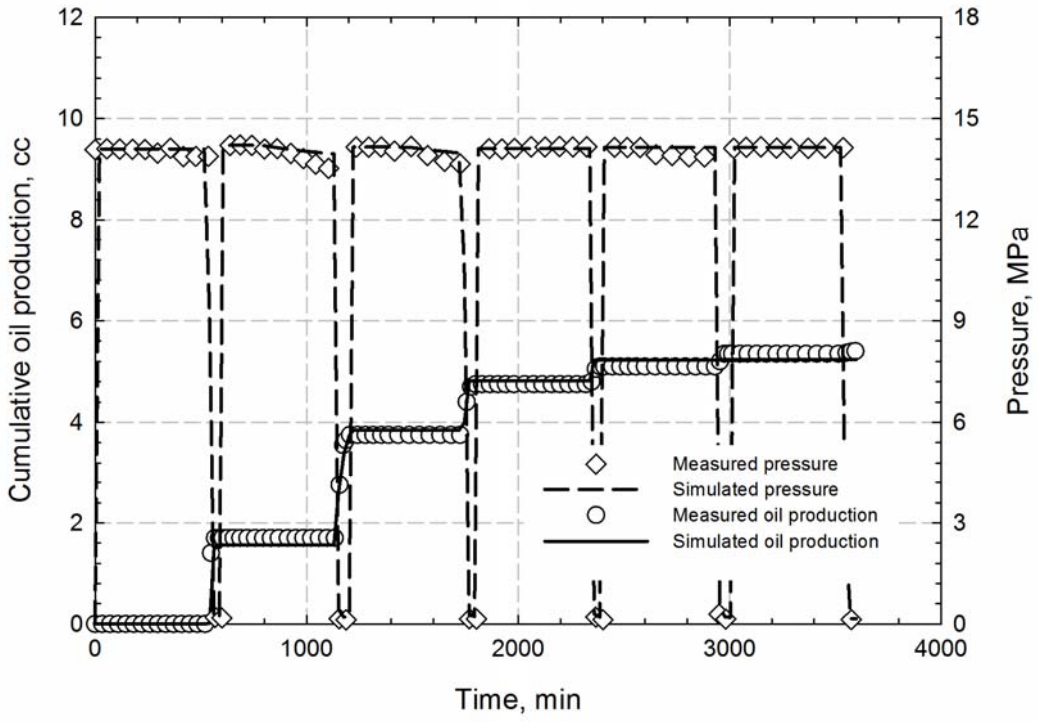


**Figure 3.30** Simulated oil production and injection pressure versus time for Scenario #9

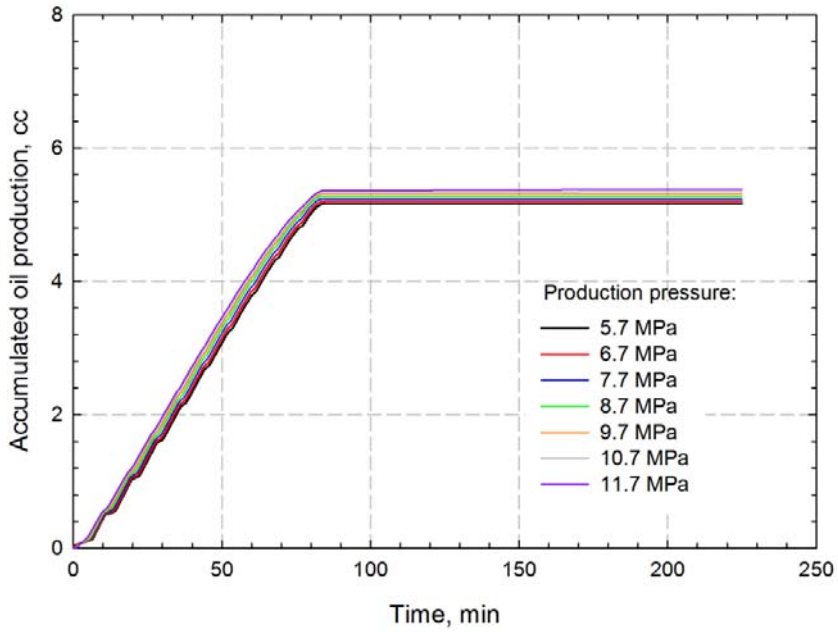


**(a)**

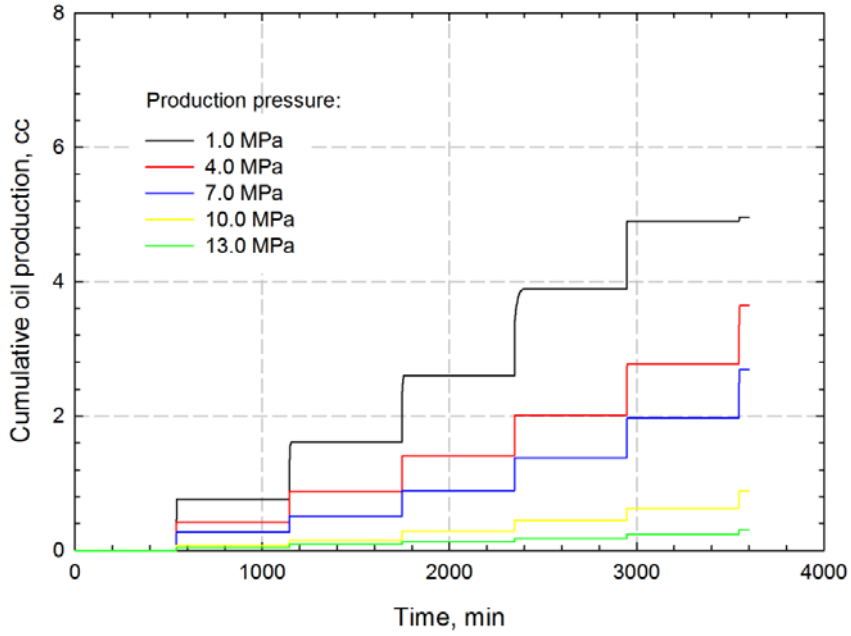


**(b)**

**Figure 3.31** Production profiles with different production pressures for **(a)** Scenario #2 and **(b)** Scenario #9

The high ultimate oil recovery of $CO_2$ flooding process at both low and high production pressures indicates that $CO_2$ flooding is efficient for recovering oil from tight formations under either near-miscible or miscible condition.

***$CO_2$ huff-n-puff process***: The tuned numerical model used in Scenario #9 is implemented to numerically examine the effect of production pressure on the recovery performance of $CO_2$ huff-n-puff process (See **Figure 3.31b**). Various production pressures including 1.0, 4.0, 7.0, 10.0, and 13.0 MPa are applied in this analysis, while the number of injecting cycles is kept as six in the simulation. Oil recovery is found to significantly improve when production pressure decreases from 13.0 to 1.0 MPa due to a larger differential pressure, leading to more dissolved $CO_2$ produced out of oil in the core sample, and hence a higher oil recovery.

**2) WAG ratios**

The tuned numerical model used in Scenario #4 is employed to numerically examine the effect of WAG ratios on the oil production performance and corresponding fluid injectivity. Five WAG ratios (i.e., 0.5, 1.0, 2.0, 4.0 and 8.0) together with continuous miscible $CO_2$ flooding (WAG ratio is 0) and waterflooding (WAG ratio is infinite) are applied in the simulations, while the injecting cycles are three for various WAG ratios (see **Figure 3.32**). The oil recovery is found to significantly enhance with an increase in the WAG ratio from 0.0 to 2.0. However, a further increase of WAG ratio leads to less enhancement effect on the oil recovery performance. When the WAG ratio increases from 4.0 to 8.0, the final oil recovery

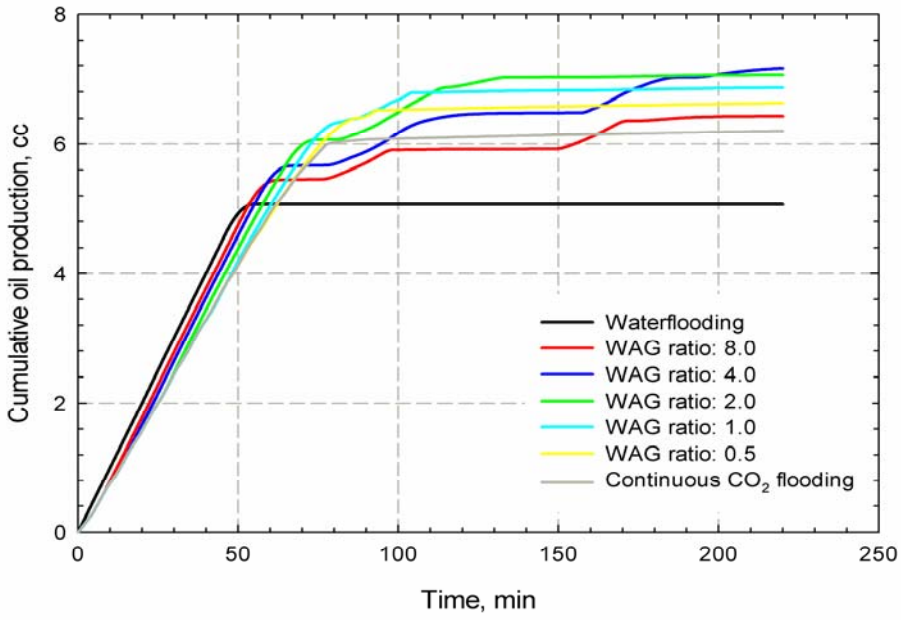


**(a)**

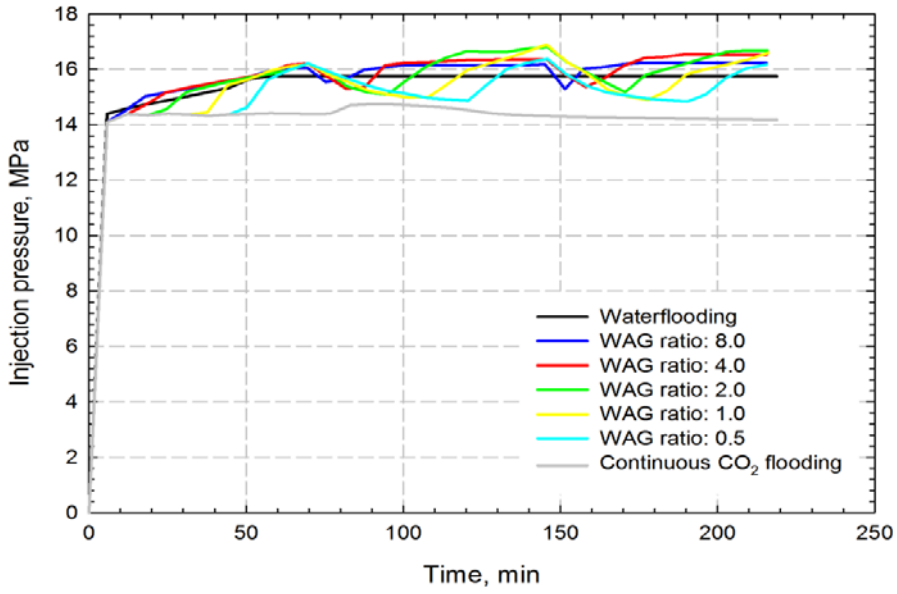


**(b)**

**Figure 3.32** Sensitivity analysis for Scenario #4: **(a)** WAG ratio and **(b)** Injection pressures

even starts to decrease. As such, the optimum WAG ratio is found to fall in the range of 2.0 to 4.0.

As shown in **Figure 3.32b**, when WAG ratio increases from 0.0 to 2.0, the peak of injection pressure for each scenario keeps increasing. Subsequently, a further increase of WAG ratio leads to a decrease of the injection pressure peak. This is attributed to the fact that resistance of water in the cores keeps increasing as more water is injected at first (Wayne *et al.*, 1982; Torabzadeh and Handy, 1984). With further increase of water slug size and decrease of $CO_2$ slug size, however, water saturation keeps increasing, leading to a higher liquid phase relative permeability, and thus a decrease of injection pressure.

Also, it can be observed that a smaller WAG ratio usually results in a larger reduction of injection pressure during $CO_2$ injection processes in each cycle. When the WAG ratio is further decreased to lower than 0.5, the injection pressure usually decreases at the beginning and then remains almost constant. This finding is aligned with the experimental results of Scenario #6. Accordingly, fluid injectivity of water injection tends to decrease with an increase of WAG ratio from 0.0 to 2.0, whereas it is increased with a further increase of WAG ratio from 2.0 to infinite (i.e., waterflooding). Fluid injectivity is more significantly improved during $CO_2$ injection period of each cycle with a smaller WAG ratio, whereas it becomes difficult to be further improved when the WAG ratio remains very low.

**3) Cycle times**

The tuned numerical model implemented in Scenario #4 is also applied to examine the influence of cycle time on recovery performance and corresponding fluid injectivity in miscible $CO_2$-WAG process. As can be seen in **Figures 3.33a** and **b**, the WAG ratio is set to be 4.0, and simulation time is kept the same throughout simulation processes. It is found that, when cycle time decreases from 200 min to 16 min, oil recovery keeps increasing. This is because that a shorter slug size of both water and $CO_2$ results in less chance to breakthrough when being injected, leading to better recovery efficiency during the injection process of each cycle. When the cycle time is smaller than 33 min of 0.250 PV, the oil recovery is no longer sensitive to the cycle time. Thus, a cycle time of 33 min may be the optimum.

The peak of injection pressure in each scenario appears to be higher with a longer cycle time due to larger resistance for water flowing at higher water saturation, while the minimum injection pressure in each scenario tends to be lower with a longer cycle time since gas phase relative permeability increases as gas saturation increases. This indicates that a longer cycle time results in lower fluid injectivity during water injection period in each cycle, leading to higher fluid injectivity during $CO_2$ injection period. Similarly, it is difficult to further increase the fluid injectivity at the later period of $CO_2$ injection process if $CO_2$ injection period remains long enough.

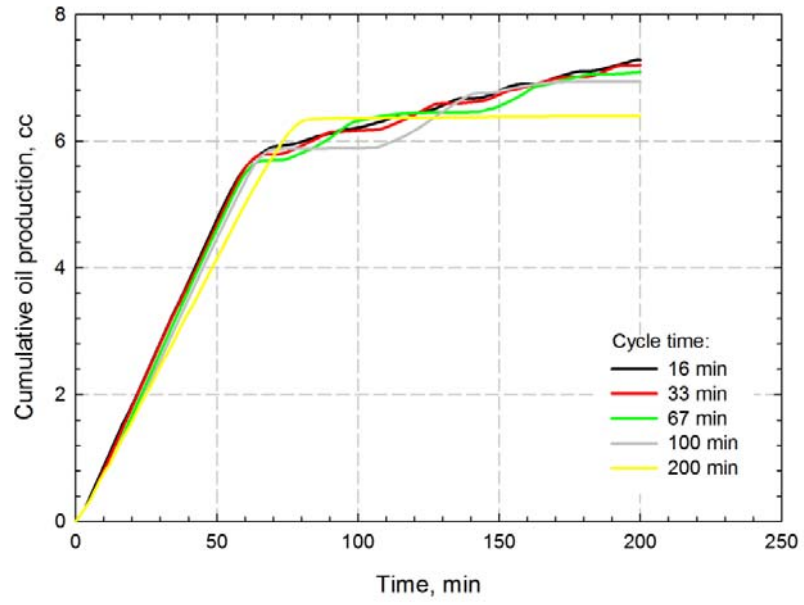


**(a)**

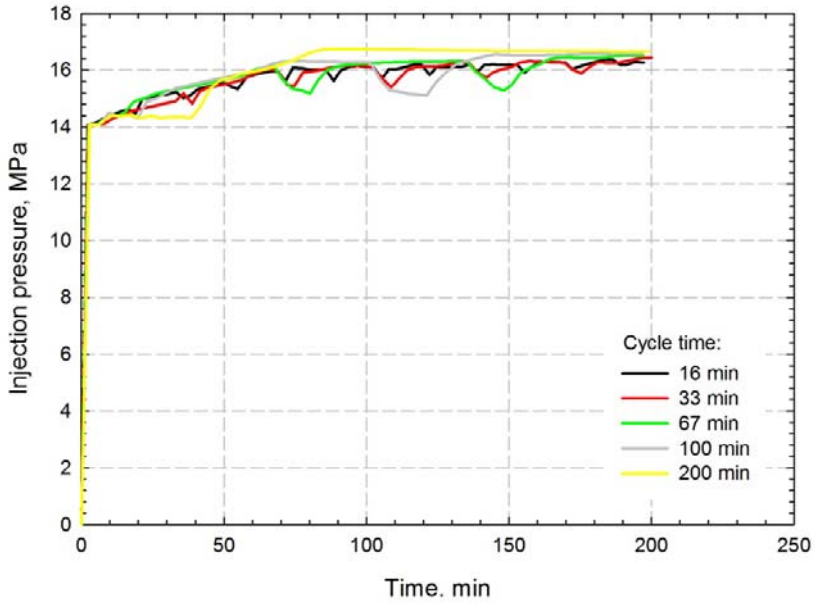


**(b)**

**Figure 3.33** Sensitivity analysis for Scenario #4: **(a)** Cycle time and **(b)** Injection pressure

**4) Water slug size**

As observed in previous experimental results, the introduction of water into $CO_2$ flooding process has significantly improved the oil recovery. Thus, the influence of various water slug sizes on the recovery performance and corresponding fluid injectivity in $CO_2$-WAG flooding is examined with numerical models tuned in Scenario #4.

In the simulation processes, the $CO_2$ slug size is kept the same as that in Scenario #4, while the water slug size increases from 0.125 PV to 1.000 PV, and three cycles are conducted. As shown in **Figures 3.34a** and **b**, though oil recovery tends to increase with water slug size, the enhancement effect of recovery remains minor when water slug size larger 0.250 PV. This means that it is difficult to further improve the sweep efficiency with water slug size longer than 0.250 PV. On the other hand, when water slug size is smaller than 0.250 PV, an increase in water slug size leads to an increase in both maximum and minimum injection pressure for each scenario due to the increase of resistance between water and rock at a higher water saturation.

If water slug size is larger than 0.250 PV, the maximum injection pressure is almost the same for each scenario with various water slug sizes, while reduction of injection pressure by $CO_2$ flooding in each cycle is almost the same for each scenario. This indicates that the water saturation in core samples is nearly unchanged as water slug size is larger than 0.250 PV, resulting in a nearly constant liquid phase relative permeability together with a constant injection pressure. Therefore, the amount of $CO_2$ injected dominates the degree of fluid injectivity improvement in $CO_2$-WAG

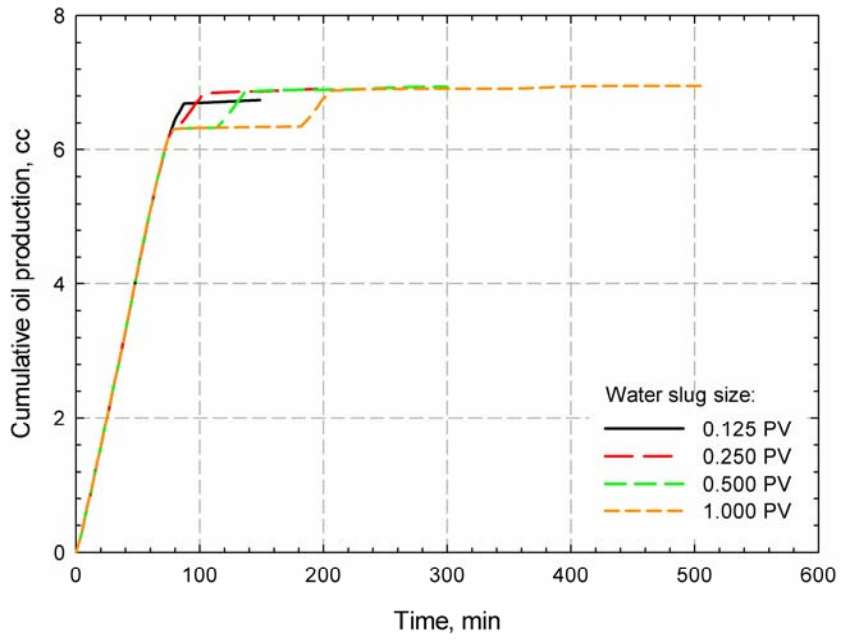


**(a)**

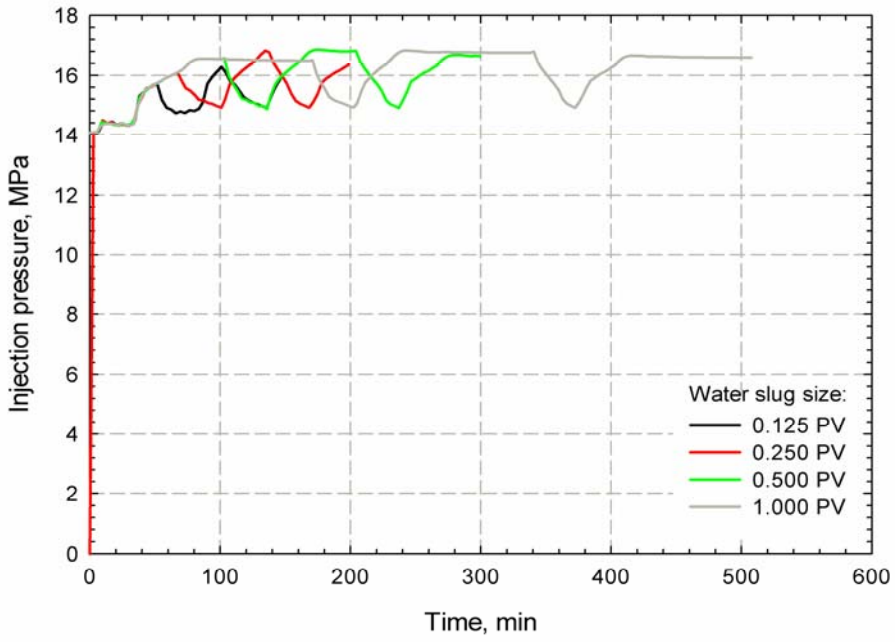


**(b)**

**Figure 3.34** Sensitivity analysis for Scenario #4: **(a)** Water slug size and **(b)** Injection pressure

processes, provided that a long water slug size is initiated. Otherwise, fluid injectivity may be improved with a decrease in water slug size if it remains smaller than a certain value.

**5) Injection pressure**

The tuned numerical model in Scenario #9 is utilized to examine the effect of injection pressure on recovery performance of $CO_2$ huff-n-puff process. The injection pressure ranges from 5.0 to 25.0 MPa. As can be seen from **Figure 3.35**, six cycles are performed during the simulation. As for the first five cycles, cumulative oil production increases with injection pressure. However, the enhancement effect of oil recovery becomes less significant when the injection pressure is higher than 9.0 MPa. This is attributed to the fact that it is difficult for the recovery performance of $CO_2$ injection to be significantly improved when the injection pressure is higher than the MMP between crude oil and $CO_2$.

Six sets of simulation in this study results in very similar ultimate recovery factor under various injection pressures. This means that $CO_2$ huff-n-puff process in tight oil formations usually results in similar recovery factors under both miscible and immiscible conditions, provided that the huff-n-puff process lasts long enough (Zhang *et al*., 2006).

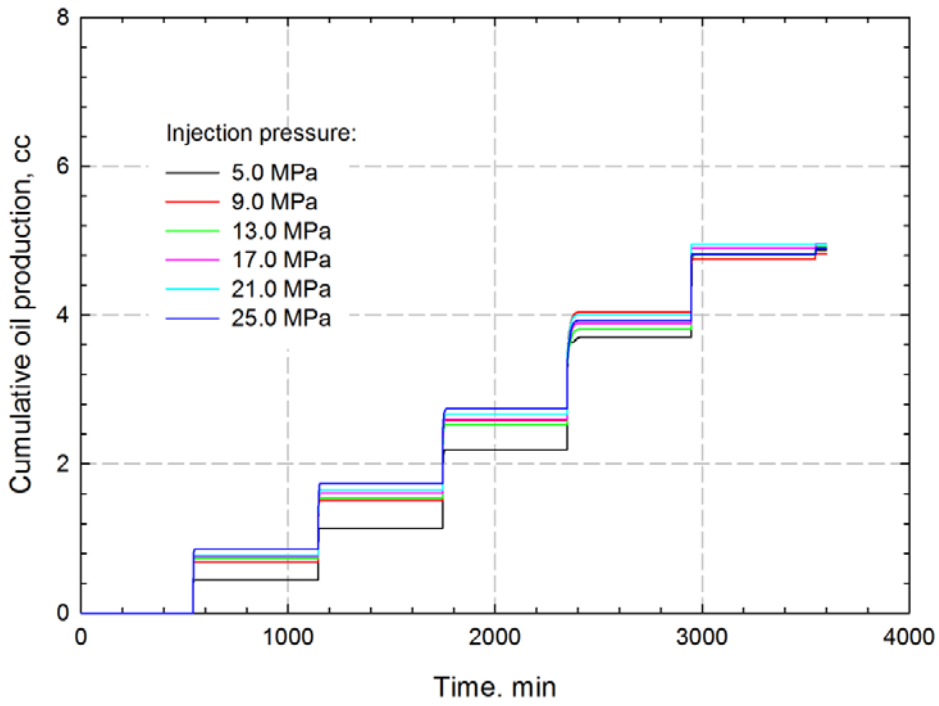


**Figure 3.35** Production profiles with different injection pressure for Scenario #9

**6) Soaking time**

The displacement model from Scenario #9 is applied to examine effect of soaking time on recovery performance during $CO_2$ huff-n-puff process. The simulation results are illustrated in **Figure 3.36**. The injection pressure is set to be 14.0 MPa throughout the simulation, while the soaking time changes from 3 to 9 h. It is found that the oil recovery is enhanced when soaking time increases from 3 to 6 h, while the ultimate recovery factor keeps nearly constant with a further increase of soaking time from 6 to 9 h. This means that the injected $CO_2$ has fully dissolved into crude oil when soaking time is longer than 6 h, then a further increase of the soaking time will hardly contribute to the improvement of oil recovery.

## 3.4 Summary

A coreflooding system has been developed and used to evaluate recovery performance of $CO_2$ injection in tight oil formations. Coreflooding experiments with various injection-production strategies are performed. It is found that $CO_2$ injection maintains superior recovery efficiency compared to waterflooding. The $CO_2$-WAG flooding is found to have advantages of higher sweeping efficiency and lower $CO_2$ consumption compared to continuous $CO_2$ flooding. Although recovery factor of $CO_2$ huff-n-puff processes prove to be lower than that of $CO_2$ flooding, the oil recovery will be improved with a higher injection pressure, provided that it is lower than the corresponding MMP.

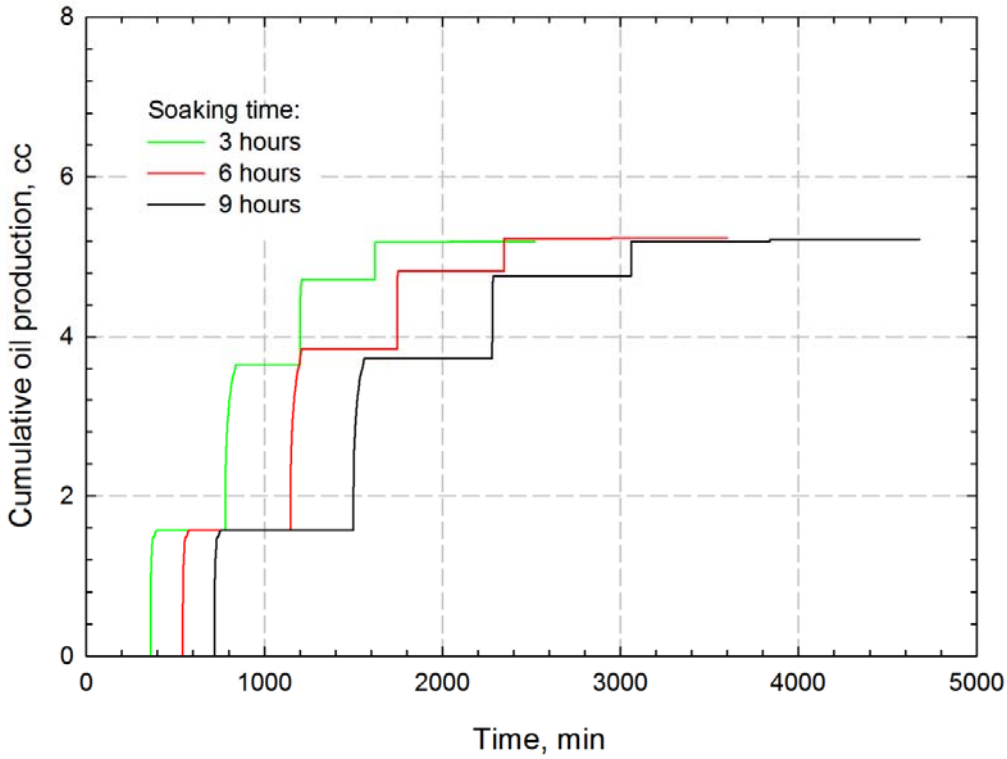


**Figure 3.36** Production profiles with different soaking times for Scenario #9

Numerical simulations are performed to history match the experimental measurements. There exists a good agreement between numerical and experimental results, demonstrating that numerical simulation have captured the general mechanisms of waterflooding and $CO_2$ EOR in tight oil formations. Effects of production pressure, WAG ratio, slug size, cycle time, injection pressure, and soaking time on recovery performance have been examined, while these operational parameters can be optimized so as to maximize the ultimate oil recovery while improving fluid injectivity in tight oil formations. The injection pressure, WAG ratio and production pressure prove to be dominant on oil recovery during the $CO_2$ injection processes.

# CHAPTER 4 PERFORMANCE EVALUATION OF FIELD-SCALE $CO_2$ INJECTION

Comprehensive field-scale reservoir simulation is conducted in this chapter to evaluate performance of various $CO_2$ injection strategies in a targeted tight oil formation. With the analyzed fluid properties and findings from the laboratory experiments, a reservoir geological model is developed with the field data collected from the Bakken formation located in Saskatchewan, Canada. Once history match is completed, the tuned reservoir geological model is utilized to evaluate performance of various $CO_2$ injection strategies, while sensitivity analysis is conducted to examine effects of operational parameters on oil recovery from the tight oil formation.

## 4.1 Field Background

The targeted reservoir is the Bakken formation located in the south Saskatchewan, Canada. The selected region is shown in **Figure 4.1**, covering an area of 4.0 × 2.8 km with a payzone thickness ranging from 6-14 m. The formation matrix permeability ranges from 0.05-0.70 mD, while the porosity ranges from 5-10%. The initial water saturation ranges from 15-20%, while initial oil saturation ranges from 80-85%. The initial reservoir pressure and temperature are 27.7 MPa and 63ºC,

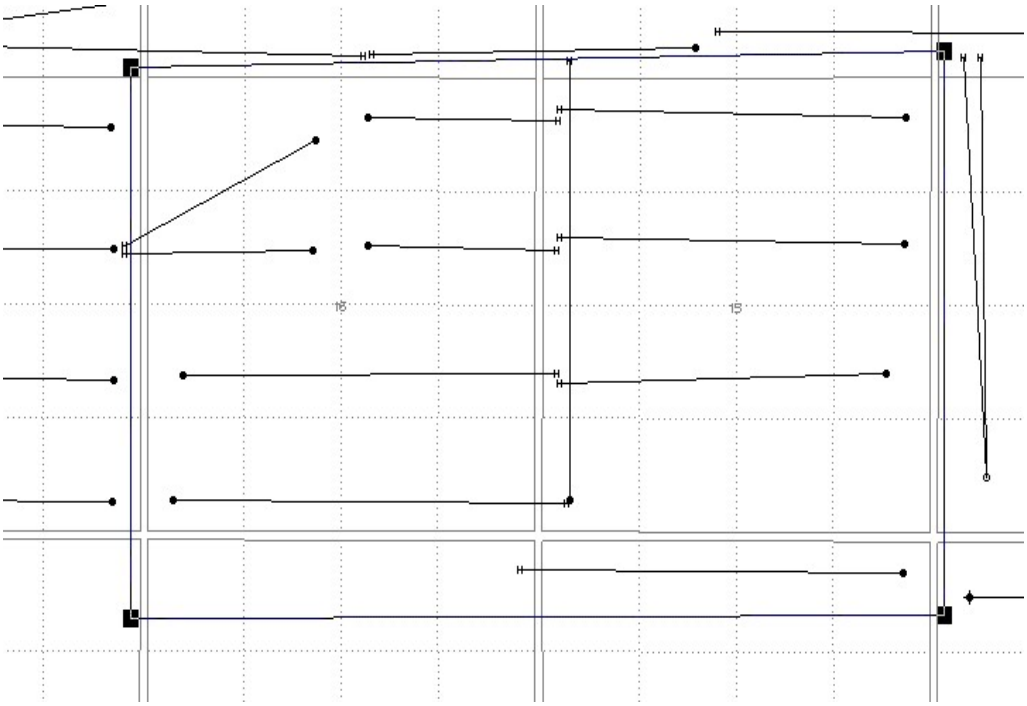

**Figure 4.1** Location map of an oilfield selected in the Bakken formation

respectively. Density and viscosity of crude oil are measured to be 801.2 kg/$m^3$ and 2.17 cP at 20ºC and atmospheric pressure, respectively, while compositional analysis results of the oil are tabulated in **Table 3.2**.

There are 11 horizontal wells in the selected region, all of which have been massively fractured. According to the field data, the width of the facture in the Bakken formation is measured to be 0.03 m with the fracture permeability of 4850 mD, while the half length of the fracture is 100 m with an interval between fractures of 100 m.

The selected field started to produce from July 2010 at its primary recovery stage. The oil production, water production and gas production of each well are shown in **Figures 4.2a-c**, while the details can be found in Appendix. By November 2012, only 1.48% of OOIP is recovered from this field during the primary recovery stage.

## 4.2 Reservoir Geological Model

A reservoir geological model is created by using the CMG GEM module according to the geological data collected from the oilfield. The CMG Winprop module (version 2009, Computer Modelling Group Ltd.) is used to prepare the fluid properties for the GEM simulator (version 2009, Computer Modelling Group Ltd.). The fluid properties used in the reservoir geological model are the same as those of Chapter 3 (see **Tables 3.1-3.2**).

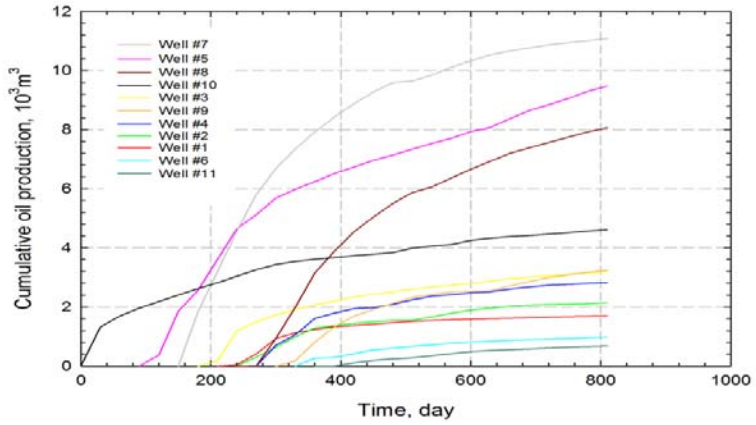


**(a)**

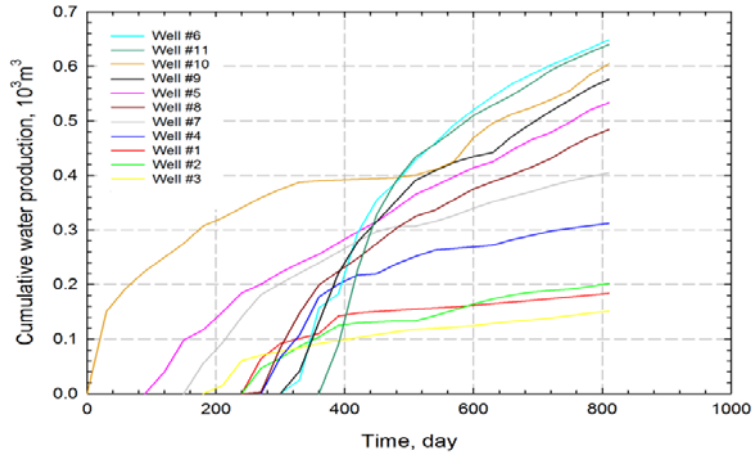


**(b)**

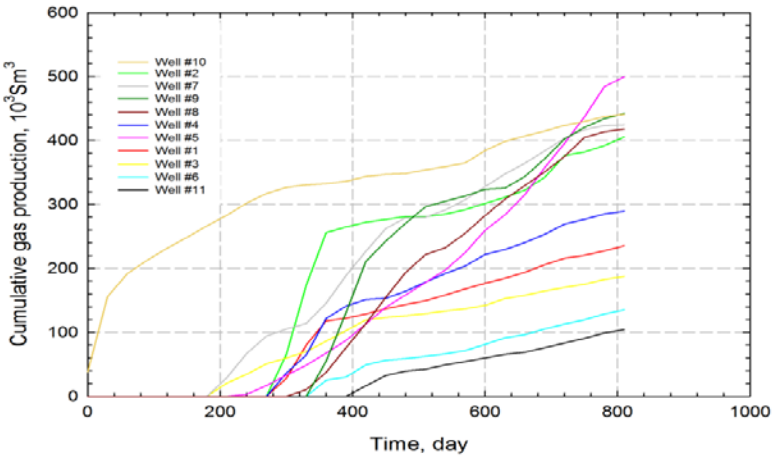


**(c)**

**Figure 4.2 (a)** Cumulative oil production, **(b)** Cumulative water production, and **(c)** Cumulative gas production of each well in the selected region

The 3D view of the model is shown in **Figure 4.3**, where 11 horizontal wells are placed with massive fractures whose properties are the same as that described in the previous section. The reservoir geological model is divided into 5 layers, each of which has a slightly different distribution of initial oil saturation (see **Figures 4.4a-e**).

## 4.3 Simulation Procedure

According to field production history (i.e., water production, oil production and gas production), average reservoir pressure is consequently estimated from July 2010 to October 2012 by using the material balance principles, which are detailed as follows (Economides *et al*., 1993):

$$N_p\left[B_{o2} + \left(R_p - R_{so2}\right)B_{g2}\right] + W_pB_{w2} = N\left(E_o + mE_g + E_{f,w}\right) + (W_l + W_e)B_{w2} + G_lB_{g2} \quad [4\text{-}1]$$

where $N_p$ is the cumulative oil production; $B_o$ is formation volume factor for oil; $R_p$ is cumulative producing gas-oil ratio; $R_{so}$ is the solution gas-oil ratio; $B_g$ is formation volume factor for gas; $W_p$ is cumulative water production; $B_w$ is formation volume factor for water; $N$ is original oil in place; $m$ is initial gas cap size; $W_l$ is cumulative water injected; $W_e$ is cumulative aquifer influx; and $G_l$ is cumulative gas injected.

$E_o$ is associated with oil and solution gas expansion:

$$E_o = (B_{o2} - B_{o1}) + (R_{so1} - R_{so2})B_{g2} \quad [4\text{-}2]$$

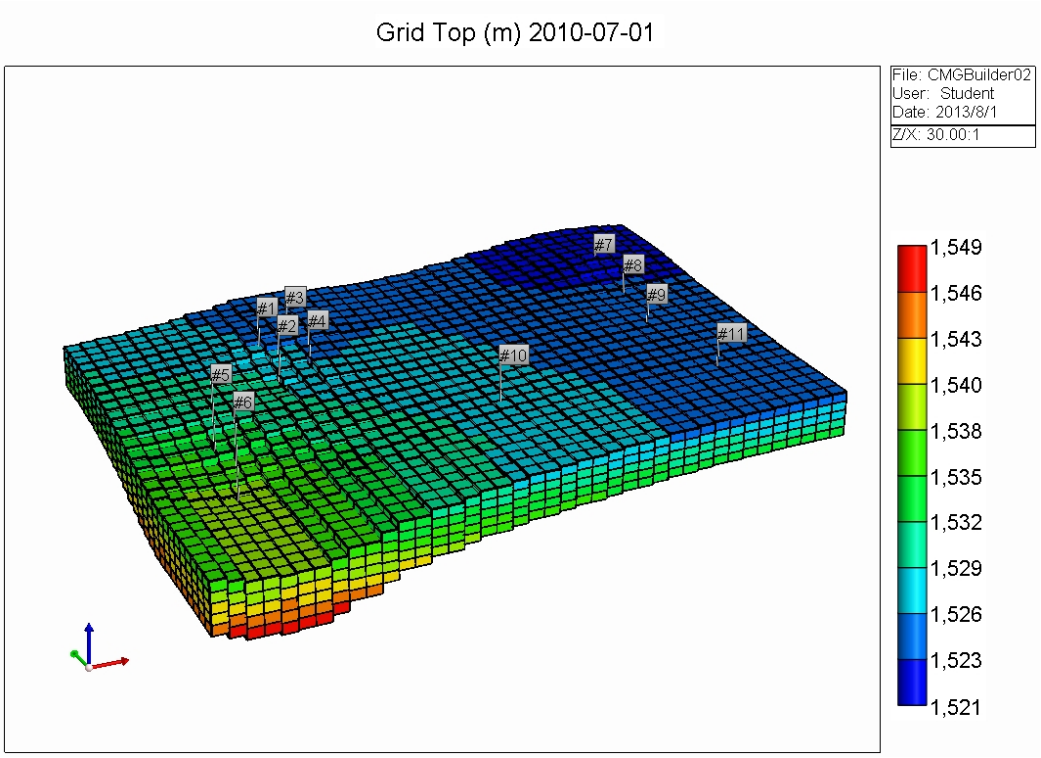


**Figure 4.3** Schematic diagram of 3D view of the reservoir geological model

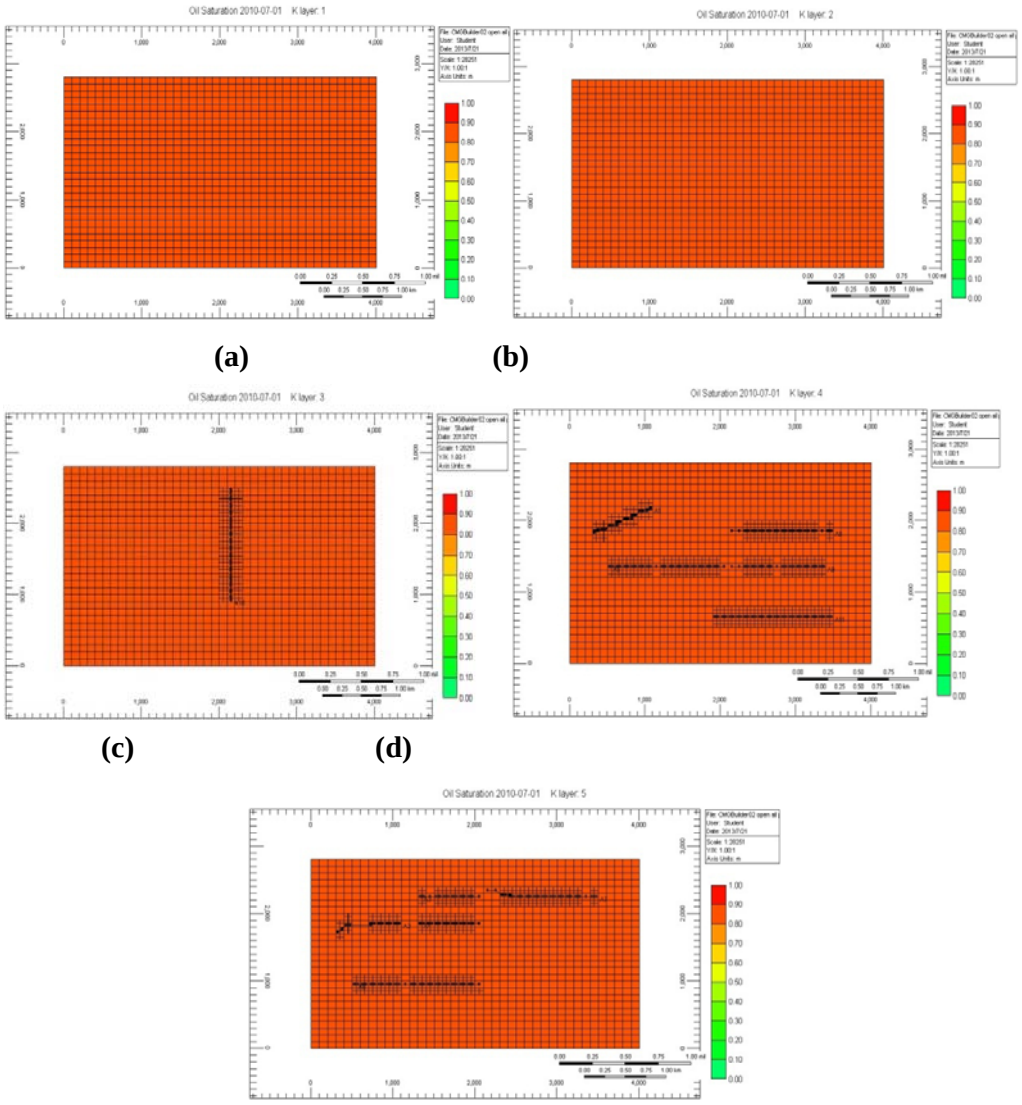


**Figure 4.4** Distribution of initial oil saturation for **(a)** Layer #1, **(b)** Layer #2, **(c)** Layer #3, **(d)** Layer #4, and **(e)** Layer #5

$E_g$ is gas cap expansion term:

$$E_g = B_{o1}\left(\frac{B_{g2}}{B_{g1}} - 1\right) \quad [4\text{-}3]$$

$E_{f,w}$ is the rock and water compression/expansion term:

$$E_{f,w} = -(1+m)B_{o1}\frac{c_r + c_w S_{w1}}{1 - S_{w1}}\Delta P c_r c_w S_w \quad [4\text{-}4]$$

where $c_r$ represents pore compressibility; $c_w$ represents water compressibility; and $S_w$ represents water saturation.

With oil production rate for each well as the input constraints, relative permeability curves and capillary pressure curves are subsequently tuned to history match the average reservoir pressure profile obtained from the reservoir pressure decline analysis. With the tuned reservoir geological model, recovery performance of waterflooding, continuous $CO_2$ flooding, miscible $CO_2$-WAG flooding, and $CO_2$ huff-n-puff processes is evaluated. Sensitivity analysis is further performed on the operational parameters including production pressure, WAG ratio, slug size, injection pressure, and soaking time during $CO_2$ injection processes.

## 4.4 Result and Discussion

### 4.4.1 Reservoir pressure estimation

According to the material balance principles (see Equations 4-1 to 4-4), calculated reservoir pressure as a function of time for the primary recovery process is shown in **Figure 4.5**. The reservoir pressure decreases slightly for the first 6

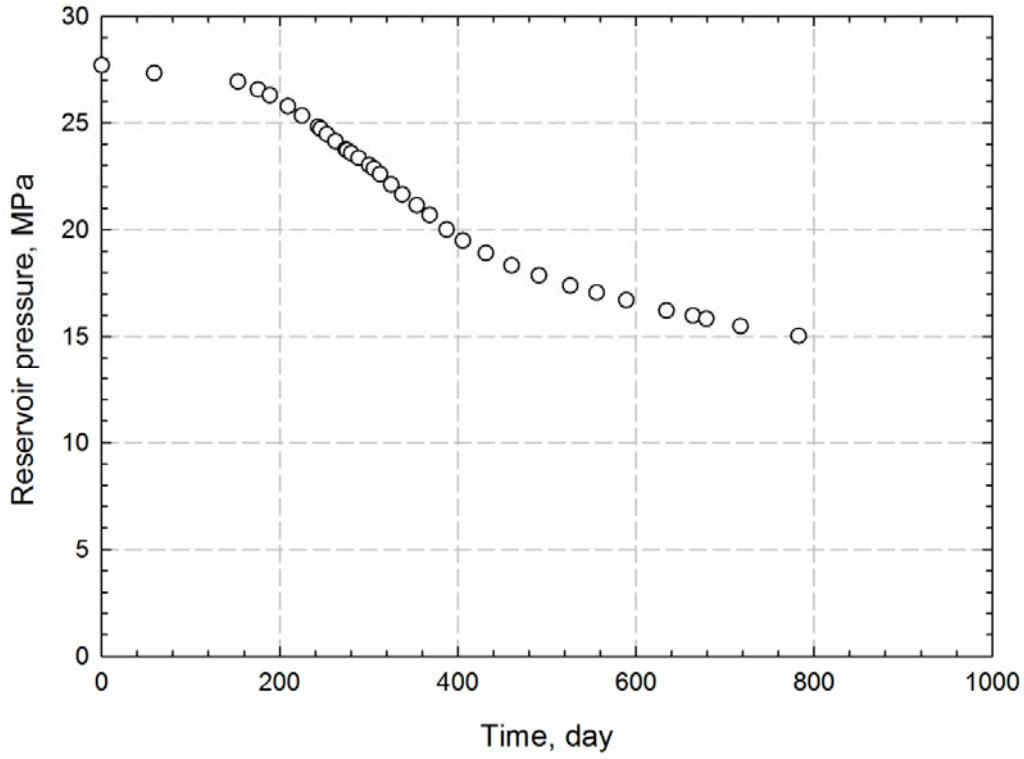


**Figure 4.5** Calculated reservoir pressure versus time

months due to only two wells under production. As more wells start producing, pressure decline becomes more significant, though the trend of pressure decrease becomes gentle again at the later time period. This is due to a decrease in oil production, resulting in a minor pressure decline in the reservoir.

### 4.4.2 History matching

With actual oil production for each well as the input constraints, relative permeability curves and capillary pressure curves are tuned to history match the average reservoir pressure profile obtained from previous pressure decline analysis. **Figures 4.6a** and **b** show the tuned water and oil relative permeability curves, gas and liquid relative permeability curves and capillary pressure curves, respectively. It is found that the relative permeability curves and capillary pressure curves have similar trends as the coreflooding results of Chapter 3, indicating that the reservoir model in this study has similar geological properties as the core samples used in previous experiments.

**Figure 4.7** presents the history matching results for primary recovery process, where the average reservoir pressure calculated from the decline analysis is well matched by simulation. The distributions of residual oil, water, and gas saturation in each layer after primary recovery are shown in **Figure 4.8**, **Figure 4.9**, and **Figure 4.10**, respectively. Compared to the initial condition, change of residual oil saturation is minor due to only 1.48% of OOIP recovered by November 2012, while

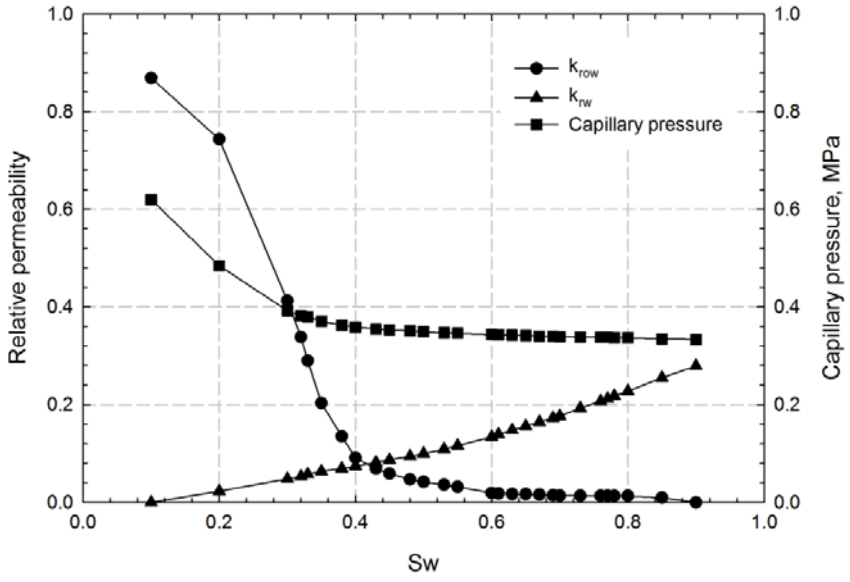


**(a)**

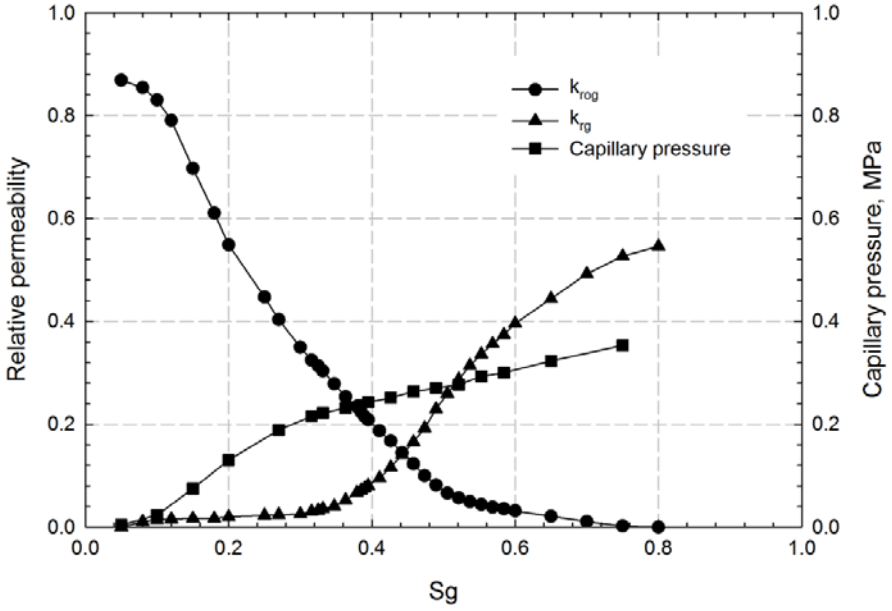


**(b)**

**Figure 4.6** Relative permeability for **(a)** Water-oil system and its capillary pressure and **(b)** Gas-liquid system and its capillary pressure for the field-scale reservoir simulation

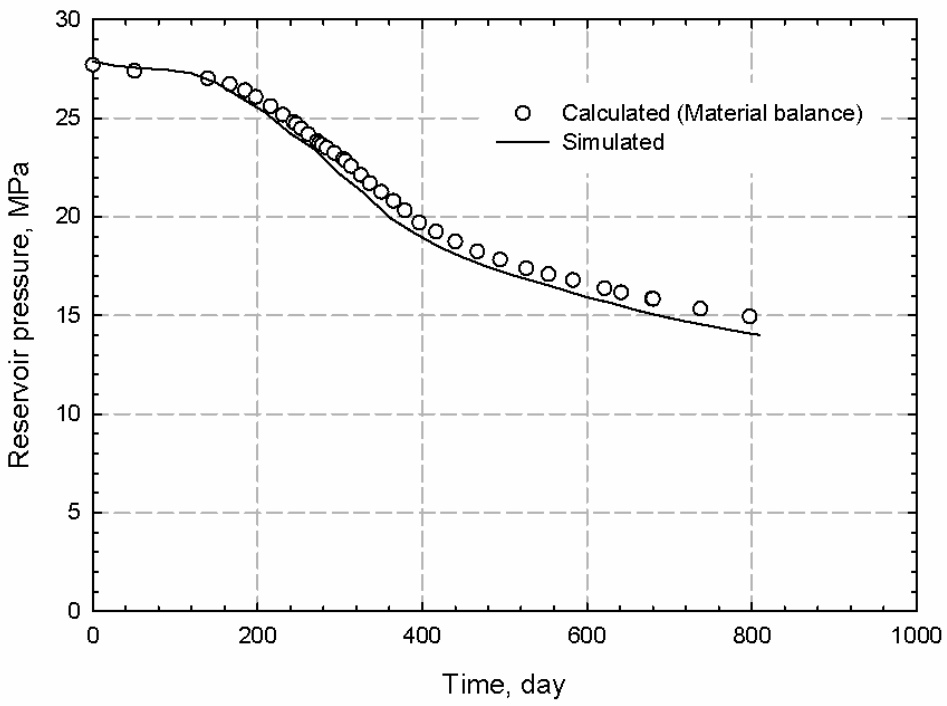


**Figure 4.7** Simulated reservoir pressure and its calculated value from material balance versus time

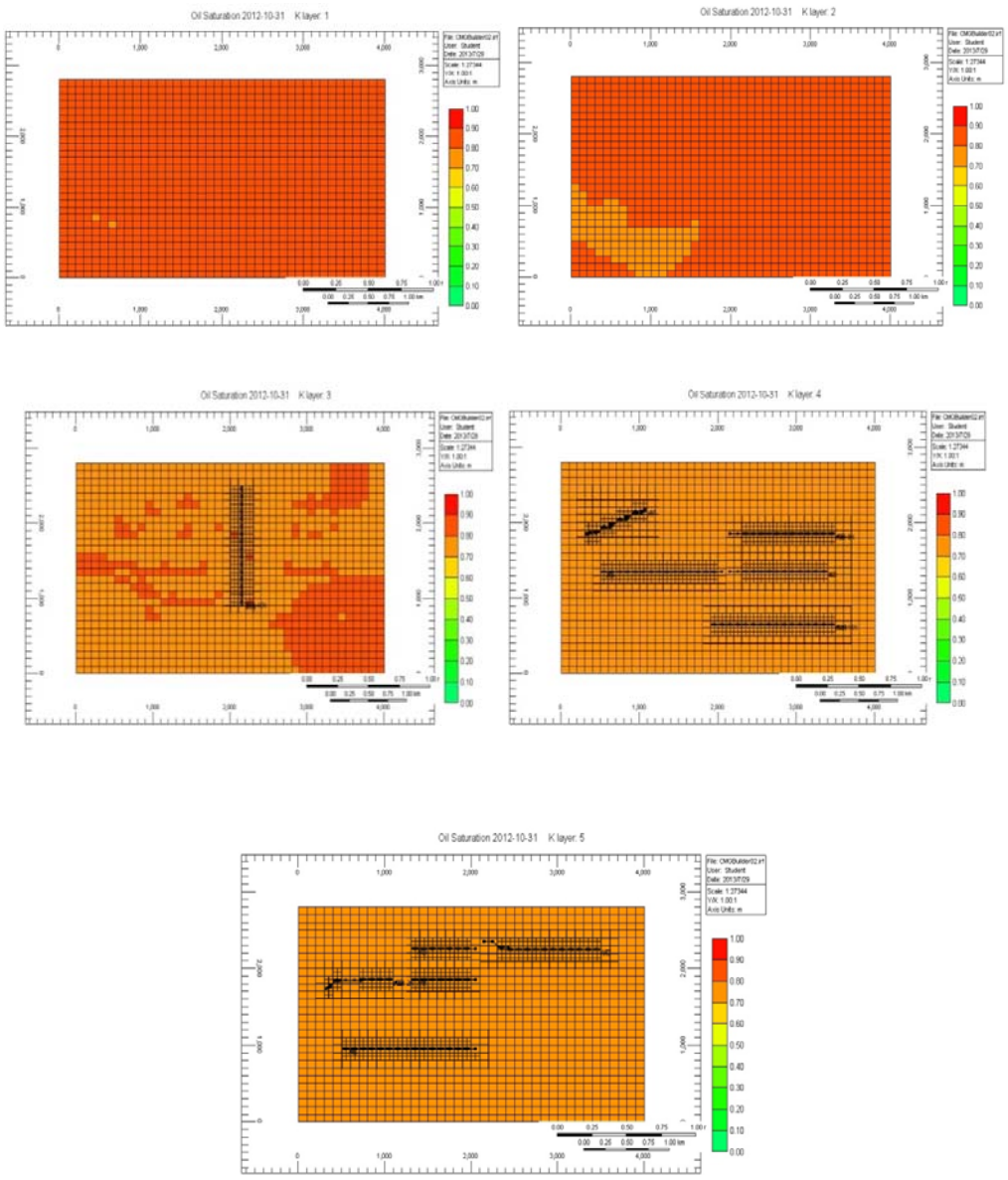


**Figure 4.8** Distribution of residual oil saturation after primary recovery process for **(a)** Layer #1, **(b)** Layer #2, **(c)** Layer #3, **(d)** Layer #4, and **(e)** Layer #5

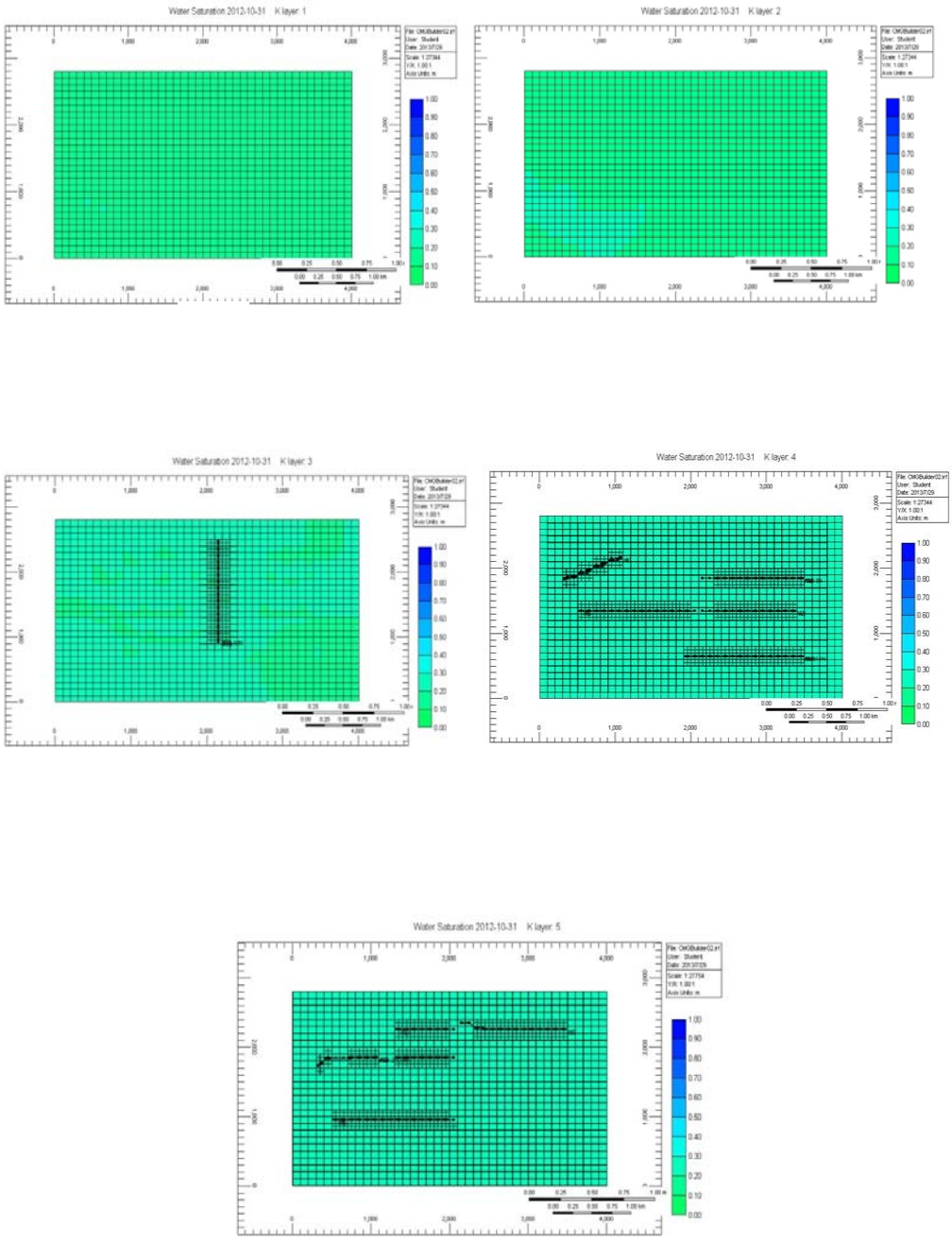


**Figure 4.9** Distribution of residual water saturation after primary recovery process for **(a)** Layer #1, **(b)** Layer #2, **(c)** Layer #3, **(d)** Layer #4, and **(e)** Layer #5

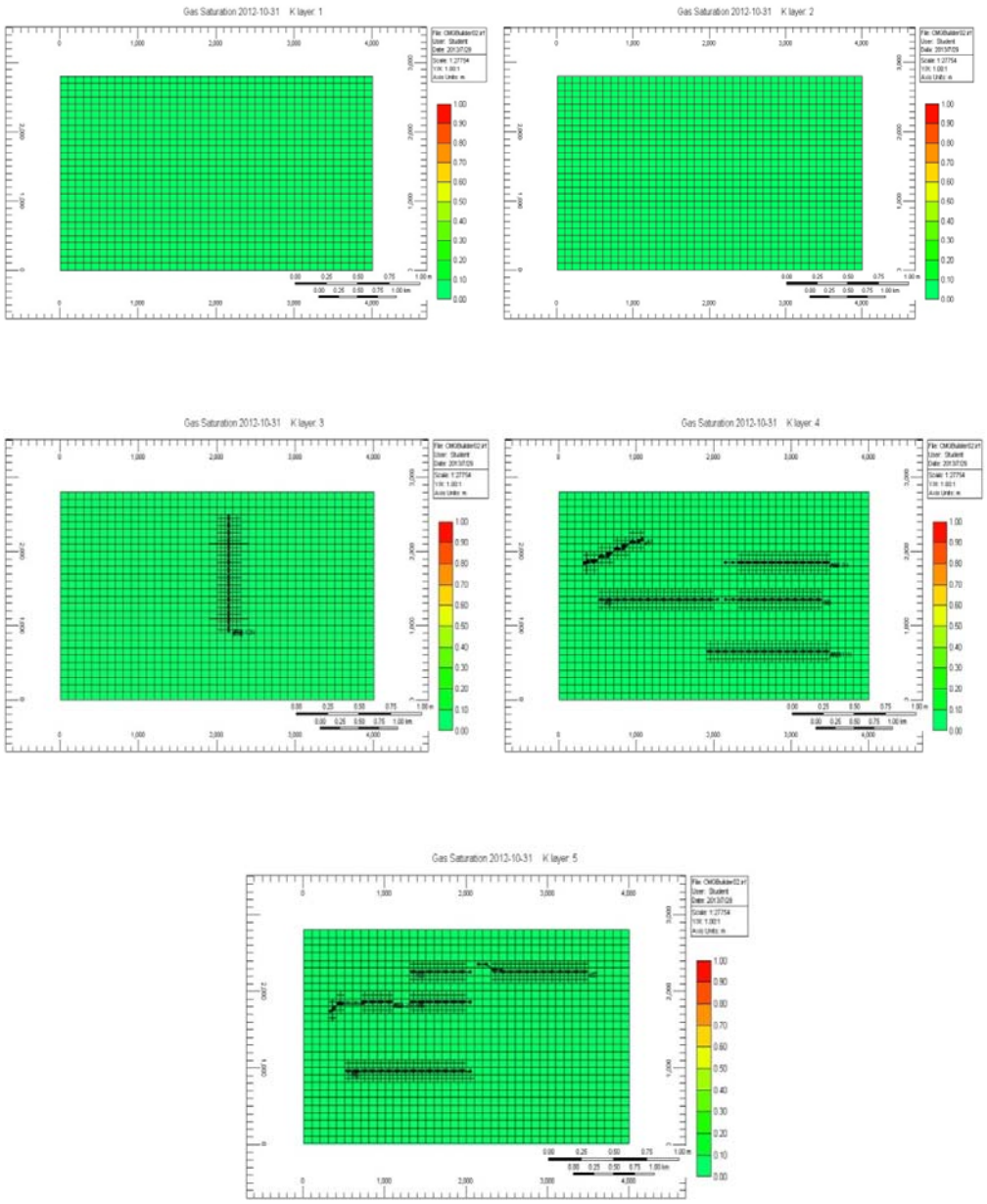


**Figure 4.10** Distribution of residual gas saturation after primary recovery process for **(a)** Layer #1, **(b)** Layer #2, **(c)** Layer #3, **(d)** Layer #4, and **(e)** Layer #5

a minor difference is also observed for the residual gas saturation in each layer. This is attributed to the fact that the average reservoir pressure is 14.5 MPa, which is higher than the bubble-point pressure.

### 4.4.3 Sensitivity analysis

#### 1) Well pattern

With the tuned reservoir model, recovery performance of waterflooding is evaluated for 20 years with various well patterns. As shown in **Figures 4.11a-c**, three well patterns (i.e., Patterns #1, #2, and #3) are evaluated, where the injection wells are highlighted. Simulation is performed with constant water injection rate of 35 $m^3$/d for each injector, while oil is produced under a constant production pressure of 11.5 MPa. According to field operation practice, a production well will be terminated once the oil rate is lower than 0.5 $m^3$/d (Pinto Oilfield, 2012). Recovery performance of various well patterns is shown in **Figure 4.12**. Ultimate oil recovery of Patterns #1, #2, and #3 is estimated to be 11.4%, 8.3% and 12.7% of OOIP, respectively. It is found that Pattern #3 results in the highest oil recovery compared to Patterns #1 and #2. As such, Pattern #3 is thereafter to be applied for performance evaluation in the following continuous $CO_2$ flooding and $CO_2$-WAG flooding.

The residual oil, water, and residual gas saturations in each layer of Pattern #3 are distributed as shown in **Figure 4.13**, **Figure 4.14**, and **Figure 4.15**, respectively. Oil recovery is found to be favourable in the region with high permeability. The

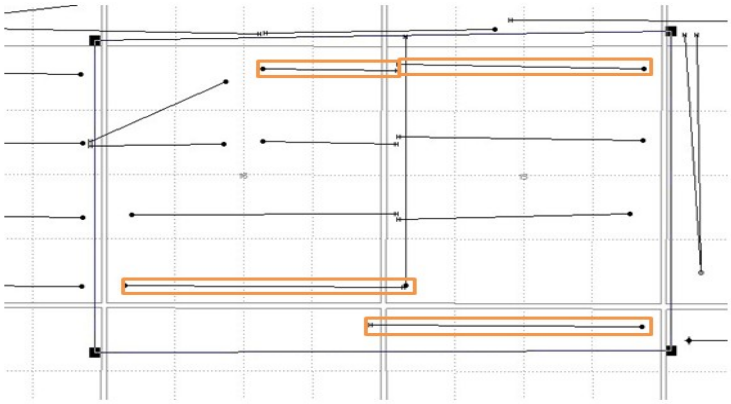

**(a)**

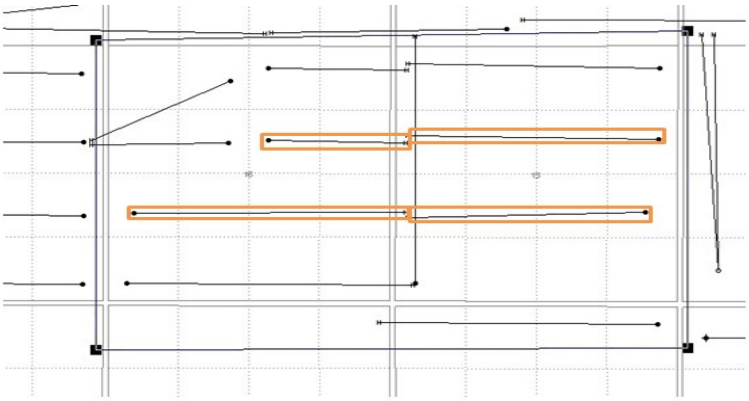

**(b)**

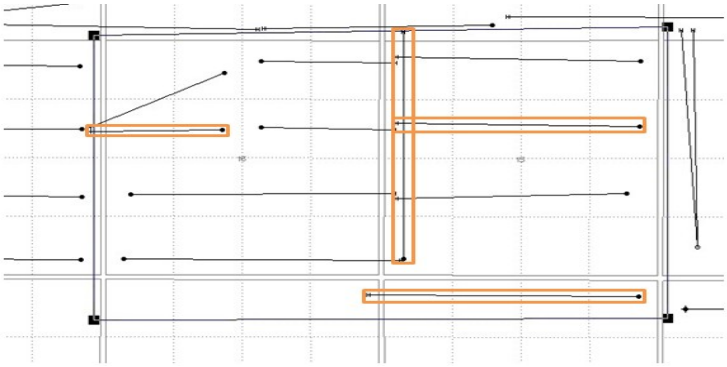

**(c)**

**Figure 4.11** Schematic diagram of **(a)** Pattern #1, **(b)** Pattern #2, and **(c)** Pattern #3 for waterflooding processes (Injector: Orange color; Producer: Black color)

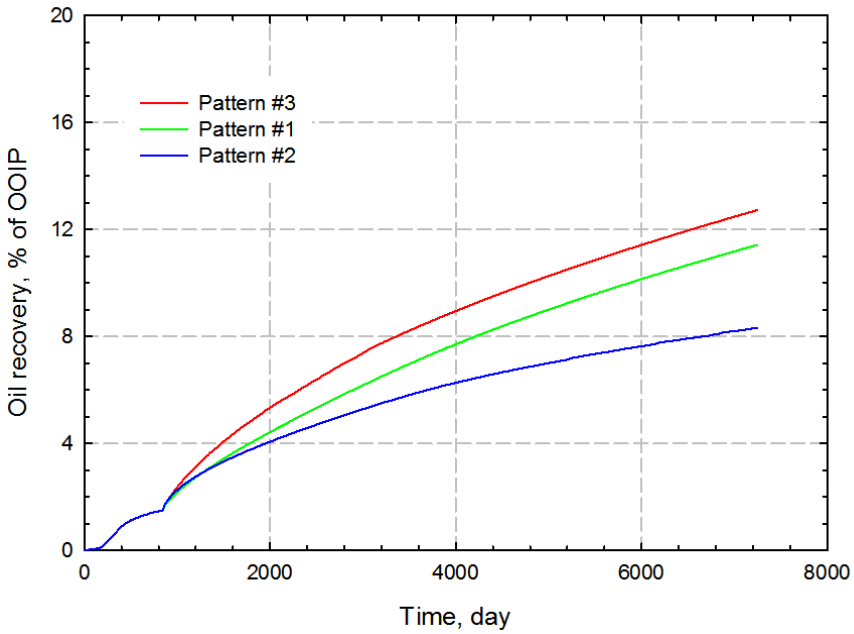


**Figure 4.12** Simulated oil recovery versus time for different well patterns of waterflooding processes

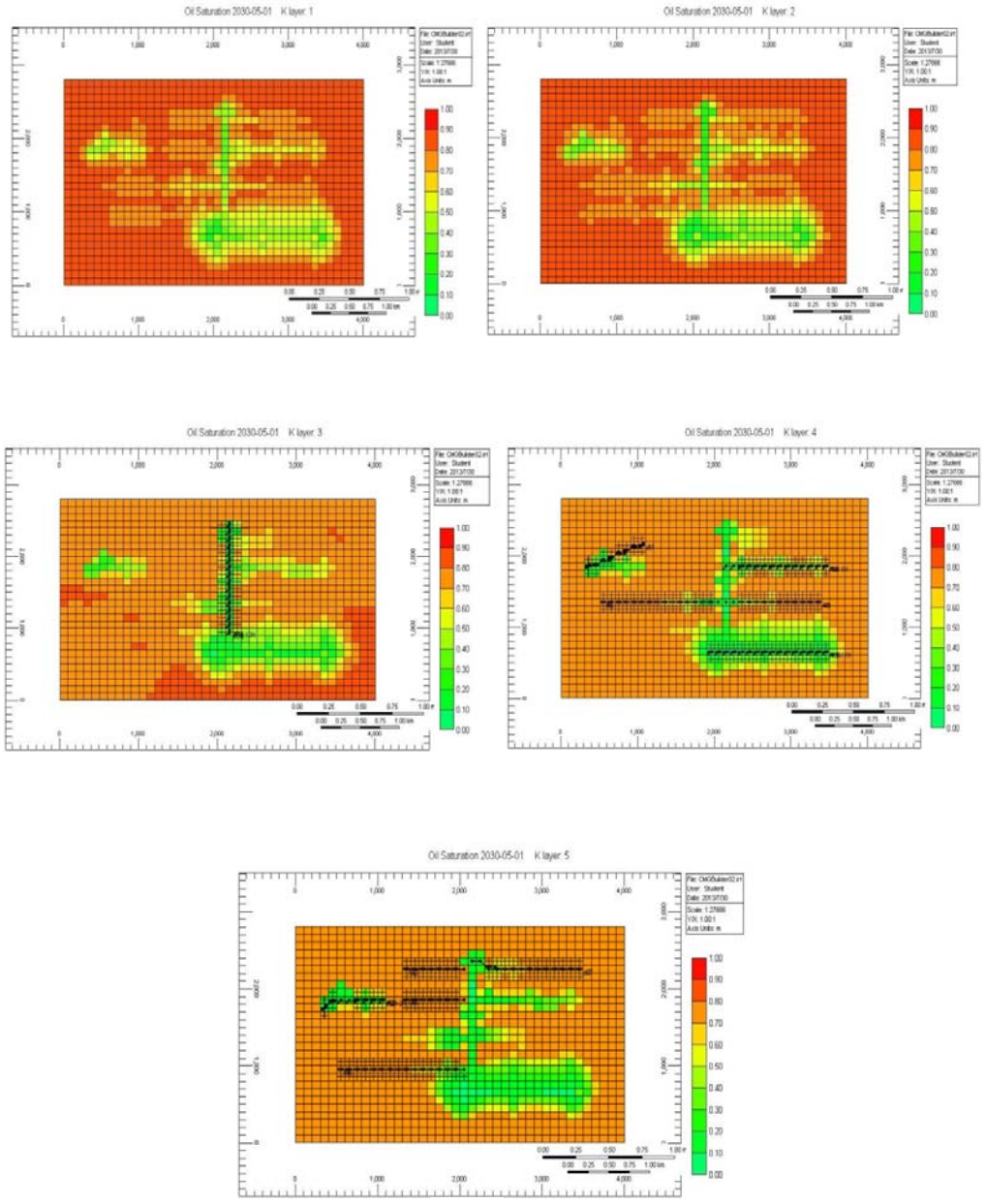


**Figure 4.13** Distribution of residual oil saturation in waterflooding processes for **(a)** Layer #1, **(b)** Layer #2, **(c)** Layer #3, **(d)** Layer #4, and **(e)** Layer 5

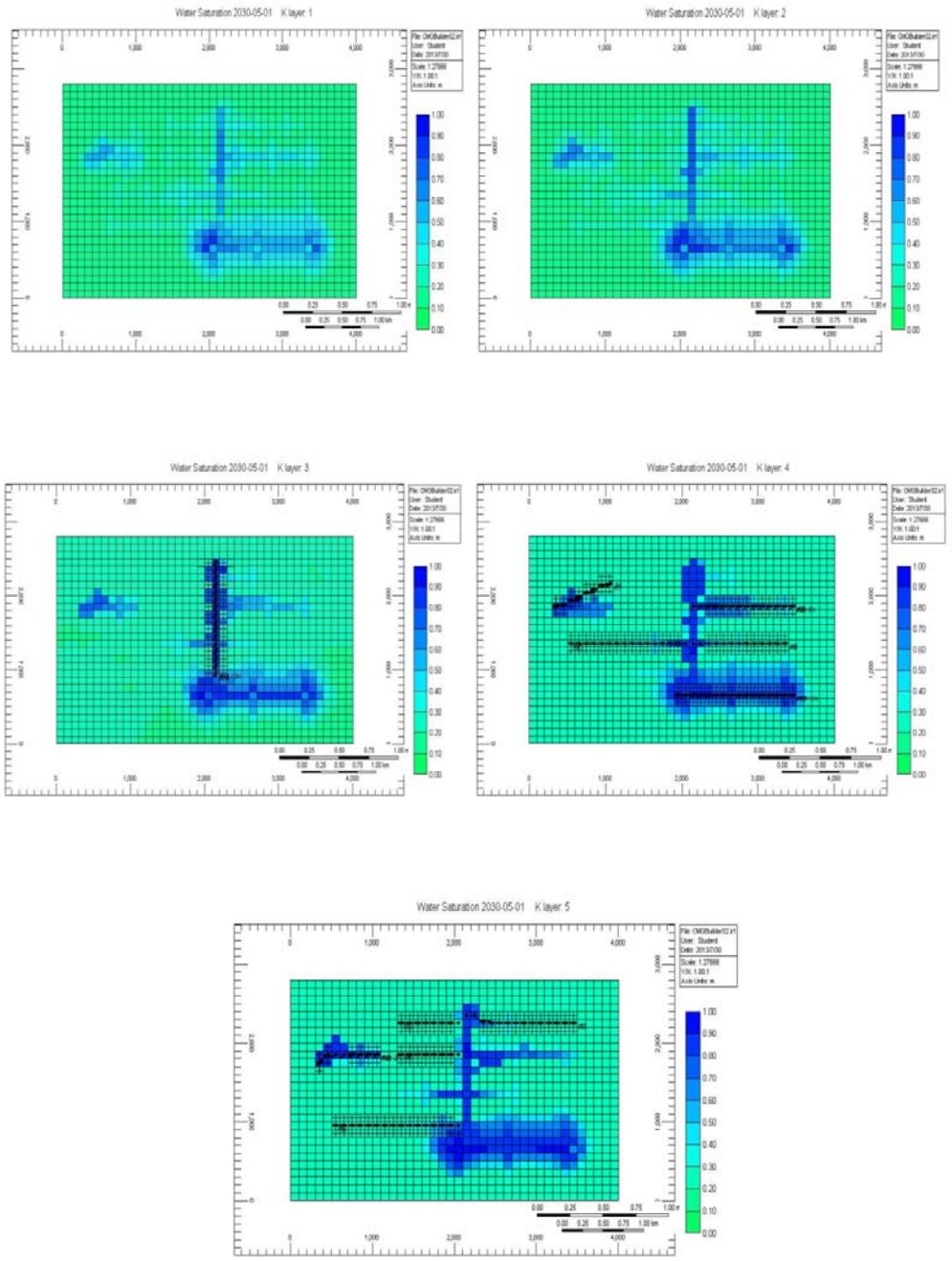


**Figure 4.14** Distribution of residual water saturation in waterflooding processes for **(a)** Layer #1, **(b)** Layer #2, **(c)** Layer #3, **(d)** Layer #4, and **(e)** Layer 5

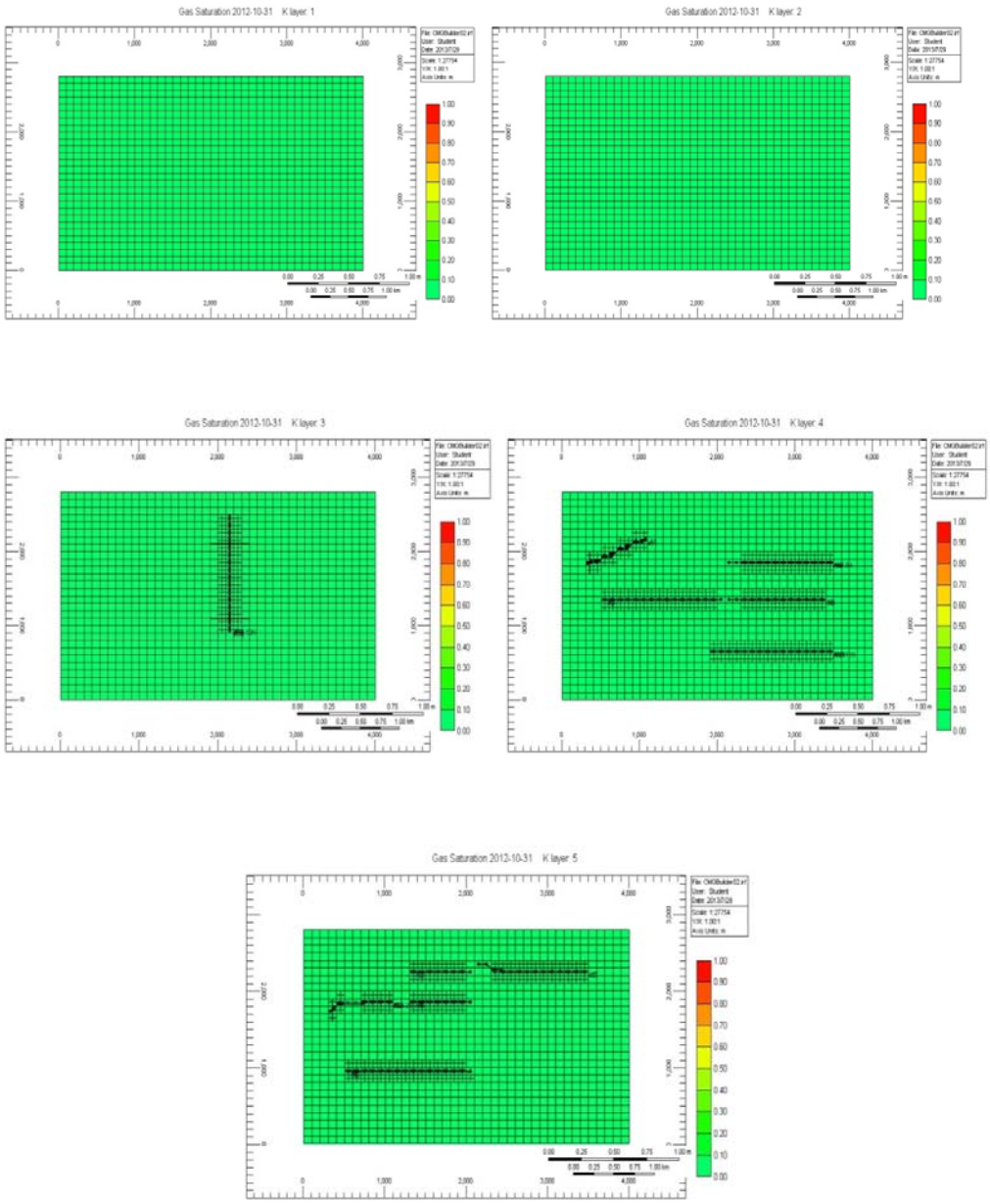


**Figure 4.15** Distribution of residual gas saturation in waterflooding processes for **(a)** Layer #1, **(b)** Layer #2, **(c)** Layer #3, **(d)** Layer #4, and **(e)** Layer 5

residual oil saturation of the upper layers is higher compared to that of lower layers. This is because all the horizontal wells are drilled in the bottom layers. As for the gas saturation, a minor difference is observed in each layer. This is attributed to the fact that the average reservoir pressure of waterflooding is still higher than the bubble-point pressure, resulting in little free gas formed in the reservoir.

**2) Production pressure**

The tuned reservoir model is utilized to numerically examine effect of different bottomhole pressures (BP) of the producers ranging from 6.5 MPa to 11.5 MPa on oil recovery of continuous $CO_2$ flooding. As can be seen in **Figure 4.16**, when the production pressure is lower than 9.5 MPa, ultimate oil recovery keeps increasing with an increase in BP of producers. However, the BP of the injectors exceeds the MMP of 9.7 MPa when the BP of producers is higher than 9.5 MPa. As such, ultimate oil recovery becomes no longer sensitive to the increase of the BP for the producers so that the optimum BP for the producers in continuous $CO_2$ flooding process is usually considered to be around MMP between the crude oil and $CO_2$ (Dong *et al*., 2001). This finding is consistent with that obtained from the previous coreflooding experiments.

The recovery factor at production pressure of 9.5 MPa is calculated to be 12.0% of OOIP, which is nearly the same as that of waterflooding. This is attributed to the low sweep efficiency and early breakthrough during $CO_2$ flooding process. The corresponding distributions of residual oil, water, and gas saturation in each layer are illustrated in **Figure 4.17, Figure 4.18**, and **Figure 4.19**, respectively. Although the

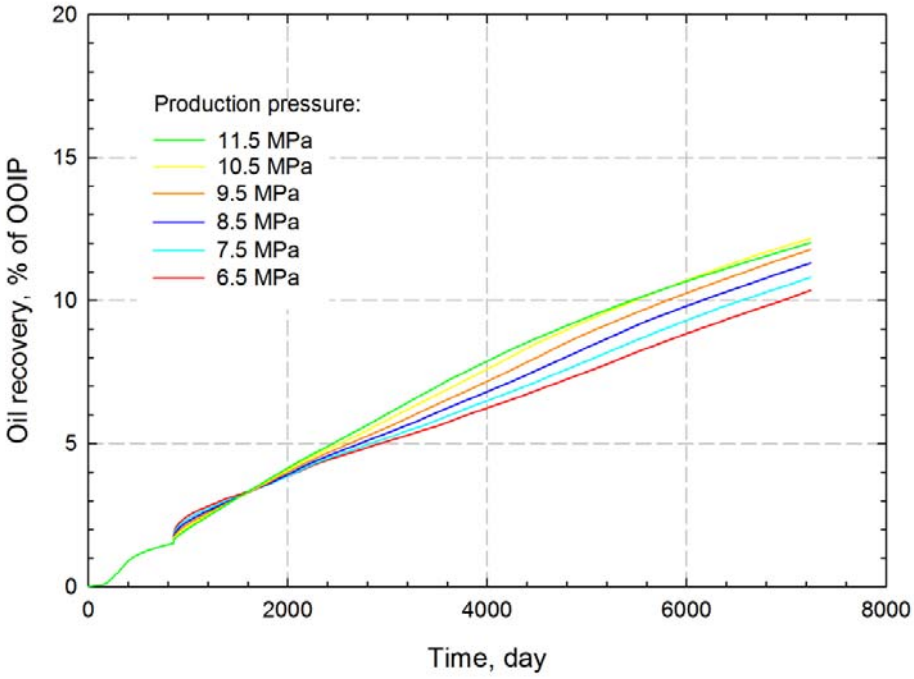


**Figure 4.16** Oil recovery of continuous $CO_2$ flooding with different production pressures

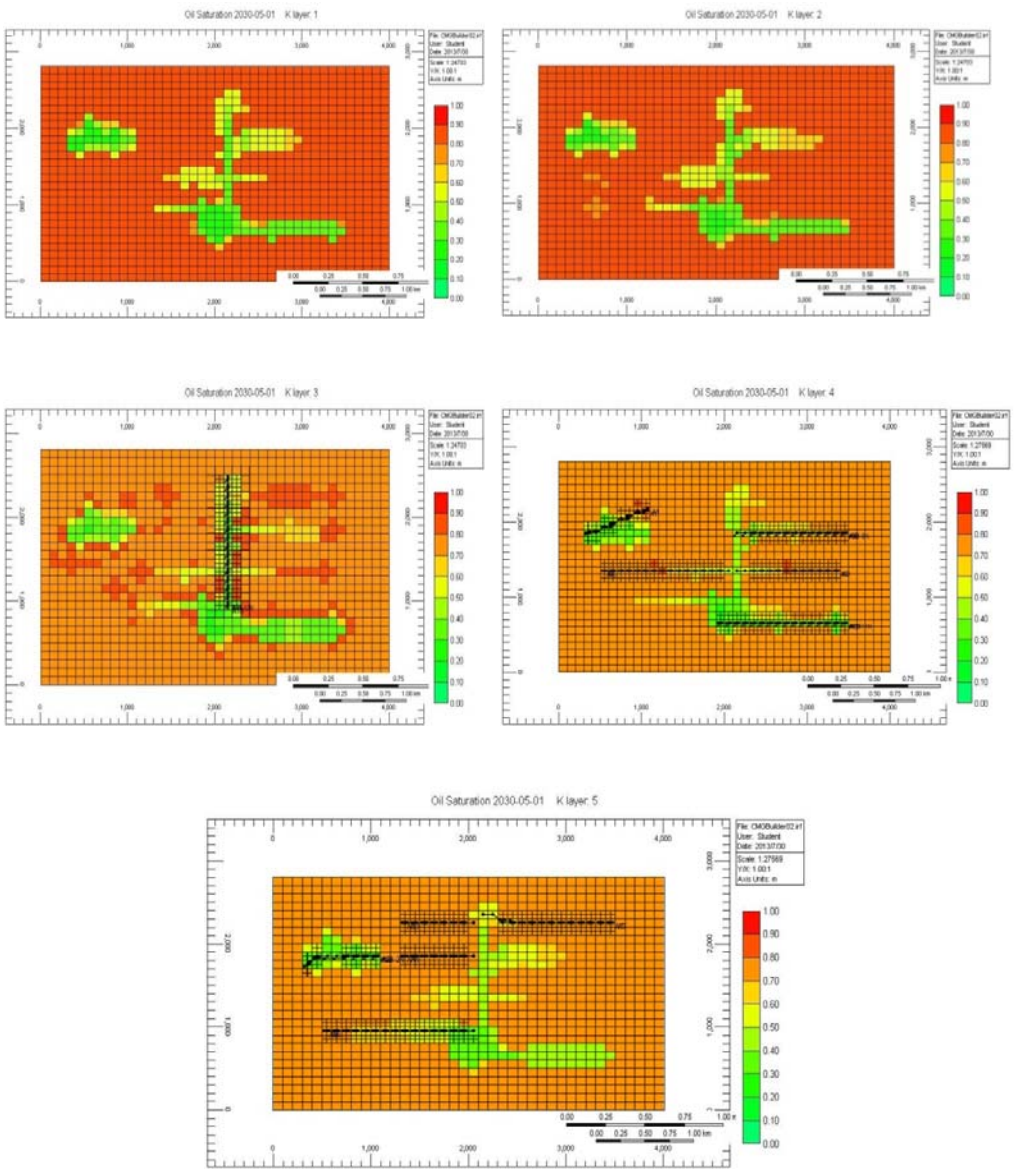


**Figure 4.17** Distribution of residual oil saturation in continuous $CO_2$ flooding processes for **(a)** Layer #1, **(b)** Layer #2, **(c)** Layer #3, **(d)** Layer #4, and **(e)** Layer #5

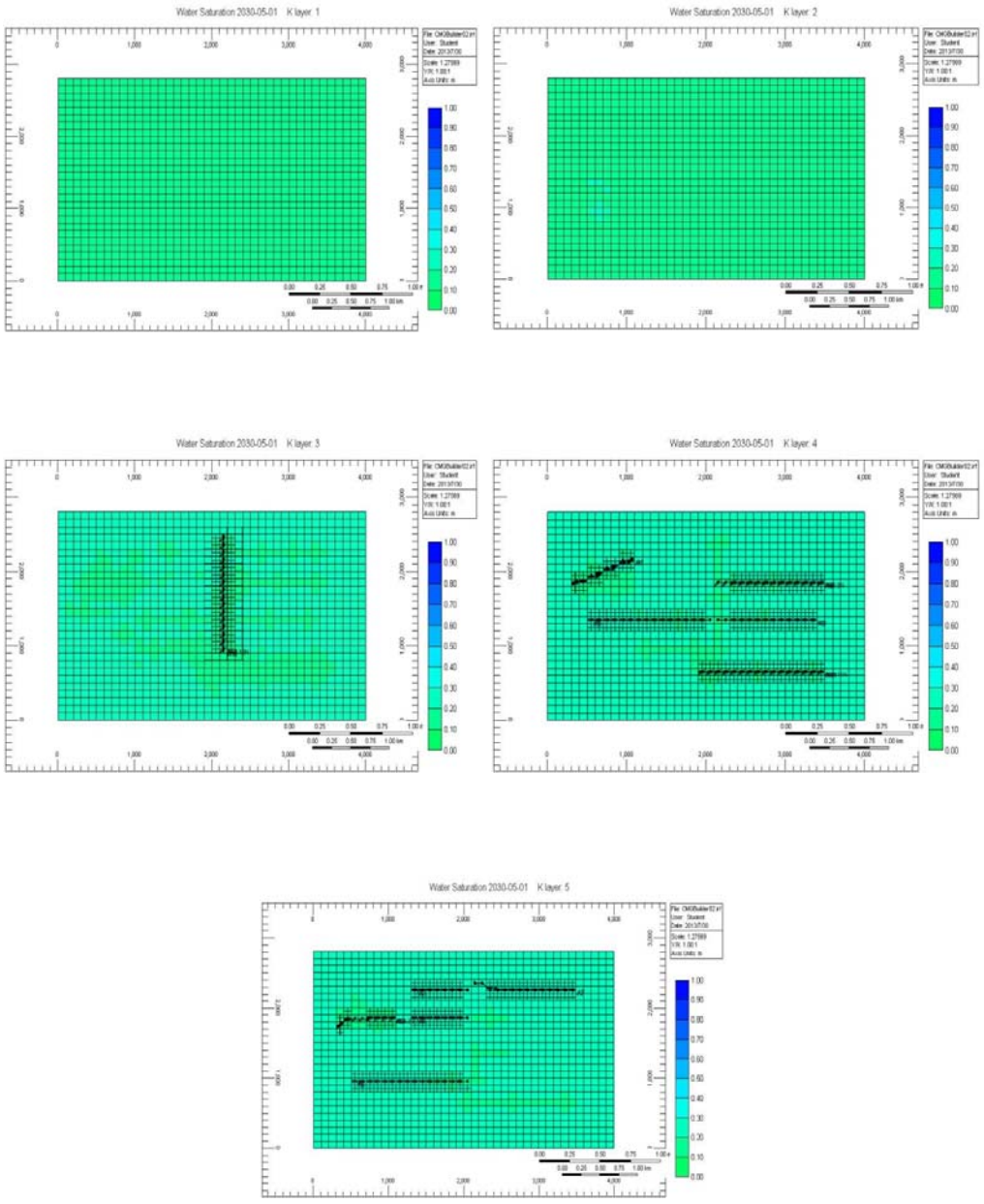


**Figure 4.18** Distribution of residual water saturation in continuous $CO_2$ flooding processes for **(a)** Layer #1, **(b)** Layer #2, **(c)** Layer #3, **(d)** Layer #4, and **(e)** Layer #5

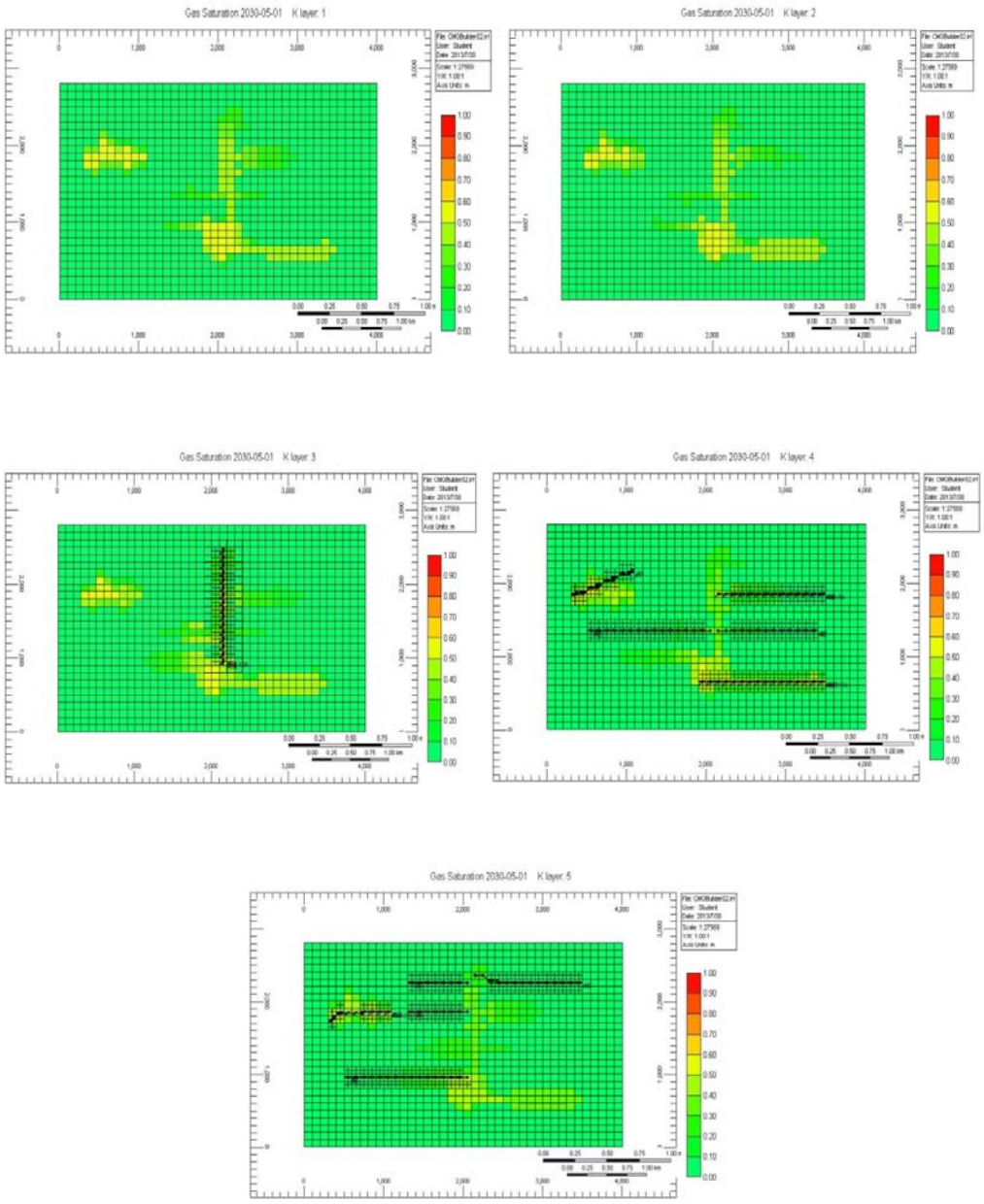


**Figure 4.19** Distribution of residual gas saturation in continuous $CO_2$ flooding processes for **(a)** Layer #1, **(b)** Layer #2, **(c)** Layer #3, **(d)** Layer #4, and **(e)** Layer #5

area swept by continuous $CO_2$ flooding is smaller compared to that of waterflooding, the recovery efficiency remains higher in the region where $CO_2$ is able to sweep, leading to a lower residual oil saturation. However, the residual gas saturation of each layer is generally low, except for the region around wells. This is because the gas tends to break through shortly after $CO_2$ is injected, leading to both low sweep efficiency and low residual gas saturation.

**3) WAG ratio**

The tuned reservoir geological model same as the one for continuous $CO_2$ flooding is implemented to examine the effect of WAG ratios on oil recovery during miscible $CO_2$-WAG flooding processes. Either water or $CO_2$ is injected with a constant rate, while oil is produced under a constant BP of 10.5 MPa. To allow pragmatic field implementation, a cycle time of 6 months is applied for each scenario (Chen *et al.*, 2010). As can be seen from **Figure 4.20**, an increase in water slug size contributes to improving sweep efficiency, though the enhancement of oil recovery is not significant when WAG ratio is increased from 0.5 to 2.0. This means that it is difficult to further increase the sweep efficiency under the above conditions due mainly to early gas and water breakthrough and nearly constant water saturation in the formation rock. Thus, the optimum WAG ratio of field production can be set to be 2.0 with an oil recovery up to 14.2% of OOIP.

**4) Cycle time**

The tuned reservoir model is further implemented to examine the effect of

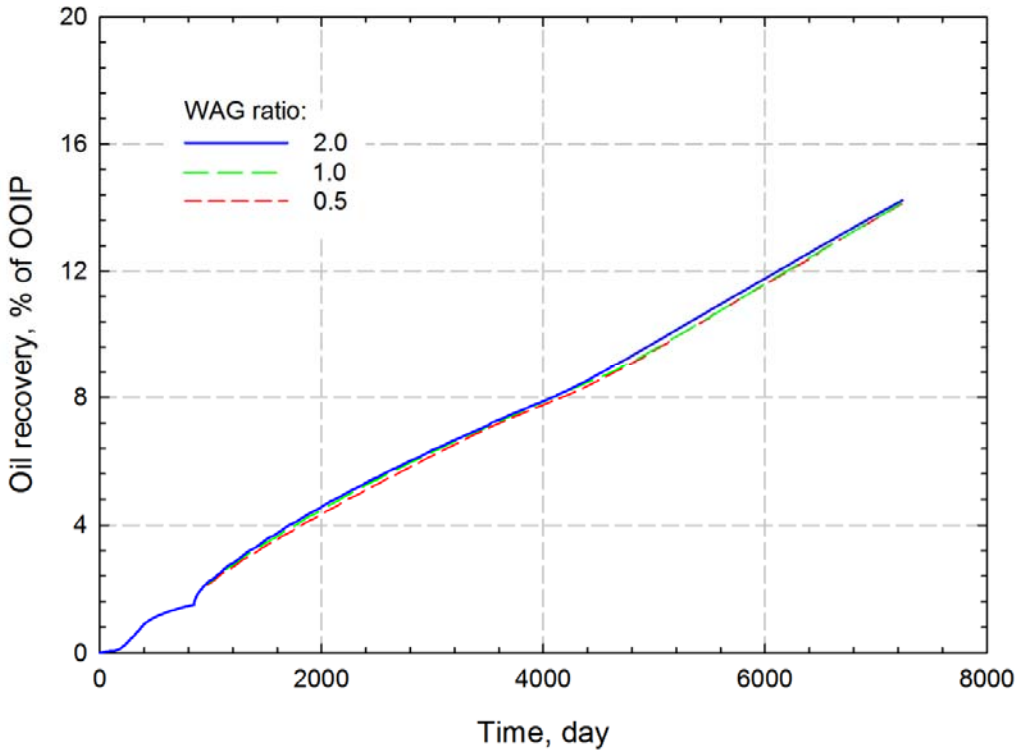


**Figure 4.20** Oil recovery profiles with different WAG ratios for miscible $CO_2$-WAG flooding processes

cycle time on oil recovery in a miscible $CO_2$-WAG process. The WAG ratio is set to be 2.0. The cycle time changes from 6 to 12 months. The simulation results are presented in **Figure 4.21**. It is found that a shorter cycle time usually results in a higher oil recovery. This is because a shorter cycle time results in a shorter slug size for both water and $CO_2$ so that there exists less chance to induce an early breakthrough, and hence a higher recovery efficiency. The ultimate oil recovery of $CO_2$-WAG flooding process is found to be 14.2%, 14.0%, and 13.9% of OOIP at the cycle time of 6, 9, and 12 months, respectively. Obviously, the cycle time of 6 months together with a WAG ratio of 2.0 is considered to be optimum for the $CO_2$-WAG flooding process.

The distributions of residual oil, water, and gas saturation in each layer under the optimum condition are depicted in **Figure 4.22**, **Figure 4.23,** and **Figure 4.24**, respectively. Compared to the previous continuous $CO_2$ flooding, the swept area is improved due to the introduction of water, indicating a higher sweep efficiency, and thus a lower residual oil saturation of each layer.

**5) Soaking time**

In this study, the tuned numerical model is further applied to evaluate the recovery performance of miscible $CO_2$ huff-n-puff processes under various soaking times ranging from 6-15 days. The BP for the injectors and producers are set to be 18.0 MPa and 9.5 MPa, respectively. For each well, $CO_2$ is continuously injected for 1 month at first. Then the well is shut in to soak for 6, 10 and 15 days, respectively. Finally, oil is produced for another 6 months under constant pressure of 9.5 MPa. A

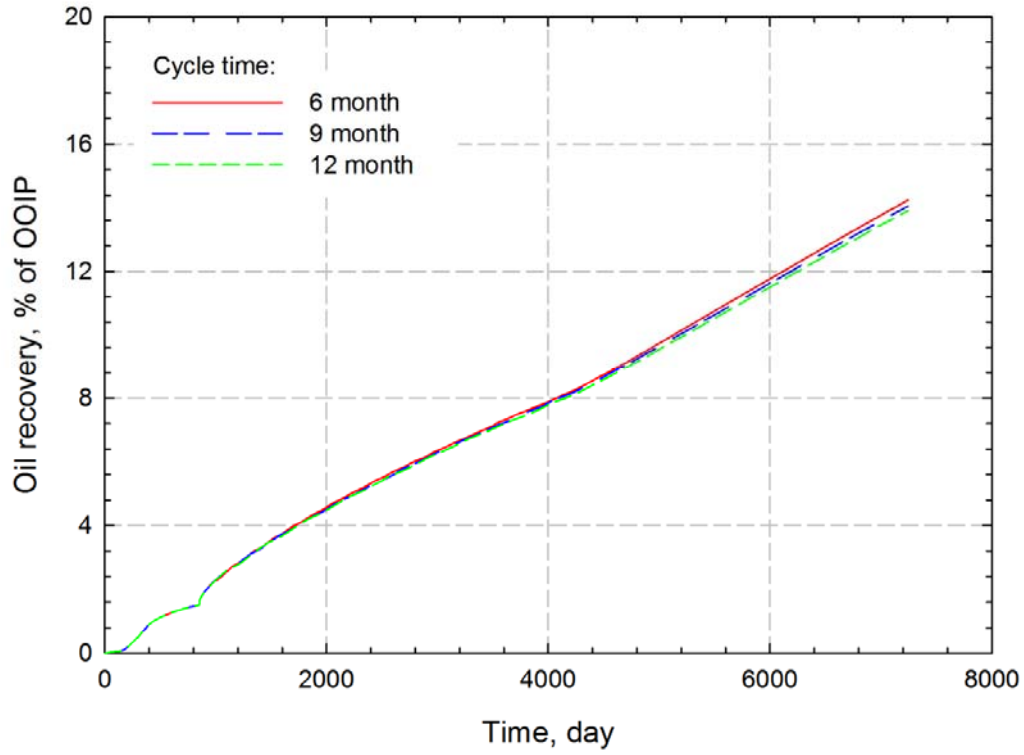


**Figure 4.21** Oil recovery profiles with different cycle time for miscible $CO_2$-WAG flooding processes

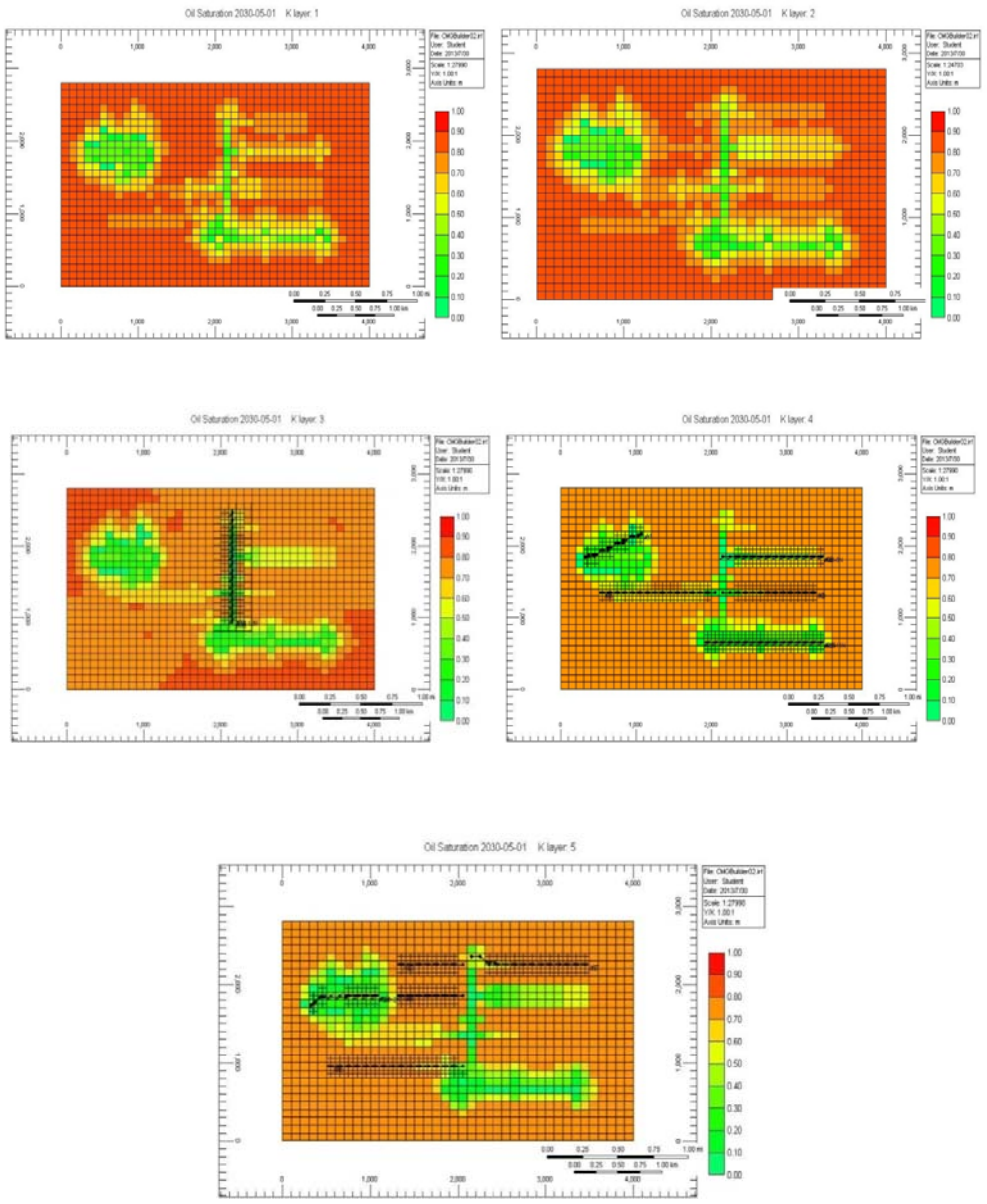


**Figure 4.22** Distribution of residual oil saturation in $CO_2$-WAG flooding processes for **(a)** Layer #1, **(b)** Layer #2, **(c)** Layer #3, **(d)** Layer #4, and **(e)** Layer #5

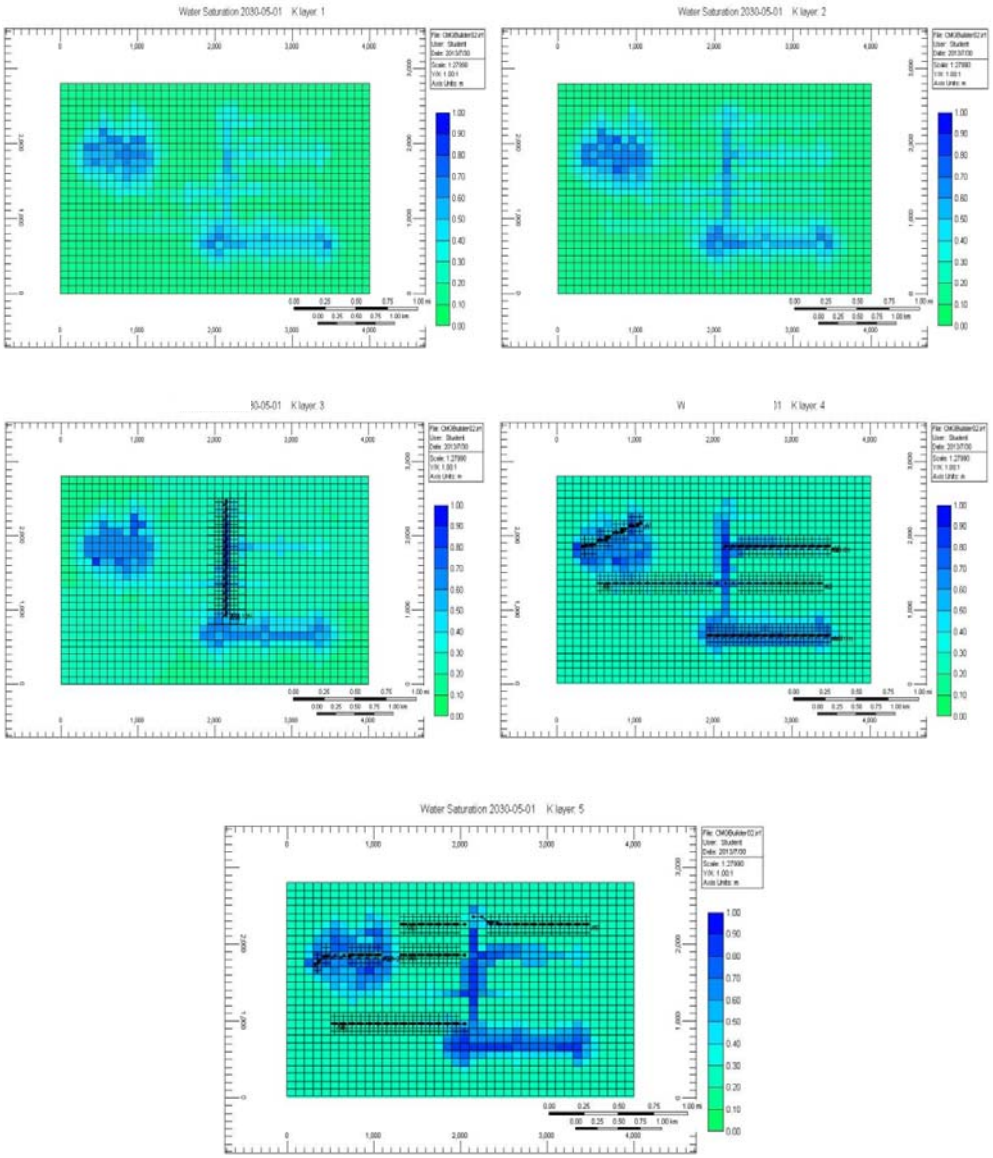

**Figure 4.23** Distribution of residual water saturation in $CO_2$-WAG flooding processes for **(a)** Layer #1, **(b)** Layer #2, **(c)** Layer #3, **(d)** Layer #4, and **(e)** Layer #5

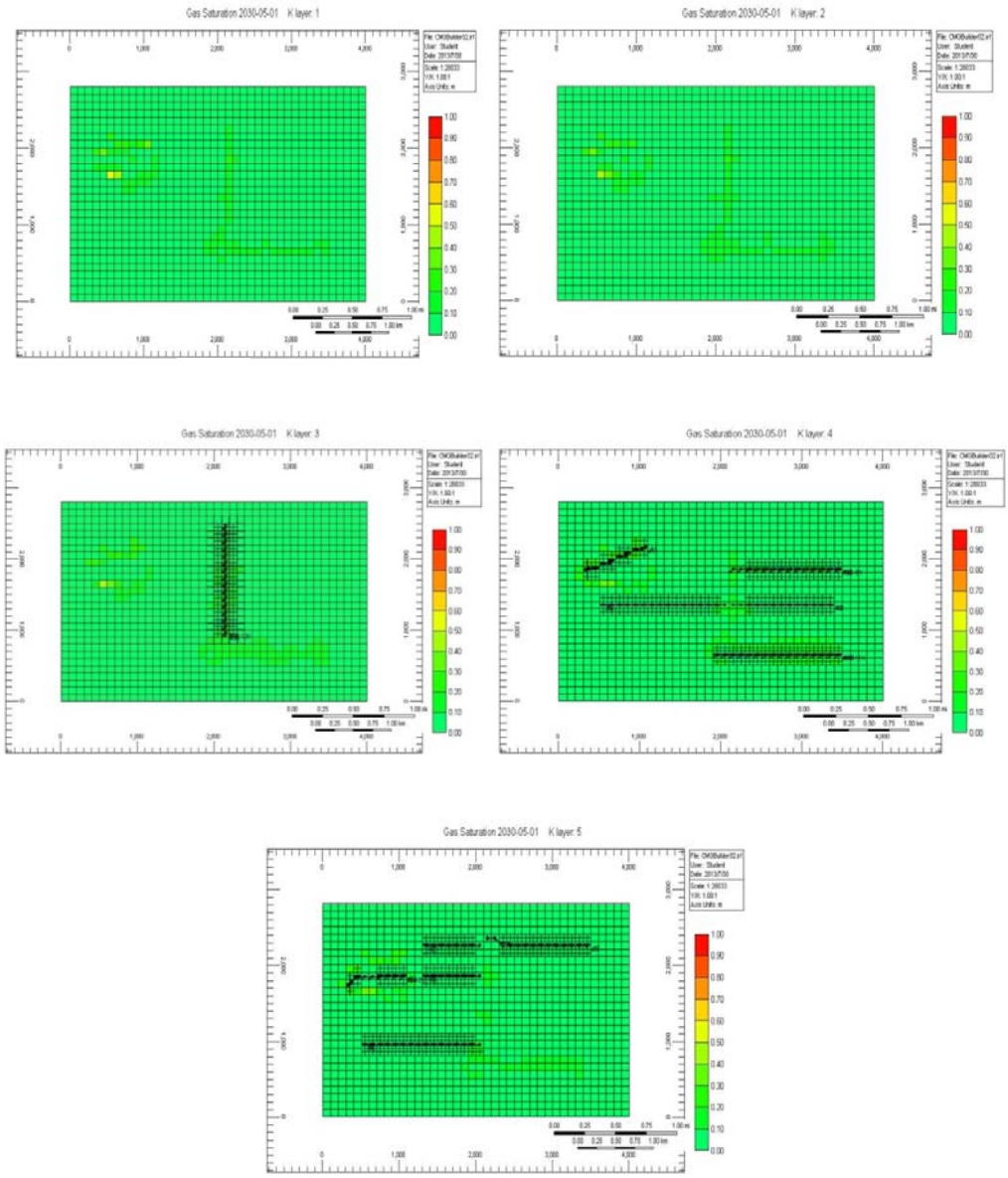


**Figure 4.24** Distribution of residual gas saturation in $CO_2$-WAG flooding processes for **(a)** Layer #1, **(b)** Layer #2, **(c)** Layer #3, **(d)** Layer #4, and **(e)** Layer #5

total of 10 cycles are performed in each scenario.

The simulated recovery performance is shown in **Figure 4.25**, where oil recovery is enhanced by a longer soaking time. This is attributed to the fact that more $CO_2$ is dissolved into crude oil if the soaking time remains longer. Similar findings are also documented in the literature (Haskin and Alston, 1989). The recovery factor with a soaking time of 15 days is found to be 15.9%, which is 0.2% higher than that of 10 days of soaking time, and 0.4% higher than that of 6 days of soaking time, while a longer soaking time usually results in more benefits loss during a limited period of time. In this way, the optimum soaking time of $CO_2$ huff-n-puff process needs to balance the oil production and the field economic benefits.

**6) Injection pressure**

Sensitivity analysis of injection pressure is subsequently conducted for miscible $CO_2$ huff-n-puff process with the tuned reservoir model. As for each well, $CO_2$ is injected for the first 1 month. Then, the well is shut in to soak for 15 days. Finally, oil is produced for 6 months with a constant pressure of 9.5 MPa as the constraint. The BP for the injectors changes from 15.0 MPa to 21.0 MPa. There are 8 wells in the reservoir used for $CO_2$ injection and oil production, while the $CO_2$ injection, soaking and oil production are repeated for 10 cycles.

As can be seen in **Figure 4.26**, the ultimate oil recovery factors under injection pressure of 15.0 MPa, 18.0 MPa and 21.0 MPa are found to be 12.9%, 15.9% and 18.2% of OOIP, respectively. A higher injection pressure results in a better oil

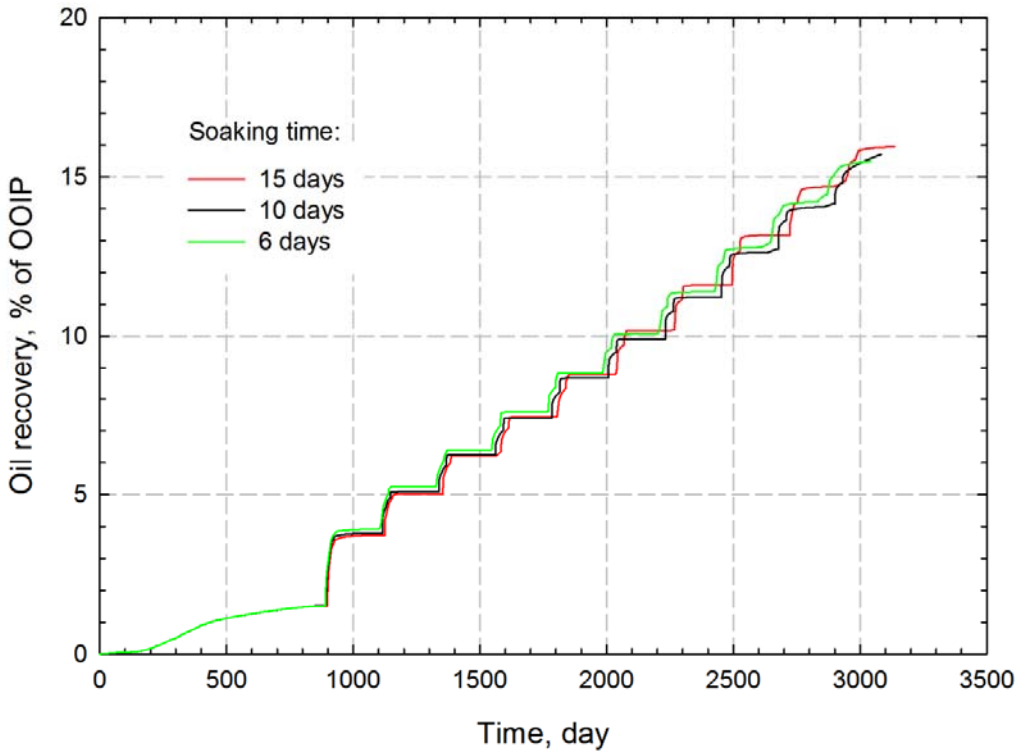


**Figure 4.25** Oil recovery profiles with different soaking times for miscible $CO_2$ huff-n-puff processes

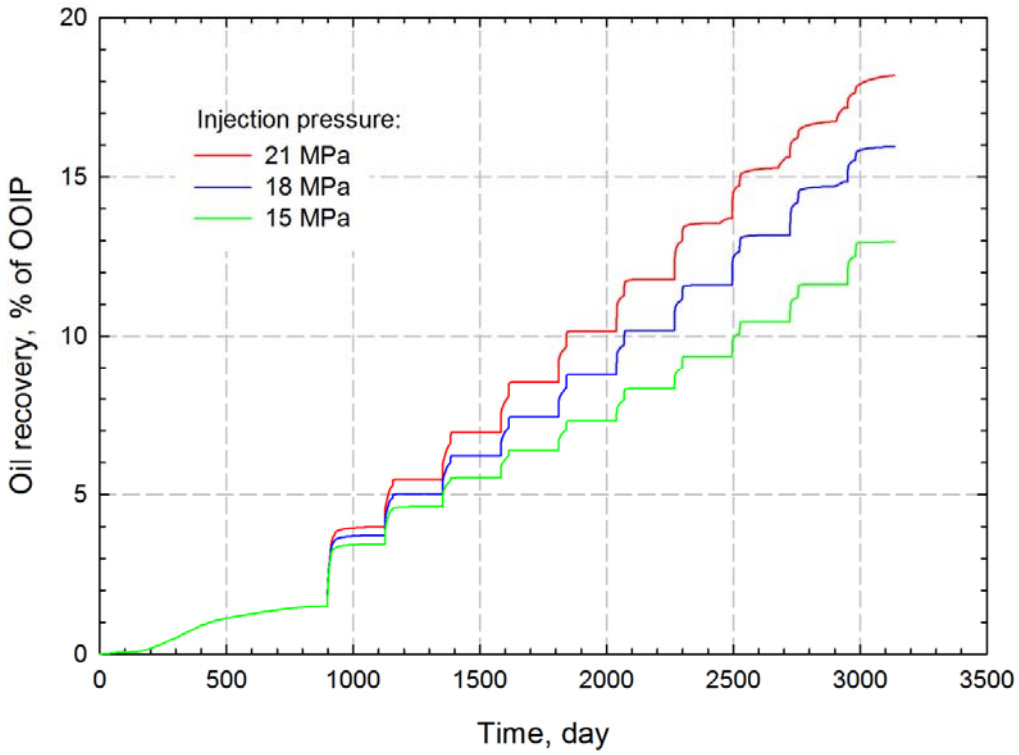


**Figure 4.26** Oil recovery profiles with different injection pressures for $CO_2$ huff-n-puff processes

recovery due to more $CO_2$ injected and a higher pressure drop during production. In general, a higher injection pressure usually requires a larger capacity of surface compressors. In this way, the optimum injection pressure of $CO_2$ huff-n-puff process needs to balance the oil recovery and the capital investment.

The distributions of residual oil, water, and gas saturation for each layer at injection pressure of 18.0 MPa and 15 days of soaking time are presented in **Figure 4.27**, **Figure 4.28**, and **Figure 4.29**, respectively. Although the $CO_2$ huff-n-puff process is only able to affect a limited region around each well, the residual oil saturation is still found to be low. This is because more wells are included in oil production processes compared to previous $CO_2$ flooding, resulting in a larger area affected by $CO_2$ injection, and hence a higher recovery factor of $CO_2$ huff-n-puff process.

## 4.5 Summary

A reservoir geological model with massively fractured horizontal wells is developed and used to evaluate the recovery performance of $CO_2$ injection in tight oil formations. The reservoir pressure history obtained from material balance for the primary recovery process is well matched by simulation. With the tuned reservoir geological model, recovery performance and residual oil distribution by various recovery schemes (i.e., waterflooding, continuous $CO_2$ flooding, $CO_2$-WAG flooding, and $CO_2$ huff-n-puff process) have been evaluated.

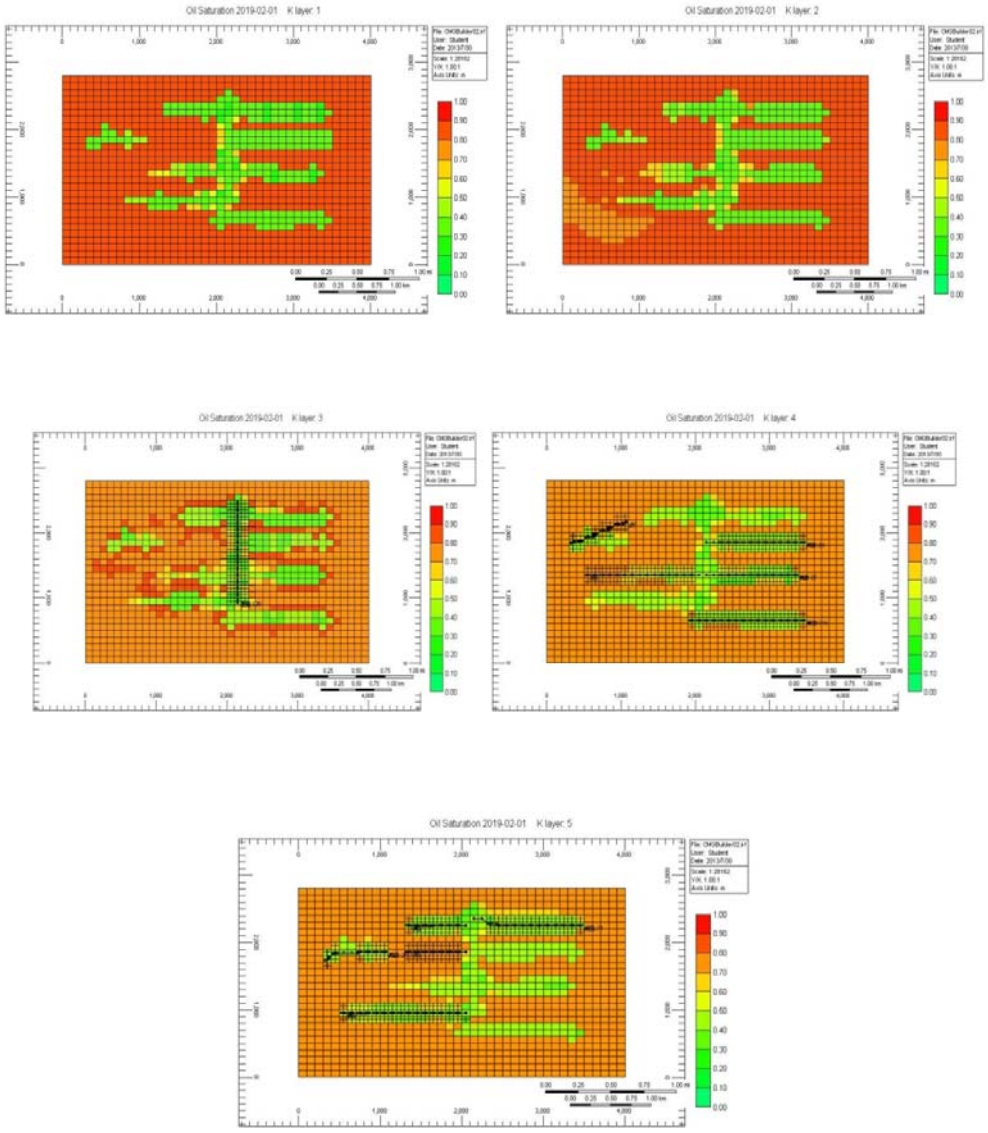


**Figure 4.27** Distribution of residual oil saturation in $CO_2$ huff-n-puff processes for **(a)** Layer #1, **(b)** Layer #2, **(c)** Layer #3, **(d)** Layer #4, and **(e)** Layer #5

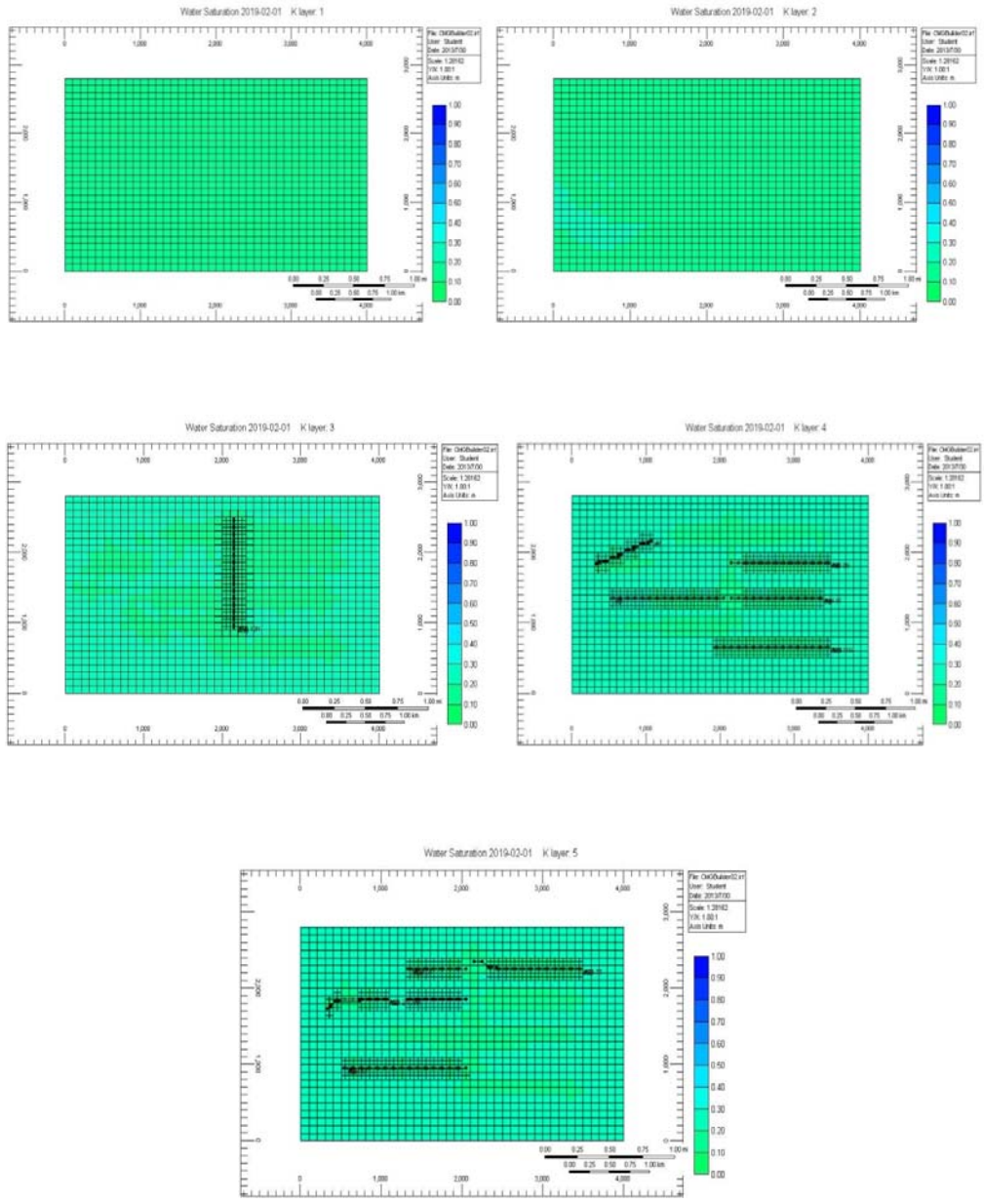


**Figure 4.28** Distribution of residual water saturation in $CO_2$ huff-n-puff processes for **(a)** Layer #1, **(b)** Layer #2, **(c)** Layer #3, **(d)** Layer #4, and **(e)** Layer #5

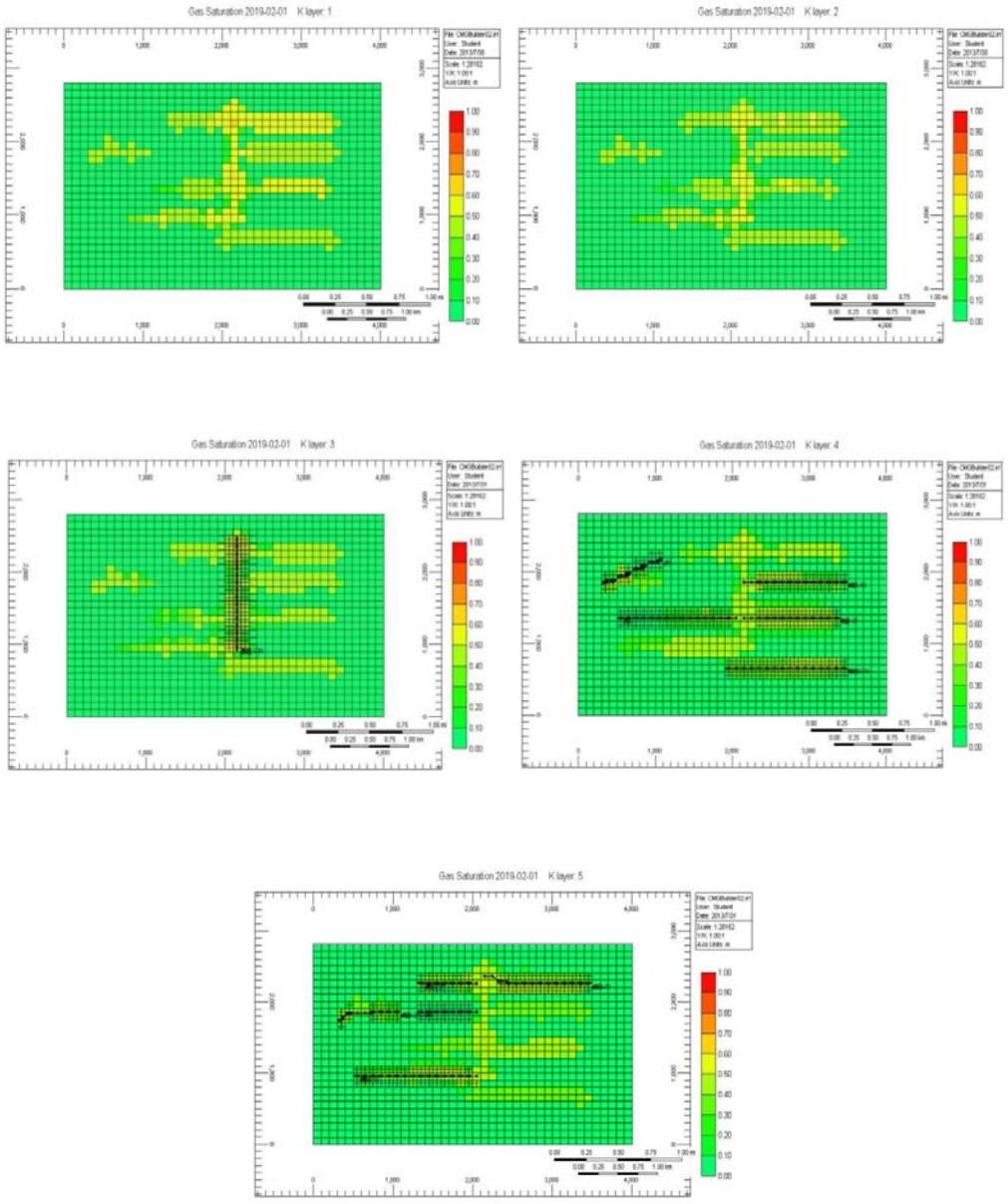


**Figure 4.29** Distribution of residual gas saturation in $CO_2$ huff-n-puff processes for **(a)** Layer #1, **(b)** Layer #2, **(c)** Layer #3, **(d)** Layer #4, and **(e)** Layer #5

Miscible $CO_2$-WAG flooding is found to have a larger sweep area and higher oil recovery efficiency compared to other $CO_2$ flooding schemes, while $CO_2$ huff-n-puff is able to obtain favourable recovery performance, provided that enough wells in the field are put into production. The sensitivity of operational parameters (i.e., well pattern, production pressure, WAG ratio, cycle time, soaking time, and injection pressure) on recovery performance has been analyzed. Oil recovery in the tight oil reservoir is found to be improved by optimizing these parameters, while the production pressure and injection pressure is proved to be dominant on oil recovery.

# CHAPTER 5 CONCLUSIONS AND RECOMMENDATIONS

## 5.1 Conclusions

In this thesis, comprehensive studies have been conducted on development of $CO_2$ EOR techniques for unlocking resources from tight oil formations. Experimentally, nine coreflooding tests are performed to evaluate recovery performance of different injection-production strategies with tight core samples. Numerically, simulation techniques have been developed to history match the experimental measurements, while sensitivity analysis is conducted with the tuned numerical model in order to maximize the recovery from tight oil formations. Subsequently, comprehensive field-scale simulation is initiated to evaluate the reservoir performance under various $CO_2$ injection strategies in a tight oil formation.

The major conclusions of this thesis study can be summarized as follows:

1) $CO_2$ injection is experimentally found to achieve superior recovery efficiency compared to that of waterflooding. The $CO_2$-WAG flooding is considered to have advantages of higher sweep efficiency and lower $CO_2$ consumption than the continuous $CO_2$ flooding. Although recovery factor of $CO_2$ huff-n-puff processes proves to be lower than that of $CO_2$ flooding, its oil recovery will be improved with a higher injection pressure, provided that it is lower than the corresponding MMP.

2) There exists a good agreement between the experimentally measured and numerically simulated oil production and pressure, indicating that the

underlying mechanisms governing $CO_2$ injection processes in tight oil formations have been well simulated and incorporated.

3) During continuous $CO_2$ flooding processes, the high ultimate oil recovery is obtained at both low and high production pressures, indicating that $CO_2$ flooding is efficient for recovering oil from tight formations under either near-miscible or miscible condition.

4) As for $CO_2$-WAG processes, the oil recovery is significantly enhanced with an increase in the WAG ratio from 0.0 to 2.0. However, a further increase of WAG ratio leads to a minor increase in oil recovery. When the WAG ratio increases from 4.0 to 8.0, the ultimate oil recovery even starts to decrease. As such, the optimum WAG ratio is found to fall in the range of 2.0 to 4.0 in this study.

5) Either a smaller cycle time or a longer water slug size of $CO_2$-WAG flooding is found to result in higher oil recovery, while the enhancement effect becomes minor when the cycle time is smaller than a certain value, or the water slug size remains longer than a certain value. For a coreflooding experiment, the optimum cycle time and water slug size are numerically determined to be 33 min and 0.250 PV, respectively.

6) During $CO_2$ huff-n-puff processes, a higher injection pressure is found to result in a higher recovery factor. However, the enhancement effect of oil recovery becomes less significant when the injection pressure is higher

than 9.7 MPa of MMP between the crude oil and $CO_2$. The oil recovery is improved when the soaking time increases from 3 to 6 h, while a further increase of the soaking time will hardly contribute to the improvement of oil recovery due to the fact that no more $CO_2$ is able to be dissolved into the crude oil.

7) As for field-scale simulation, miscible $CO_2$-WAG flooding is found to have a larger sweep area and higher oil recovery efficiency compared to other $CO_2$ flooding schemes, while the $CO_2$ huff-n-puff process is able to obtain favourable recovery performance, provided that enough wells in the field are put into production. Oil recovery in the tight oil reservoir is able to be improved by optimizing the operational parameters during $CO_2$ injection processes, while the operational parameters of production and injection pressure are proved to be dominant on oil recovery in tight oil formations.

## 5.2 Recommendations

Based on the thesis study, the following recommendations for future research are made:

1) Due to the low permeability and low porosity in tight oil formations, massive fractures along the horizontal wells have been initiated to improve both injectivity and productivity. The existence of fractures in

tight formations may lead to different flow behaviour, and thus a different recovery performance. Effective coreflooding experiments with consideration of hydraulic fractures should be designed and implemented to evaluate recovery performance of $CO_2$ injection in the fractured tight oil formations.

2) Various $CO_2$ injection strategies, i.e., continuous $CO_2$ flooding, $CO_2$-WAG flooding, and $CO_2$ huff-n-puff, shall work together in a sequential order during one coreflooding experiment, instead of using only one strategy for the whole experiment. The underlying mechanisms of such development methods should be consequently identified, while the optimum working situation should be determined.

3) Due to the inherent nature of low permeability and low porosity of tight formations, asphaltene precipitation may significantly affect reservoir performance during $CO_2$ injection. Both the onset of asphaltene precipitation together with its effect on oil recovery should be determined.

4) Sensitivity analysis should be performed in the field-scale simulation to examine effects of fracture spacing and geometry on oil recovery, and thus optimize the fracture design for maximizing oil production.

# REFERENCES


Arshad, A.; Al-Majed, A.A.; Maneouar, H.; Muhammadain, A.; and Mtawaa, B. Carbon Dioxide Miscible Flooding in Tight Oil Reservoirs: A Case Study. Paper SPE 127616, presented at the SPE Kuwait International Petroleum Conference and Exhibition, Kuwait City, Kuwait, December 14-16, 2009.

Asghari, K. and Torabi, F. Laboratory Experimental Results of Huff-n-Puff $CO_2$ Flooding in a Fractured Core System. Paper SPE 110577, presented at the SPE Annual Technical Conference and Exhibition, Anaheim, CA, November 11-14, 2007.

Ashraf, M. and Satapathy, M. The Global Quest for Light Tight Oil: Myth or Reality. *Energy Perspectives* 2013, 1st semester, 16-23.

Bagci, A.S. Immiscible $CO_2$ Flooding through Horizontal Wells. *Energy Sources, Part A: Recovery, Utilization, and Environmental Effects* 2007, 29(1), 85-95.

Bank, G.C.; Riestenberg, D.; and Koperna, G.J. $CO_2$ Enhanced Oil Recovery Potential of the Appalachian Basin. Paper SPE 111282, presented at the SPE Eastern Regional Meeting, Lexington, KY, October 17-19, 2007.

Brannan, G. and Whitington, H.M. Enriched Gas Miscible Flooding: A Case History of the Levelland Unit Secondary Miscible Project. *Journal of Petroleum Technology* 1977, 29(8), 919-924.

Cao, M. and Gu, Y. Oil Recovery Mechanisms and Asphaltene Precipitation Phenomenon in Immiscible and Miscible $CO_2$ Flooding Processes. *Fuel*

2013, 109(24), 157-166.

Chen, S.; Li, H.; Yang, D.; and Tontiwachwuthikul, P. Optimum Parametric Design for Water-Alternating-Gas (WAG) Process in a $CO_2$ Miscible Flooding Reservoir. *Journal of Canadian Petroleum Technology* 2010, 49(10), 75-82.

Christensen, J.R.; Stenby, E.H.; and Skauge, A. Review of WAG Field Experience. *SPE Reservoir Evaluation and Engineering* 2001, 4(2), 97-106.

Computer Modeling Group Ltd., 2009. *WinProp and GEM Program*, Calgary, AB, Canada.

Craig, F.F. and Owens, W.W. Miscible Slug Flooding-A Review. *Journal of Petroleum Technology* 1960, 12(4), 11-15.

Dennis, B.; David, A.P.; and Martin, M. Waterflood and $CO_2$ Flooding of the Fractured Midale Field. *Journal of Petroleum Technology* 1993, 45(9), 811-817.

Dong, M.; Huang, S.S.; and Srivastava, R. A Laboratory Study on Near-miscible $CO_2$ Injection in Steelman Reservoir. *Journal of Canadian Petroleum Technology* 2001, 40(2), 53-61.

Economides, M.J.; Hill, A.D.; and Ehlig-Economides, C. *Petroleum Production Systems*. Prentice Hall, Inc., Upper Saddle River, NJ, 1993.

Elsevier. Shale Gas, Tight Oil: Are We Entering A New Age of American Plenty? *The Electricity Journal* 2012, 25(1), 1-2.

Faltinson, J. and Gunter, B. Net $CO_2$ Stored in North America EOR Projects. *Journal of Canadian Petroleum Technology* 2011, 50(7), 55-60.

Fatemi, S.M. and Sohrabi, M. Experimental Investigation of Near-miscible Water-

alternating-gas Injection Performance in Water-wet and Mixed-wet Systems. *SPE Journal* 2013, 18(1), 114-123.

Folger, L.K. and Guillot, S.N. A Case Study of the Development of the Sundown Slaughter Unit $CO_2$ Flood Hockley County, Texas. Paper SPE 35189, presented at the SPE Permian Basin Oil and Gas Recovery Conference, Midland, TX, March 27-29, 1996.

Forrest, J.; Birn, K.; Brink, S.; Comb, T.J.; Cuthbert, B.; Dunbar, R.B.; Harju, J.A.; Isaace, E.; Jones, F.; Khanna, P.; Snarr, D.G.; Sorensen, J.A.; Wall, T.J.; and Whitney, D. Working Document of the NPC North American Resource Development Study-Unconventional Oil. Paper No. 1-6, prepared for the U.S. National Petroleum Council (NPC), September, 2011.

Ghaderi, S.M.; Clarkson, C.R.; Chen, S.; and Kaviani, D. Evaluation of Recovery Performance of Miscible Displacement and WAG Process in Tight Oil Formation. Paper SPE 152084, presented at the SPE/EAGE European Unconventional Resources Conference and Exhibition, Vienna, Austria, March 20-22, 2012.

Ghedan, S. Global Laboratory Experience of $CO_2$-EOR Flooding. Paper SPE 125581, presented at the SPE/EAGE Reservoir Characterization and Simulation Conference, Abu Dhabi, UAE, October 19-21, 2009.

Guo, X.; Du, Z.; Sun, L.; and Fu, Y. Optimization of Tertiary Water-alternate-$CO_2$ Flood in Jilin Oilfield of China: Laboratory and Simulation Studies. Paper SPE 99616, presented at the SPE/DOE Symposium on Improved Oil

Recovery, Tulsa, OK, April 22-26, 2006.

Halnes, H.K. and Monger, T.G. A Laboratory Study of Natural Gas Huff-n-Puff. Paper CIM/SPE 90-78, presented at the International Technical Meeting Jointly, Calgary, AB, June 10-13, 1990.

Haskin, H.K. and Alston, R.B. An Evaluation of $CO_2$ Huff-n-Puff Tests in Texas. *Journal of Petroleum Technology* 1989, 41(2), 177-184.

Heeremans, J.C.; Esmaiel, T.E.H.; and van Kruijsdijk, C.P.J.W. Feasibility Study of WAG Injection in Naturally Fractured Reservoirs. Paper SPE 100034, presented at the SPE/DOE Symposium on Improved Oil Recovery, Tulsa, OK, April 22-26, 2006.

Iwere, F.O.; Robin, N.H.; and Cherian, B.V. Numerical Simulation of Enhanced Oil Recovery in the Middle Bakken and Upper Three Forks Tight Oil Reservoirs of the Williston Basin. Paper SPE 154937, presented at the Americas Unconventional Resources Conference, Pittsburgh, PA, June 5-7, 2012.

Jarrell, P.M.; Fox, C.; Stein, M.; and Webb, S. *Practical Aspect of $CO_2$ Flooding*. Society of Petroleum Engineers, Dallas, TX, 2002.

Jha, K.N. A Laboratory Study of Heavy Oil Recovery with Carbon Dioxide. *Journal of Canadian Petroleum Technology* 1986, 25(2), 54-63.

Jiang, H.F.; Nuryaningsih. L.; and Hertanto, A. The Study of Timing of Cycling Injections in Miscible $CO_2$-WAG. Paper SPE 153792, presented at the SPE Western Regional Meeting, Bakersfield, CA, March 19-23, 2012.

Joshi, S.D. Cost/Benefits of Horizontal Wells. Paper SPE 83621, presented at the SPE

Western Regional/AAPG Pacific Section Joint Meeting, Long Beach, CA, May 19-24, 2003.

Kamal, N.J. A Laboratory Study of Heavy Oil Recovery with Carbon Dioxide. *Journal of Canadian Petroleum Technology* 1986, 25(2), 4-20.

Kane, A.V. Performance Review of a Large-scale $CO_2$-WAG Enhanced Recovery Project, SACROC Unit Kelly-Snyder Field. *Journal of Petroleum Technology* 1979, 31(2), 217-231.

Karimaie, H. and Torsaeter, O. Low IFT Gas-Oil Gravity Drainage in Fractured Carbonate Porous Media. *Journal of Petroleum Science and Engineering* 2010, 70(1-2), 67-73.

Kazemi, A. and Jamialahmadi, M. The Effect of Oil and Gas Molecular Diffusion in Production of Fractured Reservoir during Gravity Drainage Mechanism by $CO_2$ Injection. Paper SPE 120894, presented at SPE EUROPEC/EAGE Annual Conference and Exhibition, Amsterdam, Netherland, June 8-11, 2009.

Kovscek, A.R. and Cakici, M.D. Geologic Storage of Carbon Dioxide and Enhance Oil Recovery II: Co-optimization of Storage and Recovery. *Energy Conversion and Management* 2005, 46(11-12), 1941-1956.

Kovscek, A.R.; Tang, G.Q.; and Vega, B. Experimental Investigation of Oil Recovery from Siliceous Shale by $CO_2$ Injection. Paper SPE 115679, presented at the SPE Annual Technical Conference and Exhibition, Denver, CL, September 21-24, 2008.

Kudal, P.R.; Omkar, N.G.; and Sidharha, S. Immiscible Hydrocarbon WAG: Laboratory to Field. Paper SPE 128848, presented at the SPE Oil and Gas India Conference and Exhibition, Mumbai, India, January 20-22, 2010.

Kuo, M.C.; Dulaney, J.P.; Deer, M.W.; Evans, B.S.; and Granquit, M.R. Optimization of Waterflood Performance and $CO_2$ Flooding Design Using a Modeling Approach, Mallet Unit, Slaughter Field. Paper SPE 20377, presented at the 65$^{th}$ Annual Technical Conference and Exhibition, New Orleans, LA, September 23-26, 1990.

Li, B.Z.; Li, X.F.; Kamy, S.; and Yao, Y.D. Optimization of the Injection and Production Schemes during $CO_2$ Flooding for Tight Reservoir. *Journal of Southwest Petroleum University (Science & Technology Edition)* 2010, 32 (2), 101-107.

Li, H.; Putra. E.; Chechter, D.S.; and Grigg, R.B. Experimental Investigation of $CO_2$ Gravity Drainage in a Fractured System. Paper SPE 64510, presented at SPE Asia Pacific Oil and Gas Conference and Exhibition, Brisbane, Australia, October 16-18, 2000.

Lolon, E.P.; Cipolla, C.L.; Weijers, L.; Hesketh, R.E.; and Grigg, M.W. Evaluation Horizontal Well Placement and Hydraulic Fracture Spacing/Conductivity in the Bakken Formation, North Dakota. Paper SPE 124905, presented at the SPE Annual Technical Conference and Exhibition, New Orleans, LA, October 4-7, 2009.

MacAllister, D.J. Evaluation of $CO_2$ Flooding Performance: North Coles Levee $CO_2$

Pilot, Kern County California. *Journal of Petroleum Technology* 1989, 41(2), 185-194.

Manrique, E.J.; Muci, V.E.; and Gurfinkel, M.E. EOR Field Experience in Carbonate Reservoirs in the United States. *SPE Reservoir Evaluation and Engineering* 2007, 10(6), 667-686.

Manrique, M.; Thomas, C.; Ravikiran, R.; Izadi, M.; Lantz, M.; Romero, J.; and Alvarado, V. EOR: Current Status and Opportunities. Paper SPE 130113, presented at the SPE Improved Oil Recovery Symposium, Tulsa, OK, April 24-28, 2010.

Martin, D. and Taber, J.J. Carbon Dioxide Flooding. *Journal of Petroleum Technology* 1992, 44(4), 396-400.

Merritt, M.B. and Groce, J.F. A Case History of the Hanford San Andres Miscible $CO_2$ Project. *Journal of Petroleum Technology* 1992, 44(8), 924-929.

Miller, B.; Paneitz, J.; Yakely, S.; and Evans, K. Unlocking Tight Oil: Selective Multi-stage Fracturing in the Bakken Shale. Paper SPE 116105, presented at the SPE Annual Technical Conference and Exhibition, Denver, CO, September 21-24, 2008.

Monger, T.G. and Coma, J.M. A Laboratory and Field Evaluation the $CO_2$ Huff-n-Puff Process for Light Oil Recovery. *SPE Reservoir Engineering* 1988, 3(4), 1168-1176.

Moore, J.S. and Clark, G.C. History Match of the Maljamar $CO_2$ Pilot Performance. Paper SPE/DOE 17323, presented at the SPE/DOE Enhanced Oil Recovery

Symposium, Tulsa, OK, April 17-20, 1988.

Morel, D.; Bourbiaux, B.; Latil, M.; and Thiebot, B. Diffusion Effects in Gas Flooded Light Oil Fractured Reservoirs. *SPE Advanced Technology Series* 1993, 1(2), 100-109.

Park, R.A. Pressure Maintenance by Waterflooding North Virden Scallion Field, Manitoba. *Journal of Canadian Petroleum Technology* 5(1), 7-13.

Pinto Oilfield, SK, Canada. *AccuMap* 2012, Englewood, CO.

Pittaway, K.R.; Hoover, J.W.; and Deckert, L.B. Development and Status of the Maljamar $CO_2$ Pilot. *Journal of Petroleum Technology* 1985, 37(3), 537-544.

Prieditis, J.; Wolle, C.R.; and Notz, P.K. A Laboratory and Field Injectivity Study: $CO_2$ WAG in the San Andres Formation of West Texas. Paper SPE 22653, presented at the SPE Annual Technical Conference and Exhibition, Dallas, TX, October 6-9, 1991.

Ramsay, H.J. and Small, F.R. Use of Carbon Dioxide for Water Injectivity Improvement. *Journal of Petroleum Technology* 1964, 16(1), 25-31.

Rahman, S.; Nofel, W.; Al-Majed, A.; Arshad, A.; and Menouar, H. Phase Behavior Aspects of Carbon Dioxide ($CO_2$) Miscible Flooding in Tight Cores: A Case Study. Paper SPE 128467, presented at the SPE North Africa Technical Conference and Exhibition, Cairo, Egypt, February 14-17, 2010.

Rogers, J.D. and Grigg, R.B. A Literature Analysis of the WAG Injectivity Abnormalities in the $CO_2$ Process. *SPE Reservoir Evaluation and Engineering* 2001, 4(5), 375-386.

Sahin, S.; Kalfa, U.; and Celebioglu, D. Bati Raman Field Immiscible $CO_2$ Application Status Quo and Future Plan. *SPE Reservoir Evaluation and Engineering* 2008, 11(4), 778-791.

Saskatchewan Research Council. *Assessment of Miscible or Near Miscible Gas Flooding in Tight Oil Reservoirs.* Report Prepared for the Petroleum Technology Research Centre (PTRC). March 2012.

Shoaib, S. and Hoffman, B.T. $CO_2$ Flooding in the Elm Coulee Field. Paper SPE 123176, presented at the SPE Rocky Mountain Petroleum Technology Conference, Denver, CO, April 14-16, 2009.

Song, C. and Yang, D. Optimization of $CO_2$ Flooding Schemes for Unlocking Resources from Tight Oil Formations. Paper SPE 162549, presented at the SPE Canadian Unconventional Resources Conference, Calgary, AB, October 30-November 1, 2012a.

Song, C. and Yang, D. Performance Optimization of Water-Alternating-$CO_2$ Flooding in Tight Oil Formations. Presented at the IEA 33rd Annual Symposium on Enhanced Oil Recovery, Regina, SK, August 27-30, 2012b.

Song, C., and Yang, D. Performance Evaluation of $CO_2$ Huff-n-Puff Processes in Tight Oil Formations. Paper SPE 167217, to be presented at the SPE Unconventional Resources Conference-Canada, Calgary, AB, November 5-7, 2013.

Stalkup J.F. Status of Miscible Displacement. *Journal of Petroleum Technology* 1983, 35(4), 815-834.

Surguchev, L.M.; Ragnhild, K.; and Krakstad, O.S. Optimum Water Alternate Gas Injection Schemes for Stratified Reservoirs. Paper SPE 24646, presented at the 67th SPE Annual Technical Conference and Exhibition, Washington, DC, October 4-7, 1992.

Torabzadeh, S.J. and Handy, L.L. The Effect of Temperature and Interfacial Tension on Water/Oil Relative Permeability of Consolidated Sands. Paper SPE 12689, presented at the SPE/DOE Fourth Symposium on Enhanced Oil Recovery, Tulsa, OK, April 15-18, 1984.

Uwabe, A.; Ueno, M. and Ibuki, K. Molecular Dynamics Simulation of Partially Diffusion-Controlled Reaction between Mono and Diatomic Molecules. *Journal of Molecular Liquids* 2009, 147(1-2), 30-36.

Wang, X. and Gu, Y. Oil Recovery and Permeability Reduction of a Tight Sandstone Reservoir in Immiscible and Miscible $CO_2$ Flooding Processes. *Industrial & Engineering Chemistry Research* 2011, 50(4), 2388-2399.

Watts, R.J.; Gehr, J.B.; Wasson, J.A.; Evans, D.M.; and Locke, C.D. A Single $CO_2$ Injection Well Minitest in a Low-Permeability Carbonate Reservoir. *Journal of Petroleum Technology* 1982, 34(8), 1781-1788.

Wayne A, G.; Saul, V.; Christian, L.D.; and Shirer, J.A. A Field Test of Nitrogen WAG Injectivity. *Journal of Petroleum Technology* 1982, 34(2), 266-272.

Yang, P. and Wang, S. The Study on Porous Flow Rules of $CO_2$ Flooding in an Extra-low Permeability Reservoir. Paper 978-0-646-54471-7, presented at the 2010 International Symposium on Low-carbon Economy and Technology Science,

Beijing, China, October 29-31, 2010.

Yu, H.; Song, X.; Yang, S.; and Chen, D. Experimental and Numerical Simulation Study on Single Layer Injectivity for $CO_2$ Flooding in Low Permeability Oil Reservoir. Paper SPE 144042, presented at the SPE Enhanced Oil Recovery Conference, Kuala Lumpur, Malaysia, July 19-21, 2011.

Zekri, A.Y.; Almehaideb, R.A.; and Shedid, S.A. Displacement Efficiency of Supercritical $CO_2$ Flooding in Tight Carbonate Rocks Under Immiscible and Miscible Conditions. Paper SPE 98911, presented at the SPE EUROPEC/EAGE Annual Conference and Exhibition, Vienna, Austria, June 12-15, 2006.

Zekri, A.Y.; Mohamed, S.N.; and Abdullah, S.A. Evaluation of Oil Recovery by Water-alternating-gas (WAG) Injection Oil-wet and Water-wet Systems. Paper SPE 143438, presented at the SPE Enhanced Oil Recovery Conference, Kuala Lumpur, Malaysia, July 19-21, 2011.

Zhang, Y.P.; Sayegh, S.G.; Huang, S.; and Dong, M. Laboratory Investigation of Enhanced Light Oil Recovery by $CO_2$/Flue Gas Huff-n-puff Process. *Journal of Canadian Petroleum Technology* 2006, 45(2), 24-32.

Zhang, Y.P.; Sayegh, S.G.; Luo, P.; and Huang, S. Experimental Investigation of Immiscible Gas Process Performance for Medium Oil. *Journal of Canadian Petroleum Technology* 2010, 49(2), 32-39.

Zheng, S. and Yang, D. Pressure Maintenance and Improving Oil Recovery by Means of Immiscible Water-Alternating-$CO_2$ Processes in Thin Heavy-Oil Reservoirs. *SPE Reservoir Evaluation and Engineering* 2013, 16(1), 60-71.

Zhou, D.; Yan, M.; and Calvin, W.M. Optimization of a Mature $CO_2$ Flood-From Continuous Injection to WAG. Paper SPE 154181, presented at the 18th SPE Improved Oil Recovery Symposium, Tulsa, OK, April 14-18, 2012.

# APPENDIX: DETAILED OIL, WATER, AND GAS PRODUCTION OF EACH WELL FOR THE TRAGETED OIFIELD

**1) Well #1:**

| Time | Oil production ($m^3/d$) | Water production ($m^3/d$) | Gas production ($10^3 Sm^3/d$) |
|---|---|---|---|
| 2010-7 | 0.0 | 0.0 | 0.0 |
| 2010-8 | 0.0 | 0.0 | 0.0 |
| 2010-9 | 0.0 | 0.0 | 0.0 |
| 2010-10 | 0.0 | 0.0 | 0.0 |
| 2010-11 | 0.0 | 0.0 | 0.0 |
| 2010-12 | 0.0 | 0.0 | 0.0 |
| 2011-1 | 0.0 | 0.0 | 0.0 |
| 2011-2 | 0.0 | 0.0 | 0.0 |
| 2011-3 | 0.0 | 0.0 | 0.0 |
| 2011-4 | 0.0 | 0.0 | 0.0 |
| 2011-5 | 0.0 | 0.0 | 0.0 |
| 2011-6 | 7.6 | 0.0 | 0.0 |
| 2011-7 | 4.0 | 2.1 | 0.0 |
| 2011-8 | 5.1 | 0.9 | 0.9 |
| 2011-9 | 1.4 | 0.3 | 1.7 |
| 2011-10 | 1.4 | 0.3 | 1.2 |
| 2011-11 | 1.7 | 1.0 | 0.1 |
| 2011-12 | 1.5 | 0.2 | 0.2 |
| 2012-1 | 0.9 | 0.1 | 0.3 |
| 2012-2 | 0.8 | 0.1 | 0.2 |
| 2012-3 | 0.7 | 0.1 | 0.2 |
| 2012-4 | 0.6 | 0.1 | 0.3 |
| 2012-5 | 0.5 | 0.1 | 0.3 |
| 2012-6 | 0.6 | 0.1 | 0.3 |
| 2012-7 | 0.6 | 0.1 | 0.3 |
| 2012-8 | 0.5 | 0.1 | 0.3 |
| 2012-9 | 0.3 | 0.1 | 0.4 |
| 2012-10 | 0.0 | 0.0 | 0.0 |

**2) Well #2**

| Time | Oil production ($m^3/d$) | Water production ($m^3/d$) | Gas production ($10^3 Sm^3/d$) |
|---|---|---|---|
| 2010-7 | 0.0 | 0.0 | 0.0 |
| 2010-8 | 0.0 | 0.0 | 0.0 |
| 2010-9 | 0.0 | 0.0 | 0.0 |
| 2010-10 | 0.0 | 0.0 | 0.0 |
| 2010-11 | 0.0 | 0.0 | 0.0 |
| 2010-12 | 0.0 | 0.0 | 0.0 |
| 2011-1 | 0.0 | 0.0 | 0.0 |
| 2011-2 | 0.0 | 0.0 | 0.0 |
| 2011-3 | 0.0 | 0.0 | 0.0 |
| 2011-4 | 10.0 | 1.5 | 0.0 |
| 2011-5 | 10.6 | 0.6 | 2.1 |
| 2011-6 | 11.9 | 0.7 | 3.6 |
| 2011-7 | 9.8 | 0.6 | 2.7 |
| 2011-8 | 2.4 | 0.7 | 0.3 |
| 2011-9 | 2.6 | 0.2 | 0.2 |
| 2011-10 | 1.8 | 0.1 | 0.1 |
| 2011-11 | 1.7 | 0.1 | 0.1 |
| 2011-12 | 0.0 | 0.0 | 0.0 |
| 2012-1 | 3.6 | 0.3 | 0.1 |
| 2012-2 | 4.4 | 0.4 | 0.2 |
| 2012-3 | 3.2 | 0.3 | 0.3 |
| 2012-4 | 2.4 | 0.3 | 0.3 |
| 2012-5 | 1.9 | 0.2 | 0.4 |
| 2012-6 | 1.3 | 0.2 | 0.7 |
| 2012-7 | 0.7 | 0.1 | 1.1 |
| 2012-8 | 0.6 | 0.1 | 0.2 |
| 2012-9 | 0.6 | 0.2 | 0.3 |
| 2012-10 | 1.3 | 0.2 | 0.4 |

**3) Well #3**

| Time | Oil production ($m^3/d$) | Water production ($m^3/d$) | Gas production ($10^3 Sm^3/d$) |
|---|---|---|---|
| 2010-7 | 0.0 | 0.0 | 0.0 |
| 2010-8 | 0.0 | 0.0 | 0.0 |
| 2010-9 | 0.0 | 0.0 | 0.0 |
| 2010-10 | 0.0 | 0.0 | 0.0 |
| 2010-11 | 0.0 | 0.0 | 0.0 |
| 2010-12 | 0.0 | 0.0 | 0.0 |
| 2011-1 | 0.0 | 0.0 | 0.0 |
| 2011-2 | 5.8 | 0.5 | 0.7 |
| 2011-3 | 33.1 | 1.5 | 0.5 |
| 2011-4 | 10.1 | 0.3 | 0.5 |
| 2011-5 | 7.6 | 0.2 | 0.3 |
| 2011-6 | 6.0 | 0.2 | 0.3 |
| 2011-7 | 5.1 | 0.2 | 0.5 |
| 2011-8 | 4.5 | 0.2 | 0.5 |
| 2011-9 | 4.4 | 0.2 | 0.6 |
| 2011-10 | 3.0 | 0.2 | 0.1 |
| 2011-11 | 2.8 | 0.2 | 0.1 |
| 2011-12 | 2.8 | 0.1 | 0.1 |
| 2012-1 | 2.5 | 0.1 | 0.1 |
| 2012-2 | 2.0 | 0.1 | 0.1 |
| 2012-3 | 2.1 | 0.1 | 0.2 |
| 2012-4 | 2.6 | 0.1 | 0.4 |
| 2012-5 | 2.5 | 0.1 | 0.2 |
| 2012-6 | 1.8 | 0.1 | 0.2 |
| 2012-7 | 1.7 | 0.1 | 0.2 |
| 2012-8 | 1.6 | 0.1 | 0.2 |
| 2012-9 | 1.5 | 0.1 | 0.3 |
| 2012-10 | 1.1 | 0.1 | 0.2 |

**4) Well #4**

| Time | Oil production ($m^3/d$) | Water production ($m^3/d$) | Gas production ($10^3 Sm^3/d$) |
|---|---|---|---|
| 2010-7 | 0.0 | 0.0 | 0.0 |
| 2010-8 | 0.0 | 0.0 | 0.0 |
| 2010-9 | 0.0 | 0.0 | 0.0 |
| 2010-10 | 0.0 | 0.0 | 0.0 |
| 2010-11 | 0.0 | 0.0 | 0.0 |
| 2010-12 | 0.0 | 0.0 | 0.0 |
| 2011-1 | 0.0 | 0.0 | 0.0 |
| 2011-2 | 0.0 | 0.0 | 0.0 |
| 2011-3 | 0.0 | 0.0 | 0.0 |
| 2011-4 | 0.0 | 0.0 | 0.0 |
| 2011-5 | 22.6 | 2.1 | 1.2 |
| 2011-6 | 11.8 | 1.4 | 0.9 |
| 2011-7 | 17.8 | 2.2 | 1.8 |
| 2011-8 | 5.9 | 0.8 | 0.6 |
| 2011-9 | 5.0 | 0.6 | 0.3 |
| 2011-10 | 1.1 | 0.1 | 0.1 |
| 2011-11 | 3.8 | 0.6 | 0.4 |
| 2011-12 | 5.0 | 0.4 | 0.5 |
| 2012-1 | 4.0 | 0.4 | 0.4 |
| 2012-2 | 1.6 | 0.1 | 0.4 |
| 2012-3 | 2.1 | 0.1 | 0.6 |
| 2012-4 | 1.2 | 0.1 | 0.3 |
| 2012-5 | 3.0 | 0.3 | 0.3 |
| 2012-6 | 2.3 | 0.3 | 0.4 |
| 2012-7 | 2.0 | 0.3 | 0.5 |
| 2012-8 | 0.9 | 0.2 | 0.2 |
| 2012-9 | 1.0 | 0.2 | 0.3 |
| 2012-10 | 0.8 | 0.1 | 0.1 |

**5) Well #5**

| Time | Oil production ($m^3/d$) | Water production ($m^3/d$) | Gas production ($10^3 Sm^3/d$) |
|---|---|---|---|
| 2010-7 | 0.0 | 0.0 | 0.0 |
| 2010-8 | 0.0 | 0.0 | 0.0 |
| 2010-9 | 0.0 | 0.0 | 0.0 |
| 2010-10 | 0.0 | 0.0 | 0.0 |
| 2010-11 | 12.1 | 1.3 | 0.0 |
| 2010-12 | 48.2 | 1.9 | 0.1 |
| 2011-1 | 22.4 | 0.6 | 0.5 |
| 2011-2 | 37.3 | 1.2 | 0.5 |
| 2011-3 | 33.8 | 1.2 | 0.5 |
| 2011-4 | 15.8 | 0.5 | 0.6 |
| 2011-5 | 18.0 | 0.7 | 0.6 |
| 2011-6 | 9.9 | 0.6 | 0.9 |
| 2011-7 | 8.5 | 0.5 | 0.8 |
| 2011-8 | 8.8 | 0.7 | 0.6 |
| 2011-9 | 7.4 | 0.7 | 0.6 |
| 2011-10 | 7.1 | 0.6 | 0.6 |
| 2011-11 | 6.2 | 0.8 | 0.9 |
| 2011-12 | 6.3 | 0.8 | 1.1 |
| 2012-1 | 6.4 | 0.5 | 0.8 |
| 2012-2 | 5.8 | 0.6 | 1.0 |
| 2012-3 | 7.4 | 0.5 | 1.4 |
| 2012-4 | 4.7 | 0.4 | 1.2 |
| 2012-5 | 9.5 | 0.7 | 1.3 |
| 2012-6 | 9.2 | 0.6 | 1.6 |
| 2012-7 | 6.4 | 0.4 | 0.5 |
| 2012-8 | 6.8 | 0.6 | 0.0 |
| 2012-9 | 8.2 | 0.7 | 0.1 |
| 2012-10 | 5.8 | 0.4 | 0.5 |

**6) Well #6**

| Time | Oil production ($m^3/d$) | Water production ($m^3/d$) | Gas production ($10^3 Sm^3/d$) |
|---|---|---|---|
| 2010-7 | 0.0 | 0.0 | 0.0 |
| 2010-8 | 0.0 | 0.0 | 0.0 |
| 2010-9 | 0.0 | 0.0 | 0.0 |
| 2010-10 | 0.0 | 0.0 | 0.0 |
| 2010-11 | 0.0 | 0.0 | 0.0 |
| 2010-12 | 0.0 | 0.0 | 0.0 |
| 2011-1 | 0.0 | 0.0 | 0.0 |
| 2011-2 | 0.0 | 0.0 | 0.0 |
| 2011-3 | 0.0 | 0.0 | 0.0 |
| 2011-4 | 0.0 | 0.0 | 0.0 |
| 2011-5 | 0.0 | 0.0 | 0.0 |
| 2011-6 | 0.4 | 0.1 | 0.0 |
| 2011-7 | 8.4 | 4.3 | 0.8 |
| 2011-8 | 1.0 | 0.8 | 0.2 |
| 2011-9 | 4.2 | 3.7 | 0.6 |
| 2011-10 | 4.1 | 2.0 | 0.2 |
| 2011-11 | 1.9 | 1.1 | 0.1 |
| 2011-12 | 2.0 | 1.3 | 0.1 |
| 2012-1 | 1.6 | 1.0 | 0.1 |
| 2012-2 | 2.0 | 1.2 | 0.2 |
| 2012-3 | 1.2 | 0.9 | 0.3 |
| 2012-4 | 1.0 | 0.8 | 0.3 |
| 2012-5 | 0.9 | 0.7 | 0.2 |
| 2012-6 | 0.8 | 0.6 | 0.3 |
| 2012-7 | 0.7 | 0.5 | 0.3 |
| 2012-8 | 0.6 | 0.5 | 0.2 |
| 2012-9 | 0.8 | 0.5 | 0.3 |
| 2012-10 | 0.8 | 0.5 | 0.2 |

**7) Well #7**

| Time | Oil production ($m^3$/d) | Water production ($m^3$/d) | Gas production ($10^3$ $Sm^3$/d) |
|---|---|---|---|
| 2010-7 | 0.0 | 0.0 | 0.0 |
| 2010-8 | 0.0 | 0.0 | 0.0 |
| 2010-9 | 0.0 | 0.0 | 0.0 |
| 2010-10 | 0.0 | 0.0 | 0.0 |
| 2010-11 | 0.0 | 0.0 | 0.0 |
| 2010-12 | 0.0 | 0.0 | 0.0 |
| 2011-1 | 59.0 | 1.8 | 0.0 |
| 2011-2 | 48.4 | 1.4 | 4.2 |
| 2011-3 | 45.0 | 1.5 | 4.9 |
| 2011-4 | 40.9 | 1.4 | 3.6 |
| 2011-5 | 28.4 | 0.7 | 1.4 |
| 2011-6 | 21.9 | 0.6 | 1.2 |
| 2011-7 | 18.7 | 0.6 | 4.1 |
| 2011-8 | 16.4 | 0.6 | 5.6 |
| 2011-9 | 14.6 | 0.7 | 5.0 |
| 2011-10 | 13.0 | 0.6 | 4.6 |
| 2011-11 | 10.7 | 0.3 | 2.3 |
| 2011-12 | 1.7 | 0.0 | 0.1 |
| 2012-1 | 6.5 | 0.3 | 1.5 |
| 2012-2 | 8.8 | 0.4 | 2.2 |
| 2012-3 | 7.4 | 0.4 | 2.6 |
| 2012-4 | 6.5 | 0.4 | 2.6 |
| 2012-5 | 4.4 | 0.3 | 2.2 |
| 2012-6 | 3.5 | 0.3 | 2.6 |
| 2012-7 | 3.4 | 0.3 | 2.5 |
| 2012-8 | 2.3 | 0.3 | 1.7 |
| 2012-9 | 2.3 | 0.3 | 0.8 |
| 2012-10 | 2.3 | 0.2 | 0.2 |

**8) Well #8**

| Time | Oil production ($m^3$/d) | Water production ($m^3$/d) | Gas production ($10^3$ $Sm^3$/d) |
|---|---|---|---|
| 2010-7 | 0.0 | 0.0 | 0.0 |
| 2010-8 | 0.0 | 0.0 | 0.0 |
| 2010-9 | 0.0 | 0.0 | 0.0 |
| 2010-10 | 0.0 | 0.0 | 0.0 |
| 2010-11 | 0.0 | 0.0 | 0.0 |
| 2010-12 | 0.0 | 0.0 | 0.0 |
| 2011-1 | 0.0 | 0.0 | 0.0 |
| 2011-2 | 0.0 | 0.0 | 0.0 |
| 2011-3 | 0.0 | 0.0 | 0.0 |
| 2011-4 | 0.2 | 0.1 | 0.0 |
| 2011-5 | 30.0 | 2.6 | 0.0 |
| 2011-6 | 35.1 | 2.1 | 1.4 |
| 2011-7 | 37.4 | 1.7 | 3.5 |
| 2011-8 | 23.8 | 0.8 | 5.0 |
| 2011-9 | 21.5 | 0.8 | 5.0 |
| 2011-10 | 16.4 | 0.9 | 5.3 |
| 2011-11 | 15.4 | 0.9 | 5.2 |
| 2011-12 | 11.9 | 0.7 | 3.6 |
| 2012-1 | 6.1 | 0.4 | 1.4 |
| 2012-2 | 10.5 | 0.7 | 3.1 |
| 2012-3 | 9.6 | 0.6 | 3.6 |
| 2012-4 | 9.0 | 0.5 | 3.4 |
| 2012-5 | 8.6 | 0.4 | 2.8 |
| 2012-6 | 6.2 | 0.5 | 2.8 |
| 2012-7 | 5.9 | 0.5 | 3.2 |
| 2012-8 | 5.7 | 0.7 | 3.8 |
| 2012-9 | 6.1 | 0.6 | 1.2 |
| 2012-10 | 4.5 | 0.5 | 0.6 |

**9) Well #9**

| Time | Oil production ($m^3/d$) | Water production ($m^3/d$) | Gas production ($10^3 Sm^3/d$) |
|---|---|---|---|
| 2010-7 | 0.0 | 0.0 | 0.0 |
| 2010-8 | 0.0 | 0.0 | 0.0 |
| 2010-9 | 0.0 | 0.0 | 0.0 |
| 2010-10 | 0.0 | 0.0 | 0.0 |
| 2010-11 | 0.0 | 0.0 | 0.0 |
| 2010-12 | 0.0 | 0.0 | 0.0 |
| 2011-1 | 0.0 | 0.0 | 0.0 |
| 2011-2 | 0.0 | 0.0 | 0.0 |
| 2011-3 | 0.0 | 0.0 | 0.0 |
| 2011-4 | 0.0 | 0.0 | 0.0 |
| 2011-5 | 0.0 | 0.0 | 0.0 |
| 2011-6 | 5.8 | 1.4 | 0.0 |
| 2011-7 | 20.6 | 2.9 | 1.8 |
| 2011-8 | 16.5 | 2.9 | 2.5 |
| 2011-9 | 12.2 | 1.9 | 2.7 |
| 2011-10 | 7.2 | 1.2 | 1.0 |
| 2011-11 | 6.9 | 1.3 | 0.9 |
| 2011-12 | 6.7 | 1.2 | 0.8 |
| 2012-1 | 3.2 | 0.6 | 0.3 |
| 2012-2 | 2.8 | 0.5 | 0.3 |
| 2012-3 | 0.9 | 0.3 | 0.3 |
| 2012-4 | 0.5 | 0.3 | 0.1 |
| 2012-5 | 5.1 | 1.0 | 0.6 |
| 2012-6 | 4.9 | 0.8 | 0.9 |
| 2012-7 | 4.5 | 0.7 | 1.0 |
| 2012-8 | 2.9 | 0.7 | 0.6 |
| 2012-9 | 2.8 | 0.7 | 0.5 |
| 2012-10 | 2.3 | 0.5 | 0.3 |

**10) Well #10**

| Time | Oil production ($m^3/d$) | Water production ($m^3/d$) | Gas production ($10^3 Sm^3/d$) |
|---|---|---|---|
| 2010-7 | 17.9 | 2.5 | 2.5 |
| 2010-8 | 24.6 | 2.4 | 7.6 |
| 2010-9 | 12.4 | 1.4 | 2.4 |
| 2010-10 | 8.6 | 1.0 | 1.3 |
| 2010-11 | 7.6 | 0.8 | 1.2 |
| 2010-12 | 7.1 | 0.8 | 1.1 |
| 2011-1 | 6.9 | 1.0 | 1.1 |
| 2011-2 | 7.0 | 0.5 | 1.2 |
| 2011-3 | 7.3 | 0.6 | 1.2 |
| 2011-4 | 7.2 | 0.6 | 1.0 |
| 2011-5 | 5.8 | 0.5 | 0.6 |
| 2011-6 | 3.5 | 0.4 | 0.2 |
| 2011-7 | 2.1 | 0.1 | 0.1 |
| 2011-8 | 2.0 | 0.1 | 0.2 |
| 2011-9 | 2.1 | 0.1 | 0.5 |
| 2011-10 | 1.7 | 0.0 | 0.2 |
| 2011-11 | 1.9 | 0.1 | 0.1 |
| 2011-12 | 4.7 | 0.1 | 0.4 |
| 2012-1 | 2.4 | 0.3 | 0.3 |
| 2012-2 | 1.8 | 0.5 | 0.4 |
| 2012-3 | 4.5 | 1.4 | 1.2 |
| 2012-4 | 2.5 | 0.9 | 1.0 |
| 2012-5 | 1.6 | 0.5 | 0.5 |
| 2012-6 | 1.2 | 0.4 | 0.5 |
| 2012-7 | 1.5 | 0.5 | 0.6 |
| 2012-8 | 1.5 | 0.5 | 0.4 |
| 2012-9 | 2.1 | 0.9 | 0.5 |
| 2012-10 | 1.4 | 0.7 | 0.2 |

**11) Well #11**

| Time | Oil production ($m^3$/d) | Water production ($m^3$/d) | Gas production ($10^3$ $Sm^3$/d) |
|---|---|---|---|
| 2010-7 | 0.0 | 0.0 | 0.0 |
| 2010-8 | 0.0 | 0.0 | 0.0 |
| 2010-9 | 0.0 | 0.0 | 0.0 |
| 2010-10 | 0.0 | 0.0 | 0.0 |
| 2010-11 | 0.0 | 0.0 | 0.0 |
| 2010-12 | 0.0 | 0.0 | 0.0 |
| 2011-1 | 0.0 | 0.0 | 0.0 |
| 2011-2 | 0.0 | 0.0 | 0.0 |
| 2011-3 | 0.0 | 0.0 | 0.0 |
| 2011-4 | 0.0 | 0.0 | 0.0 |
| 2011-5 | 0.0 | 0.0 | 0.0 |
| 2011-6 | 0.0 | 0.0 | 0.0 |
| 2011-7 | 0.0 | 0.0 | 0.0 |
| 2011-8 | 2.5 | 2.9 | 0.0 |
| 2011-9 | 3.4 | 4.6 | 0.5 |
| 2011-10 | 2.6 | 3.3 | 0.5 |
| 2011-11 | 1.7 | 2.0 | 0.2 |
| 2011-12 | 1.3 | 1.4 | 0.1 |
| 2012-1 | 2.2 | 0.8 | 0.2 |
| 2012-2 | 2.5 | 0.9 | 0.2 |
| 2012-3 | 2.3 | 0.9 | 0.2 |
| 2012-4 | 1.2 | 0.6 | 0.2 |
| 2012-5 | 1.0 | 0.6 | 0.1 |
| 2012-6 | 1.1 | 0.7 | 0.2 |
| 2012-7 | 1.0 | 0.8 | 0.2 |
| 2012-8 | 0.8 | 0.6 | 0.2 |
| 2012-9 | 0.7 | 0.5 | 0.3 |
| 2012-10 | 0.6 | 0.5 | 0.2 |